**LIBRARY**
**Michigan State**
**University**

This is to certify that the
dissertation entitled

DEVELOPMENT AND APPLICATION OF A METHODOLOGY
TO EVALUATE NATURAL ATTENUATION OF
CHLORINATED SOLVENTS USING CONCEPTUAL AND
NUMERICAL MODELS

presented by
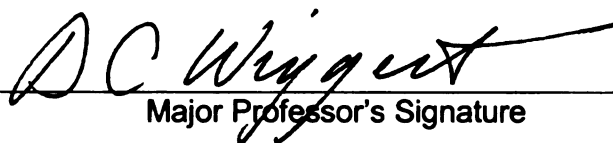
Jaime A. Graulau-Santiago

has been accepted towards fulfillment
of the requirements for the

Ph.D.        degree in        Civil and Environmental
                                            Engineering

Major Professor's Signature

December 8, 2003

Date

**PLACE IN RETURN BOX** to remove this checkout from your record.
**TO AVOID FINES** return on or before date due.
**MAY BE RECALLED** with earlier due date if requested.

| DATE DUE | DATE DUE | DATE DUE |
|----------|----------|----------|
|          |          |          |
|          |          |          |
|          |          |          |
|          |          |          |
|          |          |          |
|          |          |          |
|          |          |          |
|          |          |          |
|          |          |          |
|          |          |          |

# DEVELOPMENT AND APPLICATION OF A METHODOLOGY TO EVALUATE NATURAL ATTENUATION OF CHLORINATED SOLVENTS USING CONCEPTUAL AND NUMERICAL MODELS

By

Jaime A. Graulau-Santiago

## A DISSERTATION

Submitted to
Michigan State University
in partial fulfillment of the requirements for the degree of

DOCTOR OF PHILOSOPHY

Civil and Environmental Engineering Department

2003

# ABSTRACT

## DEVELOPMENT AND APPLICATION OF A METHODOLOGY TO EVALUATE NATURAL ATTENUATION FOR CHLORINATED SOLVENTS USING CONCEPTUAL & NUMERICAL MODELS

By

Jaime A. Graulau-Santiago

Natural attenuation of chlorinated solvents has being increasingly used by engineers and regulators as a remedial alternative to contaminated aquifers because the numerous advantages it has over more traditional engineered solutions. However, natural attenuation has been clearly demonstrated only for a selected class of organic compounds, primarily fuel hydrocarbons. The scientific community has recognized that the surge in use of natural attenuation has outpaced certain guidelines that have been developed for its application. This study evaluates a novel approach to evaluate natural attenuation of chlorinated solvents by using models incorporating important physical and biogeochemical processes that can be critical for a successful evaluation of natural attenuation.

A hydraulic characterization methodology was developed to estimate parameters that influence the transport of solutes in groundwater environments. Biogeochemical data coupled with historical development of the VOC plume were used to develop a conceptual model for the contaminated site. This model was translated into a numerical model incorporating the compiled information and two snapshots of the plume historical development were successfully validated.

The successful application of the methodology developed in this dissertation could become the foundation for the development of a series of guidelines to evaluate natural attenuation of chlorinated solvents.

# ACKNOWLEDGMENTS

I would like to express my gratitude to all of those that directly or indirectly helped me in the completion of this work.

First I would like to thank God for giving me the strength, health, patience, and the character to always work hard for the things I want.

To my parents, for teaching me essential values in life that I could not be taught in any school or college, thanks for accepting me in our Home University.

My sisters and brother, thanks for the long phone conversations during the last five years and for all the experiences we share together. You guys are my best friends.

To Parissa, for the love we share and for being with me during these tough times. Finally I can say "I'm done". I know you have heard this before but this time I think is for real. I am looking forward to our bright future together.

To Natalia Zohreh, for telling me to hurry up with the dissertation, even when she could not even talk.

To my advisor; Dr. David C. Wiggert, thanks for giving me the opportunity to reach all my academic goals. Your support during the last five years was invaluable.

Thank you, Dr. Michel J. Dybas, for showing me all the aspects of purging and sampling monitoring wells in the field. You are an inspiration for any one who wants to be a good scientist.

To Dr. David W. Hyndman; for introducing me to the wonderful world of hydrogeology and numerical modeling.

To Dr. Manta S. Phanikumar, for teaching me numerous tools that I can further apply in my career as a modeler and scientist.

Finally, to all the friends and co-workers at MSU for making my years in East Lansing more enjoyable.

# TABLE OF CONTENTS

# LIST OF TABLES

# LIST OF FIGURES

Images in this dissertation are presented in color (Figures 2.8, 3.10, 3.11, and 3.12).

# LIST OF SYMBOLS

| | |
|---|---|
| $\alpha$ | dispersivity tensor, [L] |
| b | cell endogenous decay coefficient, $[T^{-1}]$ |
| $C_a$ | contaminant concentration in soil air, $[M\ L^{-3}]$ |
| $C_k$ | dissolved concentration of the $k^{th}$ specie, $[M\ L^{-3}]$ |
| $\tilde{C}_k$ | concentration of the $k^{th}$ sorbed specie, $[M\ M^{-1}]$ |
| $C'_k$ | source-sink flux term concentration for the $k^{th}$ specie, $[M\ L^{-3}]$ |
| $C_l$ | contaminant concentration in water, $[M\ L^{-3}]$ |
| c | tracer concentration in pore fluid, $[M\ L^{-3}]$ |
| c' | tracer concentration in source or sink, $[M\ L^{-3}]$ |
| $c_{obs}$ | observed tracer concentration, $[M\ L^{-3}]$ |
| $c_{sim}$ | simulated tracer concentration, $[M\ L^{-3}]$ |
| $\mathbf{D}, D_{ij}$ | hydrodynamic dispersion coefficient tensor, $[L^2\ T^{-1}]$ |
| $D^*$ | effective molecular diffusion coefficient, $[L^2\ T^{-1}]$ |
| $[DCE\ ]$ | liquid phase DCE concentration, $[M\ L^{-3}]$ |
| $[DCE]_{soil}$ | sorbed DCE concentration $[M\ M^{-1}]$ |
| $[ethene\ ]$ | liquid phase ethene concentration, $[M\ L^{-3}]$ |
| $[ethene]_{soil}$ | sorbed ethene concentration $[M\ M^{-1}]$ |
| $\xi[DCE]$ | first-order DCE mass transfer rate coefficient $[T^{-1}]$ |
| $\xi[ethene]$ | first-order ethene mass transfer rate coefficient $[T^{-1}]$ |
| $\xi[tol]$ | first-order mass solid-liquid mass transfer coefficient, $[T^{-1}]$ |
| $\xi[PCE]$ | first-order PCE mass transfer rate coefficient $[T^{-1}]$ |
| $\xi[TCE]$ | first-order TCE mass transfer rate coefficient $[T^{-1}]$ |
| $\xi[VC]$ | first-order VC mass transfer rate coefficient $[T^{-1}]$ |
| $f_{oc}$ | fraction of total organic carbon, $[M\ M^{-1}]$ |
| H | dimensionless Henry's constant |
| h | hydraulic head [L] |
| K | hydraulic conductivity tensor $[L\ T^{-1}]$ |
| $K_d$ | solid-liquid partition coefficient, $[L^3\ M^{-1}]$ |
| $K_d[DCE]$ | solid-liquid DCE partitioning coefficient, $[L^{-3}\ M^{-1}]$ |
| $K_d[ethene]$ | solid-liquid ethene partitioning coefficient, $[L^{-3}\ M^{-1}]$ |
| $K_d[PCE]$ | solid-liquid PCE partitioning coefficient, $[L^{-3}\ M^{-1}]$ |
| $K_d[TCE]$ | solid-liquid TCE partitioning coefficient, $[L^{-3}\ M^{-1}]$ |
| $K_d[tol]$ | toluene partitioning coefficient, $[L^3\ M^{-1}]$ |
| $K_d[VC]$ | solid-liquid VC partitioning coefficient, $[L^{-3}\ M^{-1}]$ |

| | |
|---|---|
| $K_i$ | hydraulic conductivity tensor principal component, [L T$^{-1}$] |
| $K_{oc}$ | organic carbon-water partition coefficient, [L$^3$ M$^{-1}$] |
| $K_s$ [DCE] | DCE half-velocity coefficient, [M L$^{-3}$] |
| $K_s$ [PCE] | PCE half-velocity coefficient, [M L$^{-3}$] |
| $K_s$ [TCE] | TCE half-velocity coefficient, [M L$^{-3}$] |
| $K_s$ [tol] | half-velocity coefficient for toluene consumption [M L$^{-3}$] |
| $K_s$ [VC] | VC half-velocity coefficient, [M L$^{-3}$] |
| $k$ | chemical specie index |
| $\mu_{max}$ | maximum specific growth rate of dehalogenators, [T$^{-1}$] |
| [PCE ] | liquid phase PCE concentration, [M L$^{-3}$] |
| [PCE ]$_{eq}$ | equivalent PCE concentration, [M L$^{-3}$] |
| [PCE]$_{soil}$ | sorbed PCE concentration [M M$^{-1}$] |
| $\hat{q}$[DCE] | maximum specific utilization rate of DCE, [M M$^{-1}$ T$^{-1}$] |
| $\hat{q}$[PCE] | maximum specific utilization rate of PCE, [M M$^{-1}$ T$^{-1}$] |
| $q_{max}$ | maximum specific toluene utilization rate, [M M$^{-1}$ T$^{-1}$] |
| $\hat{q}$[TCE] | maximum specific utilization rate of TCE, [M M$^{-1}$ T$^{-1}$] |
| $\hat{q}$[VC] | maximum specific utilization rate of VC, [M M$^{-1}$ T$^{-1}$] |
| $\phi$ | total porosity of the soil, [L$^3$ L$^{-3}$] |
| $\phi_e$ | effective porosity |
| $R$ | retardation coefficient |
| $R_k$ | reaction term for the k$^{th}$ specie |
| $\rho$, $\rho_b$ | bulk mass density of the sediments, [M L$^{-3}$] |
| $\rho_s$ | particle mass density, [M L$^{-3}$] |
| $S_y$ | specific aquifer yield, [L$^3$ L$^{-3}$] |
| $t$ | time, [T] |
| [TCE ] | liquid phase TCE concentration, [M L$^{-3}$] |
| [TCE]$_{soil}$ | sorbed TCE concentration [M M$^{-1}$] |
| [tol] | concentration of toluene, [M L$^{-3}$] |
| [tol]$_{soil}$ | solid-phase toluene concentration, [M M$^{-1}$] |
| $v$ | groundwater velocity vector, [L T$^{-1}$] |
| $v_c$ | contaminant retarded velocity, [L T$^{-1}$] |
| $v_l$ | longitudinal advective groundwater velocity, [L T$^{-1}$] |
| [VC ] | liquid phase VC concentration, [M L$^{-3}$] |
| [VC]$_{soil}$ | sorbed VC concentration [M M$^{-1}$] |
| $W$, $C'_k$, $q_s$ | fluid source sink term, [L T$^{-1}$] |
| $x,y,z$ | Cartesian coordinates, [L] |
| $x_i$ | distance along a Cartesian coordinate, [L] |

$[X]$  biomass concentration, $[M\ L^{-3}]$

$Y_{[DCE]/[TCE]}$  stoichiometric TCE to DCE yield coefficient, $[M\ M^{-1}]$

$Y_{[ethene]/[VC]}$  stoichiometric VC to ethene yield coefficient, $[M\ M^{-1}]$

$Y_{[TCE]/[PCE]}$  stoichiometric PCE to TCE yield coefficient, $[M\ M^{-1}]$

$Y_{[VC]/[DCE]}$  stoichiometric DCE to VC yield coefficient, $[M\ M^{-1}]$

$Y_{[X]/[tol]}$  yield coefficient for cell synthesis, $[M\ M^{-1}]$

$\nabla$  gradient operator ($\partial/\partial x$, $\partial/\partial y$, $\partial/\partial z$)

# CHAPTER 1

# INTRODUCTION

## 1.1 Environmental concern of chlorinated solvents

Due to their widespread use as industrial solvents and degreasers, chlorinated

compounds are among the top five contaminants found in groundwater around the world

(Prakash and Gupta 2000). These compounds are substituted hydrocarbons in which

hydrogen atoms have been replaced with a chlorine atom. Figure 1.1 illustrates some of

the chlorinated compounds of environmental concern. Annual production levels in the

U.S. for some of these compounds are on the order of $10^5$ to $10^6$ tons per year (Table 1.1).

Halogenated hydrocarbons can be degraded under both, anaerobic and aerobic

conditions. The anaerobic degradation process is called reductive dechlorination. In this

process, halogen atoms are sequentially removed from the compound molecule and

replaced by hydrogen. The chlorinated compound in this microbially mediated reaction

is used as an electron acceptor; not as a carbon source (Holliger and Schumacher 1994;

McCarty 1997; Sims *et al.* 1991).

Reductive dechlorination depends on the redox state of the halogenated molecule,

which is determined primarily by the strength of the halogen-carbon bond. The higher

the bond strength, the less likely the halogen will be removed. In general, bromine and

iodine substitutions, which have lower bond strengths than chlorine, are easier to remove.

Fluorine, for example, forms stronger bonds with carbon than chlorine,

Cl       Cl
 \\      /
   C = C
 /      \\
Cl       Cl

*tetrachloroethene*
*(PCE)*

H        Cl
 \\      /
   C = C
 /      \\
Cl       Cl

*trichloroethene*
*(TCE)*

H        H
 \\      /
   C = C
 /      \\
Cl       Cl

*cis-1,2 dichloroethene*
*(cis-DCE)*

H        Cl
 \\      /
   C = C
 /      \\
Cl       H

*trans-1,2 dichloroethene*
*(trans-DCE)*

H        H
 \\      /
   C = C
 /      \\
H        Cl

*vinyl chloride*
*(VC)*

       Cl   H
       |    |
  Cl—  C  —  C  —H
       |    |
       Cl   H

*1,1,1 trichloroethane*
*(TCA)*

       Cl   Cl
       |    |
  H—  C  —  C  —H
       |    |
       H    H

*1,2 dichloroethane*
*(1,2 DCA)*

       Cl   Cl
       |    |
  Cl—  C  —  C  —H
       |    |
       H    H

*1,1,2 trichloroethane*
*(1,1,2 TCA)*

       Cl
       |
  Cl—  C  —Cl
       |
       Cl

*carbon tetrachloride*
*(CT)*

       Cl
       |
  H—  C  —Cl
       |
       H

*methylene chloride*

Figure 1.1.  Commonly chlorinated organic compounds found in groundwaters.

**Table 1.1. Estimated annual production of the most important hydrocarbons in the U.S. and its applications.** [a]

| Chlorinated hydrocarbon | Production ($*10^3$ tons) | Major use |
|---|---|---|
| Tetrachloroethene (PCE) | 165 | Solvent for dry cleaning, metal degreasing, textile finishing, dyeing, extraction processes; intermediate for the production of trichloroacetic acid and some fluorocarbons. |
| Trichloroethene (TCE) | 110 | Solvent for vapor degreasing in the metal industry and for dry cleaning; extraction solvent; solvent in formulations for rubbers, elastomers, and industrial paints. |
| 1,1 Dichloroethene (1,1 DCE) | N.A. | Basic material for polyvinylidene chloride and its copolymers; production of 1,1,1-trichloroethane. |
| Vinyl chloride | 6000 | Production of polyvinyl chloride (PVC); production of chlorinated solvents (primarily 1,1,1- trichloroethane). |
| 1,1,2 Trichloroethane | N.A. | Intermediate for production of 1,1,1-trichloroethane and 1,1-dichloroethane. |
| 1,1,1 Trichloroethane | 327 | Dry cleaning; vapor degreasing; solvent for adhesives and metal cutting fluids; textile processing. |
| 1,1 Dichloroethane | N.A. | Feedstock for the production of 1,1,1-trichloroethane |
| 1,2 Dichloroethane | 7200 | Production of vinyl chloride; production of chlorinated solvents such as 1,1,1 trichloroethane and tri- and tetrachloroethene: synthesis of ethylenediamines. |
| Monochloroethane | 70 | Production of tetraethyllead; production of ethylcellulose; ethylating agent for fine chemical production; solvent for extraction processes. |
| Carbon tetrachloride (CT) | 150 | Production of trichloromonofluoromethane and dichlorodifluoromethane; solvent. |
| Trichloromethane | 230 | Production of monochlorodifluoromethane (for the production of tetrafluoroethene, which is used for the manufacture of Hostaflon and Teflon); extractant for pharmaceutical products. |
| Dichloromehtane | 162 | Degreasing agent; paint remover; pressure mediator in aerosols; extraction technology |
| Monochloromethane | 390 | Production of silicones, tetramethyllead, methylcellulose; other methylation reactions. |

[a] from Fetzner (1998)
N.A. = not available

3

consequently, the energy required to remove chlorine atoms is less than fluorine.

Bouwer *et al.* (1981) and Bouwer and McCarty (1983(a); 1983(b)) were the first to demonstrate conclusively that biological transformation of these compounds not only could occur, but occurred at a faster rate than abiotic transformations. They demonstrated that a microbial consortium enriched under methanogenic conditions with acetate as a source of carbon could transform $C_1$ and $C_2$ halocarbons into carbon dioxide and methane. Of the compounds screened, only carbon tetrachloride was transformed using enrichments under denitrifying conditions.

## 1.2 Natural attenuation: overview of processes

Due to the complexities in the subsurface and the inherent problems and costs associated with conventional treatment technologies, interest in natural attenuation of groundwater contaminants has increased over the last decade (Azadpour-Keeley *et al.* 2001). Numerous potential advantages of natural attenuation over more traditional engineered approaches have been identified (Swett and Rapaport 1998):

- since it is an *in situ* process, less volume of remediation wastes are generated

- the site can be used with minimal disruption while remediation is occurring

- few surface structures are required

- implementation of natural attenuation enables managers, remediators, and regulators to differentiate between sites that are cleaning themselves from those that are not, so that engineering resources can be allocated to sites where they will provide the greatest benefit

- associated costs are lower than any engineered remediation technology

4

A challenge to acceptance of natural attenuation can be public perception since it may be viewed as a "do nothing approach" in which responsible parties were employing natural attenuation to avoid remediation costs. As scientists developed better understanding of the processes and disseminate this information, community and regulatory perceptions have changed as natural attenuation has become defined (EPA, 1998) and accepted as a remedial approach.

However, real technical challenges exist with natural attenuation. Usually, long time frames are required to achieve contaminant concentration levels that are protective of the human health and the environment. Moreover, these times are not easily predicted even with historical data. Depending on the complexity of the site hydrogeology, characterization costs can be high and long term monitoring is necessary to show the effect of changing conditions on the overall remedial effectiveness of natural attenuation.

Natural attenuation has been defined as all naturally occurring physical, chemical, and biological processes that can reduce water-phase concentration of contaminants (NRC 2000). These processes can be divided in two categories: non-destructive or destructive (EPA 1998). Non-destructive are those that reduce the contaminant's concentration but not the total contaminant mass. On the other hand, destructive processes are those that reduce both contaminant mass and concentration. They include biological and chemical transformation of the contaminants.

*Non-destructive processes*

Non-destructive processes are all physical mechanisms and include advection, hydrodynamic dispersion, molecular diffusion, sorption, dilution, and volatilization.

Advection is the migration of solutes in the direction parallel to the groundwater flow.
Transport by advection alone results in strong, sharp concentration fronts. The advective
velocity of the groundwater is given by:

$$v = -\frac{K}{\phi_e}\nabla h \qquad (1.1)$$

where $v$ is the groundwater velocity vector $[L \cdot T^{-1}]$; $\nabla$ is the gradient operator ($\partial/\partial x$, $\partial/\partial y$,
$\partial/\partial z$); x, y, z, are spatial coordinates [L]; $K$ is the hydraulic conductivity tensor $[L \cdot T^{-1}]$; h
is the hydraulic head [L]; and $\phi_e$ is the effective porosity.

Hydrodynamic dispersion results in the spreading of contaminants in directions
longitudinal and transverse to the principal groundwater flow direction. This
phenomenon is attributed to two physical processes: mechanical dispersion and molecular
diffusion. Mechanical dispersion is the mixing of contaminants that result from small
scale variability in velocity around the average linear groundwater velocity. Molecular
diffusion occurs when the contaminant migrates due to the thermal-kinetic energy of the
solute molecules. A hydrodynamic dispersion coefficient which accounts for the two
processes can be obtained from (Freeze and Cherry 1979):

$$D = \alpha\, v + D^* \qquad (1.2)$$

where $D$ is the hydrodynamic dispersion coefficient tensor, $[L^2 \cdot T^{-1}]$, $\alpha$ is the dispersivity
tensor, [L]; and $D^*$ is the effective molecular diffusion coefficient for the solute $[L^2 \cdot T^{-1}]$.

At normal groundwater velocity, mechanical dispersion is often more dominant than the spreading that occurs due to molecular diffusion.

Sorption is the process whereby contaminants partition from the water and adhere to the soil particles comprising the aquifer matrix. This mechanism results in retardation or slowing of solute migration relative to the advective groundwater velocity. The ratio of groundwater to contaminant velocity is a measure of the relative slowness of the contaminant:

$$R = \frac{v_l}{v_c} \qquad (1.3)$$

where R is the retardation coefficient; $v_l$ is the advective groundwater velocity in the longitudinal direction, $[L \cdot T^{-1}]$; and $v_c$ is the contaminant retarded velocity $[L \cdot T^{-1}]$. The retardation coefficient can be estimated from:

$$R = 1 + \frac{\rho_b K_d}{\phi} \qquad (1.4)$$

where $\rho_b$ is the bulk mass density of the sediments, $[M \cdot L^{-3}]$; $K_d$ is the partition coefficient between soil particles and water, $[L^{3} \cdot M^{-1}]$; and $\phi$ is the soil porosity, $[L^{3} L^{-3}]$. It has been found that partition coefficient values normalized to the total organic carbon content eliminates the variations observed between different soil types (EPA 1998). Therefore, the partition coefficient can be estimated by:

$$K_d = K_{oc} \, f_{oc} \qquad\qquad (1.5)$$

where $K_{oc}$ is the organic carbon-water partition coefficient, $[L^3 \cdot M^{-1}]$; and $f_{oc}$ is the

fraction of total organic carbon in the sediments $[M \cdot M^{-1}]$.

Volatilization, while not considered a destructive mechanism, does reduce the

contaminant mass in the groundwater. Factors that affect the volatilization rate of

contaminants in groundwater include concentrations, depth dependant concentration

gradients, Henry's Law and diffusion coefficients, mass transport coefficients, sorption,

and water and soil gas temperature. The partition coefficient between the contaminant

concentration in water and soil gas is given by Henry's Law:

$$C_a = H C_l \qquad\qquad (1.6)$$

where $C_a$ is the contaminant concentration in soil air, $[M \cdot L^{-3}]$; $C_l$ is the contaminant

concentration in water, $[M \cdot L^{-3}]$; and H is Henry's constant (dimensionless). The impact

of volatilization for chlorinated compounds can usually be neglected. It has been found

that volatilization could have a significant impact only for vinyl chloride removal.

*Destructive processes*

Destructive attenuation mechanisms consist of biological and abiotic processes

that result in transformation and reduction of the contaminant's mass. Biological

mediated processes for chlorinated solvents in groundwater include reductive

dechlorination, cometabolism, and direct biological oxidation. Reductive dechlorination

8

and direct biological oxidation are the most common processes responsible for biological destruction of chlorinated compounds in groundwater under natural conditions. Hydrolysis is an abiotic process in which $H_2O$ or $OH^-$ substitutes for an electron-withdrawing group such as chlorine. 1,1,1-TCA is the only chlorinated compound that can be hydrolyzed within the one to two-decade time span under conditions likely to be found in most groundwater (NRC 2000).

Reductive dechlorination of chlorinated compounds has been documented elsewhere (Ferguson and Pietari 2000; Ndon *et al.* 2000; Maymó-Gatell *et al.* 1997; Vogel *et al.* 1987; Vogel and McCarty 1987). In this process, the chlorinated compounds serve as an electron acceptor in anaerobically mediated biological processes. An appropriate source of carbon for microbial growth must be available in order for reductive dechlorination to occur. Potential carbon sources include low molecular weight organic compounds, fuel hydrocarbons, byproducts of fuel hydrocarbons, or naturally occurring organic matter. The steps involved in the biological degradation of PCE by reductive dechlorination are illustrated in Figure 1.2 (McCarty 1997).

Gibbs free energy for the reductive dechlorination of PCE to ethene with hydrogen as the electron donor is shown in Table 1.2. The $\Delta G^{o\prime}$ values in this table indicate that all these reactions are feasible at standard temperature and pressure from the thermodynamic standpoint. Also, redox potential ranges at which reductive dechlorination reactions are feasible are given in Figure 1.3 (Nyer and Duffin 1997). Due to the oxidized nature of chlorinated compounds they are unlikely to undergo direct biological oxidation. However, it has been observed that vinyl chloride can be oxidized to carbon dioxide and water via iron reduction.

9
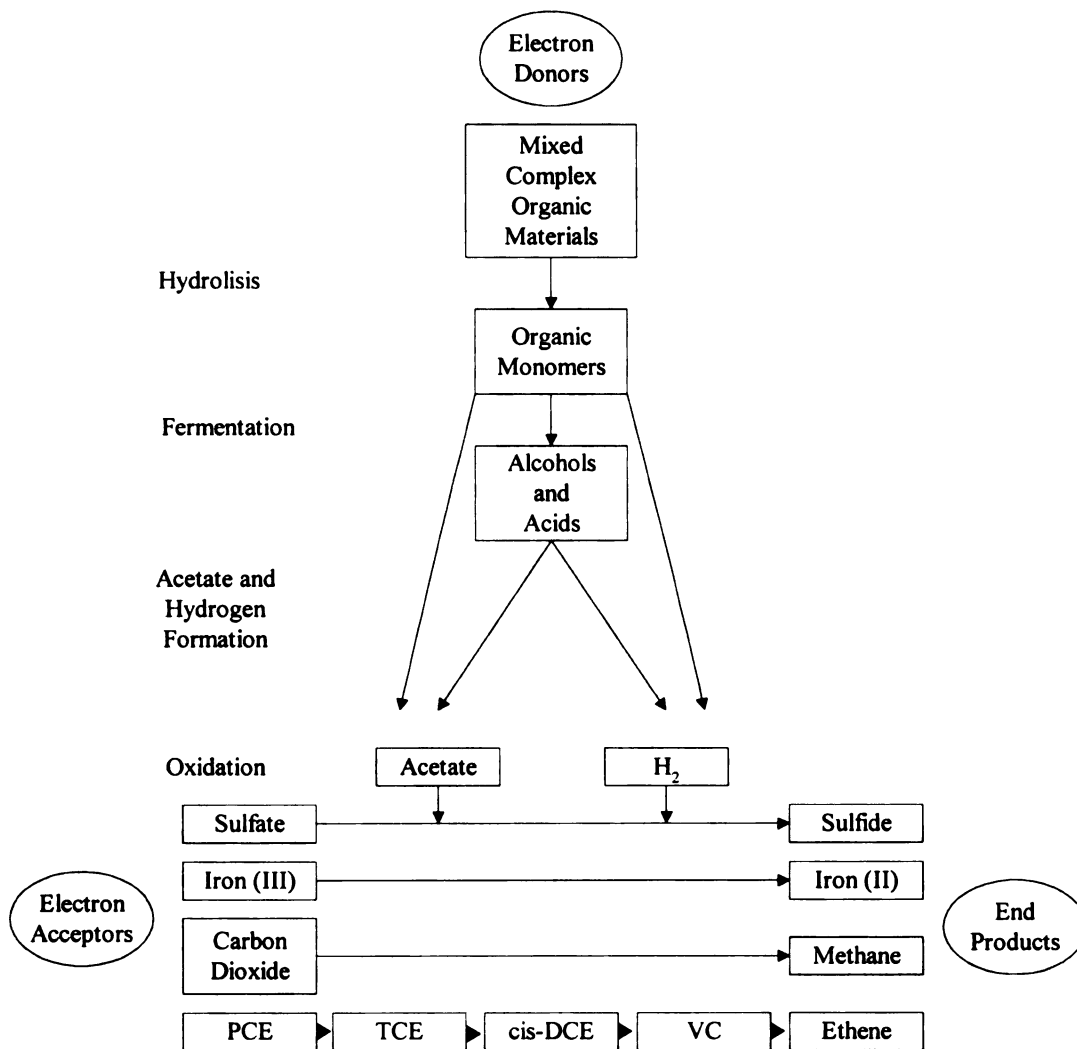
Figure 1.2.  Steps in the degradation of PCE by reductive dechlorination.
The chlorinated compounds must compete for electrons with
sulfate, iron, and carbon dioxide (from McCarty, 1997).

10

**Table 1.2. Gibbs free energy for reductive dechlorination of chlorinated ethene compounds.**

| Reductive dechlorination reaction | $\Delta G^{o\prime}$ (kJ/mol)[a] |
|---|---|
| $C_2Cl_4 + H_2 \leftrightarrow C_2HCl_3 + H^+ + Cl^-$ | -171.8 |
| $C_2HCl_3 + H_2 \leftrightarrow C_2H_2Cl_2 + H^+ + Cl^-$ | -166.1 |
| $C_2H_2Cl_2 + H_2 \leftrightarrow C_2H_3Cl + H^+ + Cl^-$ | -144.8 |
| $C_2H_3Cl + H_2 \leftrightarrow C_2H_4 + H^+ + Cl^-$ | -154.5 |

[a] from Dolfing (2000)

## 1.3 Natural attenuation of chlorinated solvents

Several investigations have demonstrated the biodegradability of chlorinated solvents in natural environments (Clement *et al.* 2002; Davis *et al.* 2002; Röling and van Verseveld 2002; Witt *et al.* 2002). However, based on field evidence, the likelihood of using natural attenuation as a stand alone approach to bring contaminant concentration to levels that do not represent a risk to the human health and the environment are moderate (Macdonald 2000). It has been estimated that only 20% of sites contaminated with chlorinated organics may be amenable to using just natural attenuation (Swett and Rapaport 1998).

Under anaerobic conditions, reductive dechlorination has been identified as the major mechanisms for the biological destruction of chlorinated compounds (McCarty 1997). A carbon source capable of creating a reduced environment is required for this process to occur naturally. This criterion imposes a limitation on the application of natural attenuation to sites where presence of carbon source ensures a long term biodegradation of chlorinated solvents.

11

1000 ——

Decreasing amount of energy released during electron transfer

possible range for reductive dechlorination

AEROBIC

$O_2 + 4H^+ + 4e^- \longrightarrow 2H_2O$   $(E_h = +820)$

$2NO_3^- + 12H^+ + 10e^- \longrightarrow 2N_2 + 6H_2O$   $(E_h = +740)$

500 ——

$MnO_2(s) + HCO_3^- + 3H^+ + e^- \longrightarrow MnCO_3(s) + 2H_2O$
$(E_h = +520)$

ANAEROBIC

0 ——

$FeOOH(s) + HCO_3^- + 2H^+ + e^- \longrightarrow FeCO_3 + 2H_2O$
$(E_h = -50)$

$SO_4^{2-} + 9H^+ + 8e^- \longrightarrow HS^- + 4H_2O$ $(E_h = -220)$
$CO_2 + 8H+ + 8e^- \longrightarrow CH_4 + 2H_2O$ $(E_h = -240)$

Optimal range
for reductive
dechlorination

-500 ——
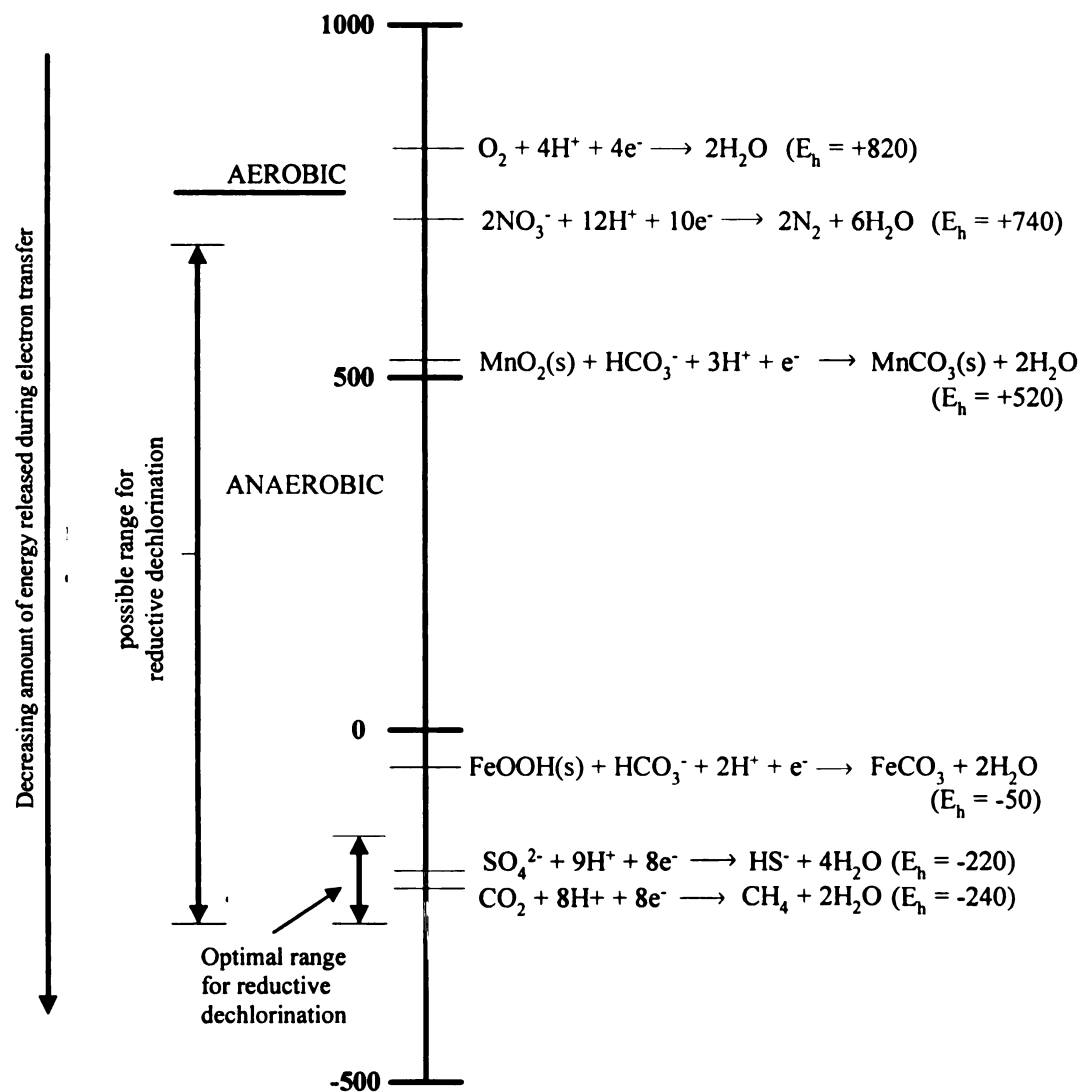
Figure 1.3.   Redox potential ($E_h$) in millivolts for various electron acceptors in groundwater.  Values for redox pairs at 25°C and pH = 7.0 (modified from Nyer and Duffin, 1997).

Numerous protocols for evaluating natural attenuation of chlorinated solvents have been developed (NRC 2000).  These protocols have been applied to document natural attenuation of chlorinated solvents at numerous sites (Clement *et al.* 2002; Wiedemeier *et al.* 1997; Witt *et al.* 2002).  However, they are used to reach conclusions about whether a site is candidate for natural attenuation based on approaches that do not

consider the field experience or the literature to date.

## 1.4 Hypothesis and research objective

The research presented in this dissertation provides an insight into the current

discussion of natural attenuation for remediation and restoration of chlorinated solvent

contaminated aquifers. It has been emphasized that existing methodologies for

evaluating natural attenuation of chlorinated solvents should be replaced by approaches

considering the specific conditions of the site.

The hypothesis for this research is that at the Schoolcraft site reductive

dechlorination was the dominant mechanism responsible in the past for the reduction of

the contaminants; however it is no longer a major contributor to the natural attenuation

process occurring at this site. The specific objective of this research is to develop a

methodology for evaluating natural attenuation of chlorinated solvents considering the

hydrogeology, microbial processes, and geochemical processes linked to the historical

development of a contaminant plume. This will help to identify which of the natural

attenuation components is the current dominant mechanism and whether or not this

technology can be applied at this site

## 1.5 Scope of work

To accomplish the specific objective, the following approach was undertaken in

this research:

- Characterization of hydraulic parameters influencing transport and distribution of contaminants in the subsurface (Chapter 2)

- Characterization of natural attenuation processes based on geochemical parameters and contaminant concentration data (Chapter 3)

- Development of a conceptual and numerical model incorporating the hydrogeology, microbial processes, and geochemical processes linked to the contamination history of the aquifer under consideration (Chapter 4)

The case study for this research is a VOC contaminated aquifer located in Schloolcraft, MI. Past industrial and commercial activities have resulted in the development of a plume of chlorinated organic contamination extending approximately 2km from the suspected source of contamination.

## 1.6 Literature cited

Azadpour-Keeley, A., Keeley, J. W., Russell, H. H., and Sewell, G. W. (2001). "Monitored natural attenuation of contaminants in the subsurface: Processes." *Ground Water Monitoring and Remediation*, 21(2), 97-107.

Bouwer, E. J., and McCarty, P. L. (1983(a)). "Transformations of 1- and 2-carbon halogenated aliphatic organic compounds under methanogenic conditions." *Applied and Environmental Microbiology*, 45, 1286-1294.

Bouwer, E. J., and McCarty, P. L. (1983(b)). "Transformations of halogenated organic compounds under denitrifying conditions." *Applied and Environmental Microbiology*, 45, 1295-1299.

Bouwer, E. J., Rittman, B. E., and McCarty, P. L. (1981). "Anaerobic degradation of halogenated 1- and 2-carbon organic compounds." *Environmental Science & Technology*, 15(5), 596-599.

Clement, T. P., Truex, M. J., and Lee, P. (2002). "A case study for demonstrating the application of US EPA's monitored natural attenuation screening protocol at a hazardous waste site." *Journal of Contaminant Hydrology*, 59(1-2), 133-162.

Davis, J. W., Odom, J. M., DeWeerd, K. A., Stahl, D. A., Fishbain, S. S., West, R. J., Klecka, G. M., and DeCarolis, J. G. (2002). "Natural attenuation of chlorinated solvents at Area 6, Dover Air Force Base: characterization of microbial community structure." *Journal of Contaminant Hydrology*, 57(1-2), 41-59.

Dolfing, J. (2000). "Energetics of anaerobic degradation pathways of chlorinated aliphatic compounds." *Microbial Ecology*, 40(1), 2-7.

U.S. Environmental Protection Agency (EPA). (1998). "Technical protocol for evaluating natural attenuation of chlorinated solvents in groundwater." *EPA/600/R-98/128*, USEPA, Cincinnati, OH.

Ferguson, J. F., and Pietari, J. M. H. (2000). "Anaerobic transformations and bioremediation of chlorinated solvents." *Environmental Pollution*, 107(2), 209-215.

Fetzner, S. (1998). "Bacterial dehalogenation." *Applied Microbiology and Biotechnology*, 50(6), 633-657.

Freeze, R. A., and Cherry, J. A. (1979). *Goundwater*, Prentice Hall, Inc.

Holliger, C., and Schumacher, W. (1994). "Reductive dehalogenation as a respiratory process." *Antonie van Leeuwenhoek*, 66, 239-246.

Macdonald, J. A. (2000). "Evaluating natural attenuation for groundwater cleanup." *Environmental Science & Technology*, 34(15), 346A-353A.

Maymó-Gatell, X., Chien, Y., Gossett, J., and Zinder, S. (1997). "Isolation of a bacterium that reductively dechlorinates tetrachloroethene to ethene." *Science*, 276(6), 1568-1571.

McCarty, P. L. (1997). "Breathing with chlorinated solvents." *Science*, 166, 1521-1522.

Ndon, U. J., Randall, A. A., and Khouri, T. Z. (2000). "Reductive dechlorination of tetrachloroethylene by soil sulfate-reducing microbes under various electron donor conditions." *Environmental Monitoring and Assessment*, 60(3), 329-336.

NRC. (2000). *Natural attenuation for groundwater remediation*, National Academy Press, Washington, D.C.

Nyer, E. K., and Duffin, M. E. (1997). "The state of the art bioremediation." *Ground Water Monitoring and Remediation*, 2, 64-69.

Prakash, B., and Gupta, S. K. (2000). "Effect of carbon source on PCE dehalogenation." *Journal of Environmental Engineering*, 126(7), 622-628.

Röling, W. F. M., and van Verseveld, H. W. (2002). "Natural attenuation: What does the subsurface have in store?" *Biodegradation*, 13(1), 53-64.

Sims, J. L., Suflita, J. M., and Russell, H. H. (1991). "Reductive dehalogenation of organic contaminants in soils and ground water." EPA Ground Water Issue.

Swett, G. H., and Rapaport, D. (1998). "Natural Attenuation: Is the Fit Right?" *Chemical Engineering Progress*, 94, 37-43.

Vogel, T. M., Criddle, C., and McCarty, P. L. (1987). "Transformation of halogenated aliphatic compounds." *Environmental Science & Technology*, 21, 722-736.

Vogel, T. M., and McCarty, P. L. (1987). "Abiotic and biotic transformation of 1,1,1-trichloroethane under methanogenic conditions." *Environmental Science & Technology*, 21, 1208-1213.

Wiedemeier, T. H., Wilson, J. T., and Kampbell, D. H. "Natural Attenuation of Chlorinated Aliphatic Hydrocarbons at Plattsburgh Air Force Base, New York." *Proceedings of the Symposium on Natural Attenuation of Chlorinated Organics in Ground Water*, 76-84.

Witt, M. E., Klecka, G. M., Lutz, E. J., Ei, T. A., Grosso, N. R., and Chapelle, F. H. (2002). "Natural attenuation of chlorinated solvents at Area 6, Dover Air Force Base: groundwater biogeochemistry." *Journal of Contaminant Hydrology*, 57(1-2), 61-80.

# CHAPTER 2

# HYDROGEOLOGIC CHARACTERIZATION OF A
# VOC CONTAMINATED AQUIFER ZONE

## 2.1 Abstract

A methodology that couples laboratory and field data with numerical optimization methods was developed to estimate aquifer physical parameters that influence distribution and migration of contaminants. Hydraulic conductivity, porosity, and tracer test data were used to characterize an aquifer zone contaminated with VOC using an optimization method for solving the generalized groundwater flow and transport equations. Based on the results a strong correlation between laboratory and field determined hydraulic conductivity was found. These tests revealed the presence of high conductivity zones that act as preferential contaminant pathways. Hydraulic conductivity values for these zones are in the range of $10^{-1}$ to 1cm/s. Based on the optimization technique, simulated depth-specific average linear velocities agreed reasonably well with observed tracer velocities. A simulated average linear velocity of 98.4 cm/day was found for the fastest zone in this aquifer, a value two times higher than the velocity at the slowest depth interval. Sensitivity analysis using the root mean square errors (RSME) showed that a 10% change in porosity field yielded a 25% average linear velocity deviation from optimal values. Although length scale dependency of longitudinal dispersivity was not taken into account, a single value per depth interval described tracer distribution reasonably well. This methodology can be used to characterize aquifer zones intended to be use for engineered remediation purposes.

17

## 2.2 Introduction

The physical characteristics composing the aquifer matrix exert a profound influence on the movement and distribution of chemical compounds in groundwater. It is widely accepted that transport of contaminants migrating to the saturated zone of an aquifer occur through high energy or less resistant stratigraphic units (Hyndman *et al.* 2000b; Lee *et al.* 2001). Therefore, study of the fate and transport of pollutants in a contaminated site must incorporate a detailed hydraulic characterization. Moreover, if an assessment of a contaminated site is being conducted, sufficient site-specific data is necessary to develop reliable numerical models that incorporate the heterogeneous nature of subsurface environments. This is critically important if numerical models are going to be used for predicting the future extent of contaminant migration (Wiedemeier *et al.* 1998). Among the many physical properties of geologic units that influence subsurface contaminant migration, the most important are hydraulic conductivity, porosity, and dispersivity. These parameters are strongly correlated to the heterogeneous nature of the aquifer matrix.

Field and laboratory methods have been developed to estimate these parameters. Hyndman *et al.* (1994) developed a theoretical algorithm, which combines field data from cross-well tomograms with tracer concentration tests to estimate transport parameters of lithologic zones in two dimensions. That methodology was further expanded and applied to a field site to estimate properties in three dimensions (Hyndman and Gorelick 1996; Hyndman *et al.* 2000b). Cho *et al.* (2000) developed a field procedure to measure vertical profiles of hydraulic conductivity using direct push methods. They identified small-scale variations in hydraulic conductivity that would have not been detected by

laboratory or conventional field methods. A similar procedure was used at a BTEX contaminated site to estimate the role of small-scale heterogeneities upon contaminant distribution (Hurt *et al.* 2001). Concentrations of BTEX compounds were highly underestimated when variations in parameters such as hydraulic conductivity and porosity were not properly measured in the field.

In the laboratory, several assays have been developed to estimate hydraulic conductivity, porosity, and dispersivity from core samples (Freeze and Cherry 1979). Although it has been recognized that it is unlikely to reproduce field conditions, a good indication of approximate values of transport parameters can be obtained with well designed laboratory experiments.

The objective of this study is to develop and test a methodology to quantify heterogeneities and physical properties of an aquifer region contaminated with volatile organic compounds. The main goal is to identify small-scale heterogeneities that influence the migration and distribution of contaminants in an unconfined aquifer. For this purpose, a series of laboratory and field tests coupled with numerical groundwater flow and transport models were developed to estimate hydraulic conductivity, porosity, and optimal depth-specific dispersivity values within the region.

## 2.3 Site description

The Village of Schoolcraft is a small rural community located approximately 16 km south of Kalamazoo, MI, USA (Figure 2.1). The unconfined aquifer underneath the village has been contaminated with organic and metal compounds as result of previous industrial and commercial activities in the village. Regional and local hydrogeologic

study area

VOC Plume (G)

SCALE IN METERS

0    300    600
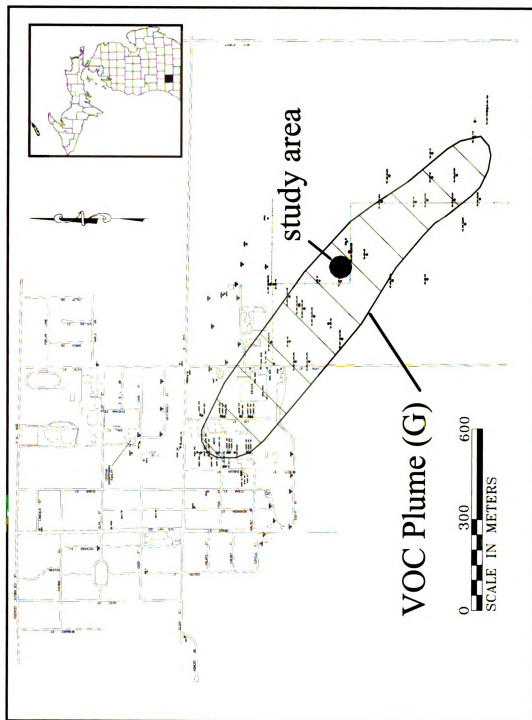
Figure 2.1. Location of study area.

conditions have been described elsewhere (Lipinski 2002; Dybas *et al.* 1998; Mayotte *et al.* 1996). The focus of this investigation is an area where a pilot scale study is being conducted to evaluate the feasibility of remediating a volatile organic compound plume in this aquifer (Figure 2.1).

Currently, bioremediation and natural attenuation studies are being conducted on-site to evaluate the potential of using a combined treatment strategy to reduce concentration of organic compounds to acceptable levels. For this purpose, two "side-by-side" delivery and monitoring well networks have been drilled approximately in the plume's center of mass (Figure 2.2). The purpose of the study on the north well network, i.e. stimulation grid, is to stimulate the native microbial flora to degrade VOC contaminants. Bioaugmentation effects on contaminant degradation are being evaluated on the south well network, i.e. the augmentation grid (Figure 2.2).

## 2.4 Methods

*Hydraulic conductivity and porosity tests*

To estimate depth-specific values of hydraulic conductivity and porosity, soil cores from 9m to 24.3m below ground surface (bgs) (in 1.5m intervals) were collected from monitoring well locations using the Waterloo cohesionless continuous sand sampler method (Dybas *et al.* 1998). These cores were visually inspected in the laboratory using the *ASTM Standard D2488-00 Practice for Description and Identification of Soils (Visual Manual Procedure)* to determine relative grain size distribution of the glaciofluvial sediments composing the unconfined aquifer. Cores from pump wells (9 – 24.3 m bgs) were inspected on-site since they were extracted in approximately 6 meter intervals and

21
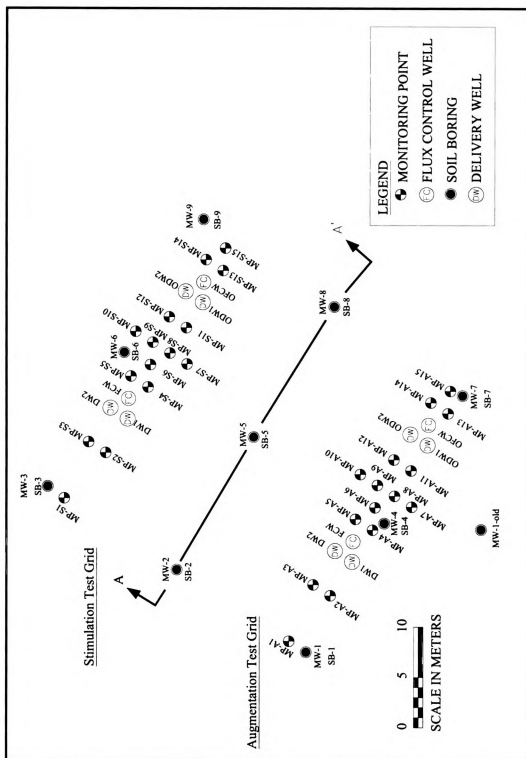
Figure 2.2. Well network in study area (stimulation and augmentation grids).

undisturbed transport to the laboratory was not possible. The Rotosonic drilling method (Lewis 2001) was used for those holes. Boring logs for all monitoring and pumping wells are given in Appendix I.

After visually classifying the cores, approximately 250 sediment samples were collected for hydraulic conductivity and porosity tests. A constant head permeameter apparatus was used to estimate the hydraulic conductivity of repacked soil samples (Hoard 2002). Bail tests were also performed on selected wells in the field screened at different depths to evaluate the accuracy of laboratory methods. The methods of Hvorslev (1951) and Bower and Rice (1976) were used.

The following equation was used to estimate the total porosity of sediment samples:

$$\phi = 1 - \frac{\rho_b}{\rho_s} \qquad (2.1)$$

where $\phi$ is the porosity; $\rho_b$ is the bulk mass density of the sample [$M \cdot L^{-3}$]; and $\rho_s$ is the particle mass density [$M \cdot L^{-3}$] (Freeze and Cherry 1979).

*Field tracer tests*

Field tracer tests were conducted on the augmentation and stimulation well networks to estimate flow and transport parameters that influence distribution of solutes within this aquifer section. The main objective of these experiments was to study the impacts that the stratigraphy exert upon contaminant migration and distribution in this region.

**Table 2.1. Details of tracer experiments.**

| Solute | Parameter value | Description[*] |
|---|---|---|
| Bromide | | *Tracer injected into DW's by* |
| injected concentration (t=0) | *100 ppm* | *pumping water from FCW's,* |
| injection into | *DWA1-DWA2* | *adding the solute to the* |
| pumping rate | $1.3 x 10^{-3} m^3/s$ *(each well)* | *pumped water and injecting it* |
| pumping time | *4 hrs* | *back into DW's.* |
| | | |
| Fluorescein | | *Same as Bromide injection.* |
| injected concentration (t=0) | *100 ppb* | |
| injected into | *DWA1-DWA2, DWS1-* | |
| pumping rate | *DWS2* | |
| pumping time | $1.3 x 10^{-3} m^3/s$ *(each well)* | |
| | *4 hrs* | |

[*] see Figure 2.2 for well notation

Fluorescein and bromide tracers were chosen because experiments have shown they are relatively conservative tracers, do not sorb to soil particles, do not affect bacterial activity, and are very easy to detect (Hyndman *et al.* 2000a). An "injection-extraction" strategy was used to deliver tracer solution to the saturated zone of the aquifer. To achieve uniform tracer delivery in the geologic formation, a 4hr injection time was chosen since preliminary numerical models predicted an approximate 80% tracer breakthrough in the extraction well at the end of the pumping period. The screened interval for the extraction and injection wells in the network is between 18.3 to 25.0m bgs. Details of the field tracer experiments are provided in Table 2.1.

Samples for tracer measurement were taken at downgradient multi-level piezometers at time and depth intervals specified in Table 2.2. A bromide electrode (Cole-Parmer) and a digital field fluorometer (Model 10-005-CE Turner Designs Inc.) were used to measure bromide and fluorescein concentrations in collected samples, respectively.

**Table 2.2. Logistics of tracer tests.**

| Sampled wells | Interval Sampled[*] (m bgs) | Sampling time (days after tracer injection) |
|---|---|---|
| **Augmentation well network** | | |
| *Bromide Tracer Test* | | |
| *MPA4 – MPA6* | *16.8 to 24.1* | *7* |
| *MPA7* | *16.8 to 24.1* | *8, 14, 15* |
| *MPA8 – MPA9* | *15.8 to 24.1* | *8, 12, 14, 15* |
| *MPA10* | *16.8 to 24.1* | *8* |
| *MPA11* | *16.8 to 24.1* | *12, 14, 15* |
| *MPA12* | *16.8 to 24.1* | *12, 14* |
| | | |
| *Fluorescein Tracer Test* | | |
| *MPA4 – MPA5* | *16.8 to 24.1* | *1-4, 6-8, 10, 14* |
| *MPA6* | *16.8 to 24.1* | *3, 4, 6-8, 10, 14* |
| *MPA7 – MPA10* | *15.8 to 24.1* | *8, 10, 14, 17, 22, 24, 27, 30* |
| *MPA11 – MPA12* | *16.8 to 24.1* | *8, 10, 14, 17, 22, 24, 27, 30* |
| **Stimulation well network** | | |
| *Fluorescein Tracer Test* | | |
| *MPA7 – MPA10* | *17.1 to 24.4* | *7, 9, 12, 15* |
| *MPA11 – MPA15* | *18.0 to 24.1* | *7, 9, 12, 15* |

[*]All multi-level wells consist of multiple 15.3cm screens spaced at 0.9 m intervals

*Conceptual and numerical models*

A conceptual model for this site was constructed to develop an understanding of the important features that affect solute transport within this region. A northwest-southeast cross section through the site (Figure 2.3) shows the main geologic features of the region. Groundwater flow in the vicinity is from northwest to southeast at an average velocity of 15cm/day (Dybas *et al.* 2002; Mayotte *et al.* 1996) and recharge for this area is approximately 23.7cm/yr. Pertinent boundary conditions were assigned based on a regional-scale model constructed by Lipinsky (2002). Figure 2.4 shows the boundaries for the regional aquifer which control groundwater flow in the study area.
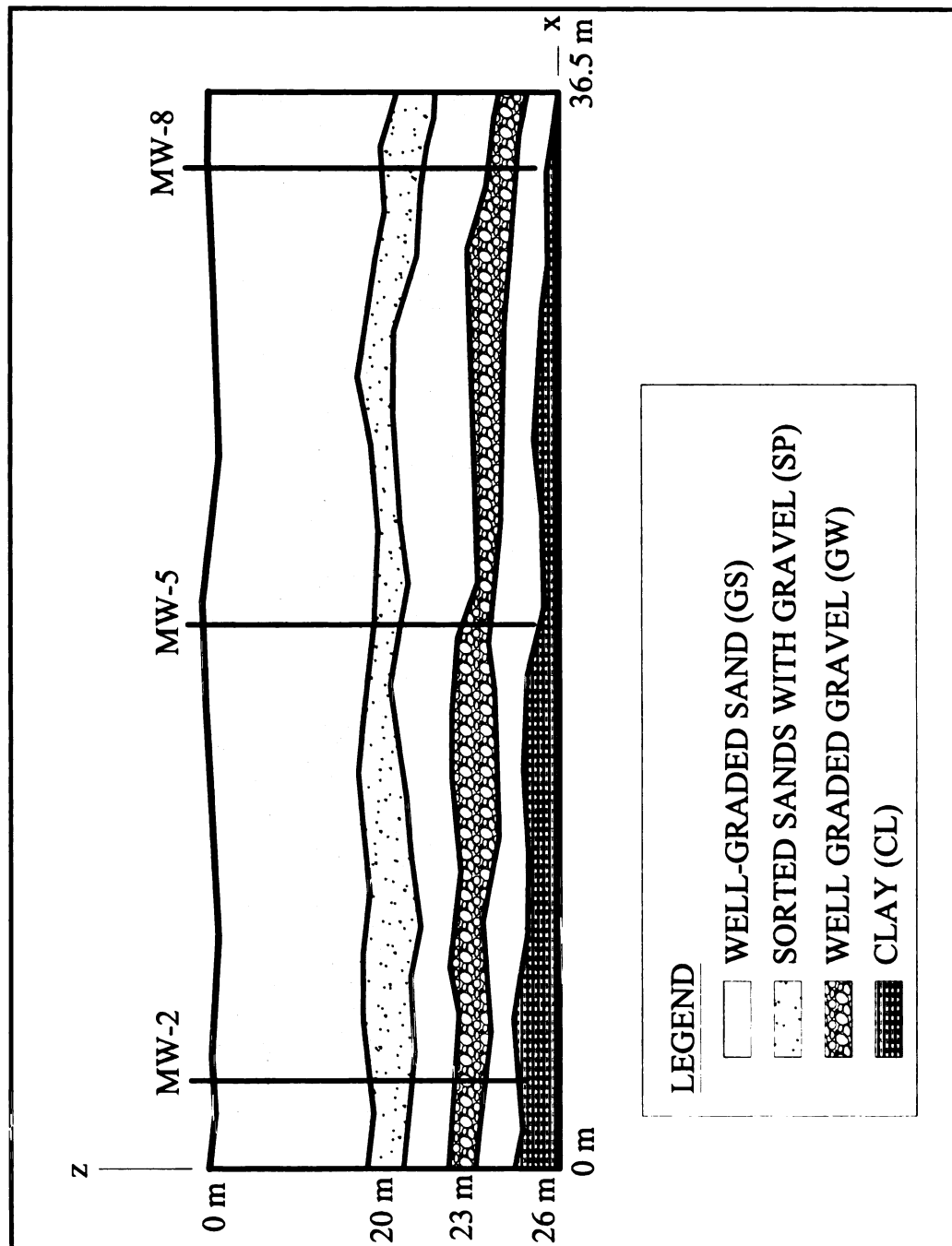
Figure 2.3. Cross section A-A' (Figure 2.2) through monitoring wells MW-2, MW-5, and MW-8.

LEGEND

☐ WELL-GRADED SAND (GS)
▦ SORTED SANDS WITH GRAVEL (SP)
○ WELL GRADED GRAVEL (GW)
▓ CLAY (CL)
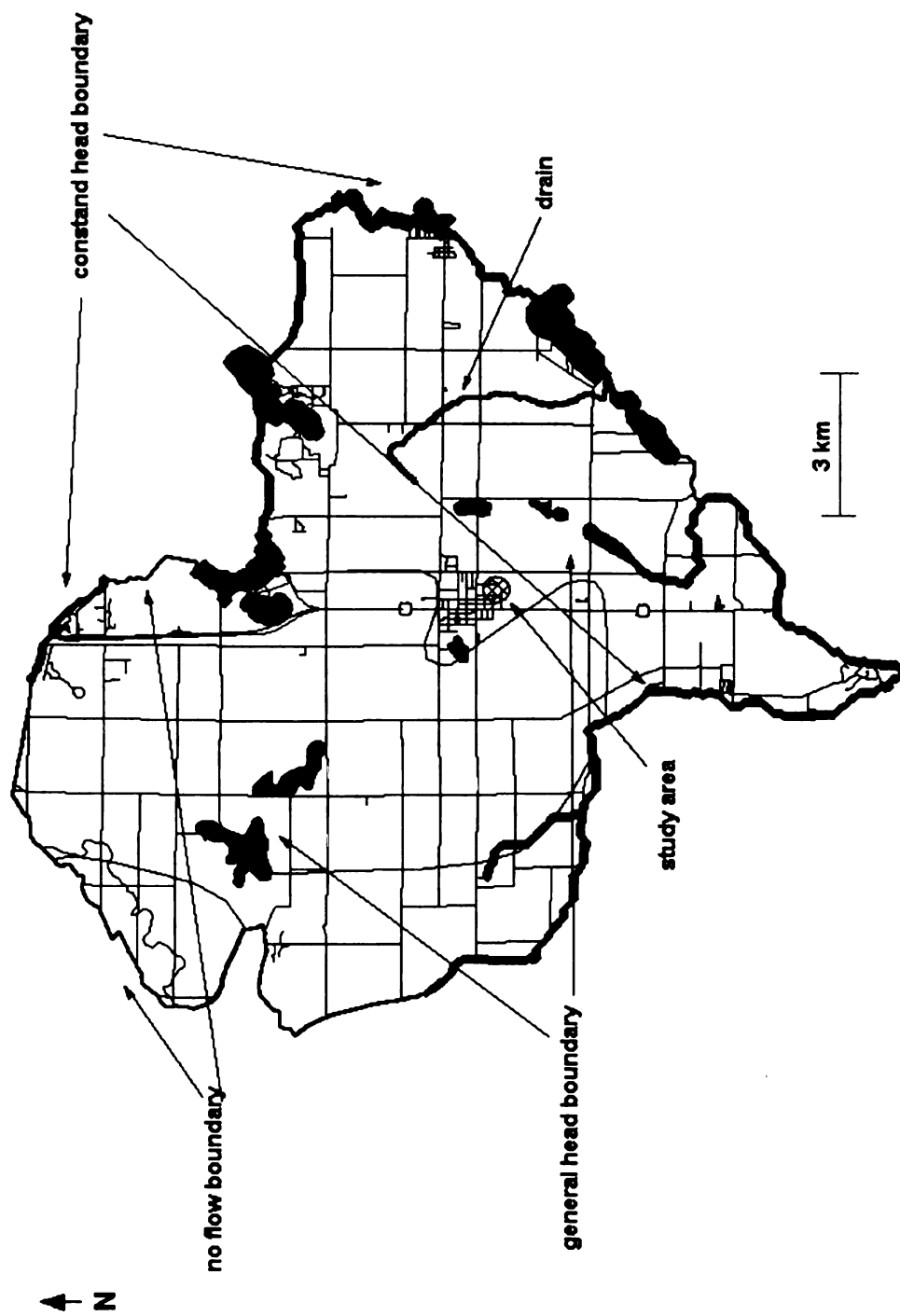
Figure 2.4. Main features that control regional groundwater flow in the unconfined aquifer (from Lipinski, 2002).

Information compiled from the conceptual model was incorporated into a three dimensional numerical groundwater flow and transport model. The objective for this experiment was to understand the influence of local heterogeneities on solute distribution in this region. By analyzing vertical profiles of tracer concentration a quantitative description of those heterogeneities can be obtained.

A three dimensional finite difference grid was constructed by telescopic mesh refinement (Anderson and Woessner 1992) from the numerical regional groundwater flow model of Lipinski (2002). The horizontal resolution of the grid was 15cm in both, longitudinal and transverse direction. Vertical resolution of the grid varied from 90cm at the bottom of the aquifer to 620cm at the top resulting in 15 model layers. This grid discretization was adequate to represent the physical resolution of the monitoring well networks on the site while minimizing artificial dispersion effects. Local boundary conditions were determined based on the regional groundwater flow model. Figure 2.5 shows the numerical model grid in horizontal and vertical directions.

Groundwater flow was simulated using the classical mathematical expression from Bear (1979):

$$\nabla \bullet (\mathbf{K} \bullet \nabla h) + W = S_y \frac{\partial h}{\partial t} \qquad (2.2)$$

where $\nabla$ is the gradient operator ($\partial/\partial x$, $\partial/\partial y$, $\partial/\partial z$); x, y, z, are spatial coordinates [L]; $\mathbf{K}$ is the hydraulic conductivity tensor [L·T$^{-1}$]; h is the hydraulic head [L]; W is the fluid source sink term [L·T$^{-1}$]; $S_y$ is the specific aquifer yield; and t is the time [T].
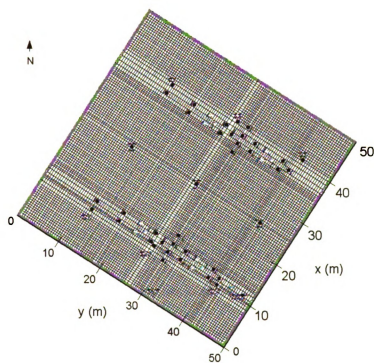
(a)
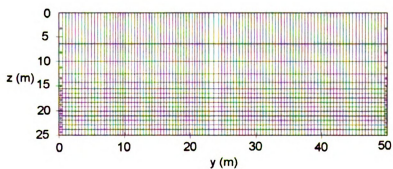


(b)

Figure 2.5. Numerical model grid in (a) horizontal, and (b) vertical directions. (No. of cells in the horizontal is 52,890, with 15 layers in the vertical direction.

This equation was coupled to the advection-dispersion equations for simulating tracer transport:

$$\frac{\partial c}{\partial t} = \nabla \bullet (\mathbf{D}\nabla c) - \nabla(\mathbf{v} \bullet c) + \frac{c'W}{\phi_e} \qquad (2.3a)$$

$$\mathbf{v} = -\frac{\mathbf{K}}{\phi_e}\nabla h \qquad (2.3b)$$

where c is the tracer concentration in pore fluid [$M \cdot L^{-3}$]; $\mathbf{v}$ is the groundwater velocity vector [$L \cdot T^{-1}$]; c' is the tracer concentration in source or sink [$M \cdot L^{-3}$]; $\phi_e$ is the effective porosity; and $\mathbf{D}$ is the hydrodynamic dispersion coefficient tensor [$L^2 \cdot T^{-1}$] with coefficients $\alpha \cdot \mathbf{v}$, where $\alpha$ is the dispersivity vector [L].

Equations 2.2 and 2.3 were solved numerically using MODFLOW (McDonald and Harbaugh 1988) and MT3DMS (Zheng and Wang 1999), respectively. For the flow model, hydraulic conductivity and porosity data obtained from field and laboratory analysis were kriged to the 3-D finite difference grid. Two stress periods were simulated: 1) 4 hr of tracer injection followed by; 2) 29.83 days of tracer transport under natural gradient influence, for a total simulation time of 30 days.

A constrained optimization method was developed to solve the objective function (Equation 2.4) and find a set of optimal dispersivity values for the geologic formation.

$$f(\alpha) = \sum_{i=1}^{N}\frac{\lambda(\alpha_i)}{\lambda_o(\alpha_i)} \qquad (2.4)$$

30

In the previous equation i is the index for the dispersivity at a particular depth; $N$ are depths at which tracer data was collected in monitoring wells; and the $\lambda$ operator is given by:

$$\lambda(\alpha_i) = \sum_{m=1}^{M} \left[ \left( \int_0^t \frac{|c_{obs} - c_{sim}|}{c_{obs}} dt \right)_i \right]_m \tag{2.5}$$

where the integral represents normalized absolute differences between observed ($c_{obs}$) and simulated ($c_{sim}$) tracer concentrations over the entire simulation time t, for depth interval i; and the summation is over all multi-level piezometers M, located at depth interval i. Simulated tracer concentrations in Equation 2.5 are given by Equation 2.3. The denominator ($\lambda_0$) in Equation 2.4 is the operator evaluated at an initial set of dispersivity values.

The objective function (Equation 2.4) was minimized by solving a set of generalized Kuhn-Tucker equations (Phanikumar *et al.* 2002). Methods for solving these equations are available in many programming packages. The sequential quadratic methods in MATLAB Optimization Toolbox (Coleman *et al.* 1999) were used in this study. The MATLAB script for this optimization is provided in Appendix II.

Depth intervals included in the objective function (Equation 2.4) were 18.6, 19.5, 20.4, 21.3, 22.3, and 23.2m bgs. Multi-level piezometers at 15.8, 16.8, and 17.7 were not included because tracer was not detected at any of these depths. This was expected since the screen top of injection wells is at 18.3m bgs. Also, piezometers with insignificant

31

tracer concentration were excluded in the formulation of Equation 2.5.

## 2.5 Results and discussion

*Hydraulic conductivity and porosity*

Figure 2.3 shows the main features found during the visual classification analysis.

Material from shallower depths (0 ~ 10m bgs) of this aquifer is mostly fine sand

changing to medium sand as one moves deeper into the formation. From 10m bgs to

approximately 18m bgs the aquifer is composed of medium to coarse sands. A layer of

poorly sorted sands with gravel and cobbles was identified at an average depth of 19m in

most of the cores. The thickness of this layer varies from 0.5m to about 1.0m. The

underlain sediments changed again to a mixture of coarse and medium sands with an

approximate thickness of 3m. A second layer of coarse material at an approximate depth

of 23m bgs was apparent from the analysis. Well graded gravels with a significant

amount of coarse gravel (40mm average diameter) were the principal materials of this

second layer. Thickness of this layer is approximately 1.2m on the average. Below this

material, a medium to coarse sand layer was deposited. Cobbles of significant size (~

100mm) were found interbedded within this layer. Hard, gray clay was found

approximately at 24.5m bgs in soil cores from MW1 to MW3. Apparently, this clayey

layer gradually slopes downward as evidenced by the location (25.9m bgs) at which clay

was found in cores from wells located at the southeast boundary of the network.

Based on the visual classification, it is evident that distinct stratigraphic units

(may act as preferential flow paths for contaminant migration) exist at average depths of

20 and 23m bgs. The extent of these layers; however, cannot be predicted since cores

were taken in a relatively small area compared to the entire extension of the VOC plume

(Figure 2.1). In a study by Dybas *et al.* (2002), cores from a location approximately

1.8km north of this site showed the underlying unconfined aquifer to be composed mostly

of medium sands.

Figure 2.6 and Table 2.3 show hydraulic conductivity results from laboratory

permeameter and field bail tests, respectively. Laboratory determined hydraulic

conductivity ranged from $1 \times 10^{-3}$ to $4 \times 10^{-1}$ cm/s with an average of $6.6 \times 10^{-2}$ cm/s and a

standard deviation of 0.066cm/s. The scatter plot in Figure 2.6(a) shows that between 5

to about 15m bgs hydraulic conductivity is in the range of $10^{-3}$ to $10^{-1.5}$ cm/s. Data is

clustered around $10^{-1.5}$ to 1cm/s below the 15m bgs interval.

Bail test results (Table 2.3) showed that values obtained by the Hvorslev method

were, in general, an order of magnitude higher than hydraulic conductivity obtained by

the Bower and Rice method. However, these values are within the expected range of

hydraulic conductivity for glacial outwash sediments (Fetter 2001). Laboratory measured

hydraulic conductivity correlated well to field values obtained by the Hvorslev (1951)

method.

A total porosity scatter plot from laboratory repacked samples is shown in Figure

2.6(b). Average total porosity was 0.331 with a standard deviation around the mean of

0.050. Maximum and minimum values were 0.504 and 0.208, respectively. Total

porosity of shallower sediments seems to be around 10% lower than deepest ones. From

Figure 2.6 an inverse correlation between hydraulic conductivity and total porosity can be

observed. A similar pattern was also reported in the study conducted by Hoard (2002).
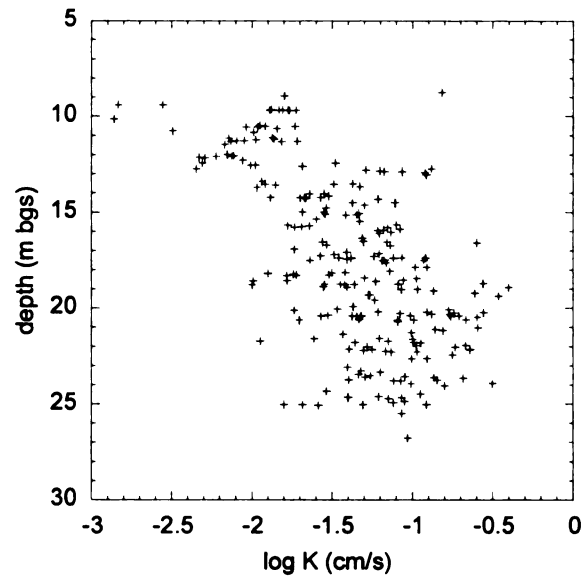
(a)
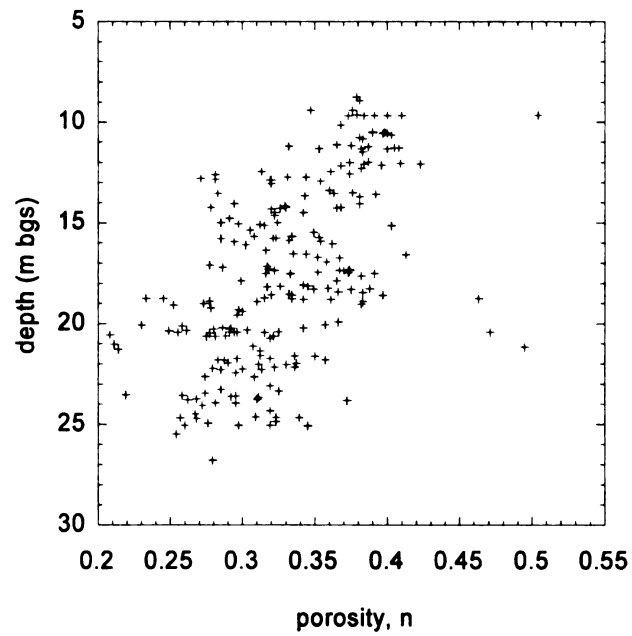


(b)

Figure 2.6. Scatter plots of (a) hydraulic conductivity and (b) porosity.

**Table 2.3. Bail test results.**

| Well id[a] | Screen depth (m bgs) | K (cm/s)[b] Bower and Rice (1976) | K (cm/s)[b] Hvorslev (1951) |
|---|---|---|---|
| MP-A2 | 23.8 – 24.4 | $2.9 \times 10^{-2}$ [d] | $1.58 \times 10^{-1}$ [d] |
| MP-A15 | 23.8 – 24.4 | $4.02 \times 10^{-2} \pm 0.001$ | $2.21 \times 10^{-1} \pm 0.008$ |
| MP-A6[c] | 22.3 – 22.9 | $4.30 \times 10^{-2} \pm 0.017$ | $2.35 \times 10^{-1} \pm 0.091$ |
| MP-S3 | 24.4 – 25.0 | $3.28 \times 10^{-2} \pm 0.004$ | $1.82 \times 10^{-1} \pm 0.021$ |
| MP-S15 | 24.4 – 25.0 | $3.15 \times 10^{-2} \pm 0.004$ | $1.72 \times 10^{-1} \pm 0.023$ |
| MP-S6[c] | 22.9 – 23.5 | $8.32 \times 10^{-2} \pm 0.027$ | $4.54 \times 10^{-1} \pm 0.146$ |
| MSU-1 | 19.2 – 19.8 | $4.11 \times 10^{-2} \pm 0.016$ | $2.25 \times 10^{-1} \pm 0.089$ |

[a] see Figure 2.2 for well location

[b] average value ± one standard deviation

[c] measurements taken on a nearby well not identified in Figure 2.2

[d] average of two bail tests; standard deviations not calculated

To incorporate hydraulic conductivity to the flow and transport model a statistical analysis of the data was performed. A log K histogram analysis showed this data to be approximately normally distributed (Figure 2.7(a)). Vertical anisotropy in this geologic formation was evident from the variogram analysis shown in Figure 2.7(b). From this analysis, horizontal and vertical correlation lengths were 18.2 m and 4.4 m, respectively. A variance at zero separation distance of $0.03 \text{cm}^2/\text{s}^2$ was found, with a log K variance of $0.13 \text{cm}^2/\text{s}^2$. These results were similar to the findings of Hyndman *et al.* (2000), and Hoard (2002).

An exponential variogram model with parameters from the experimental variograms was used to krig hydraulic conductivity data to the numerical model grid. A similar procedure was used for porosity data. Cross section images of log K and porosity are shown in Figure 2.8. High K areas in the image at approximate depths of 20m bgs and 24m bgs were found to correlate well with the two layers of coarse material identified in the conceptual model. These high K zones might act as preferential pathways for contaminant migration in this aquifer.

35
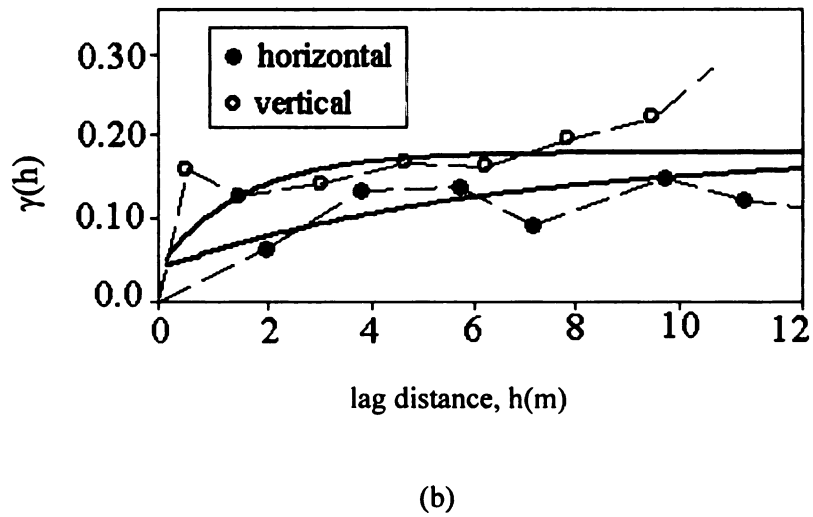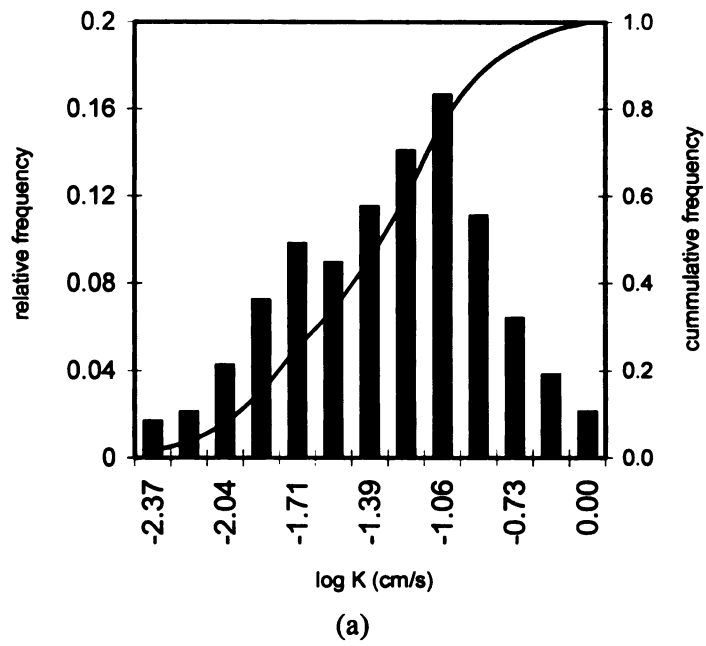
Figure 2.7. (a) log K frequency distribution, and (b) experimental and model variograms of the data.
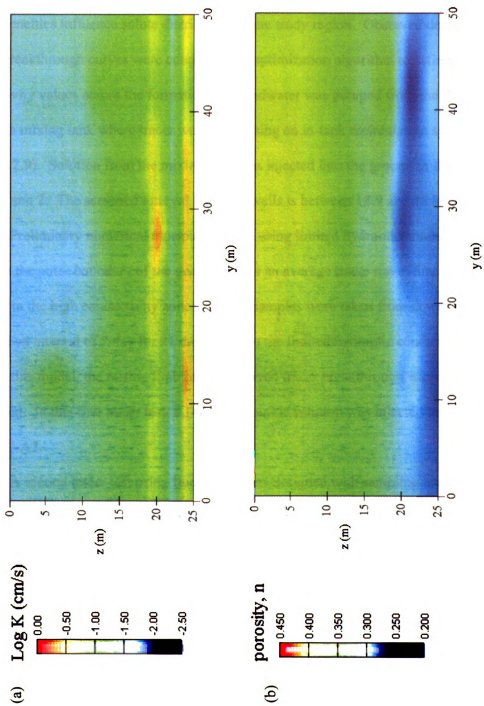
Figure 2.8. Kriged Images of (a) Log K, and (b) total porosity.

*Tracer tests and Numerical models*

A series of tracer tests were conducted to test the hypothesis that local heterogeneities influence solute distribution in the study region. Observed depth-specific tracer breakthrough curves were coupled to an optimization algorithm to estimate dispersivity values across the formation. Groundwater was pumped from the flux control well to a mixing tank where tracer was added using an in-tank recirculation system (Figure 2.9). Solution from the mixing tank was injected into the ground in delivery wells 1 and 2. The screened interval for these wells is between 18.9 and 25.0m bgs.

Preliminary numerical transport models using limited hydraulic conductivity from wells in the outer boundary of the grid predicted an average tracer travel time of 3.5 days/m in the high conductivity zones. Tracer samples were taken from downgradient wells at an interval of 7 day for 21 days. Due to the limited hydraulic conductivity data used in this model, the raising limb of the observed tracer breakthrough was not properly described. In this first tracer test, a 140ppm bromide solution was injected into DW-A1 and DW-A2.

A second tracer test using fluorescein was designed with sampling intervals of 1 and 2 days. Figure 2.10(a) and 2.10(b) show breakthrough curves during tracer injection at the flux control and delivery wells, respectively. Hydraulic conductivity results from sediment samples of monitoring and delivery wells were incorporated into the flow and transport model and simulation results validated field observations reasonably well. Based on these results, about 60% tracer breakthrough occurred in the flux control after 170min of pumping time. Tracer breakthrough at delivery wells reached a maximum relative concentration ($C/C_0$) of 1.8 at 4hr of pumping. Relative concentration in delivery
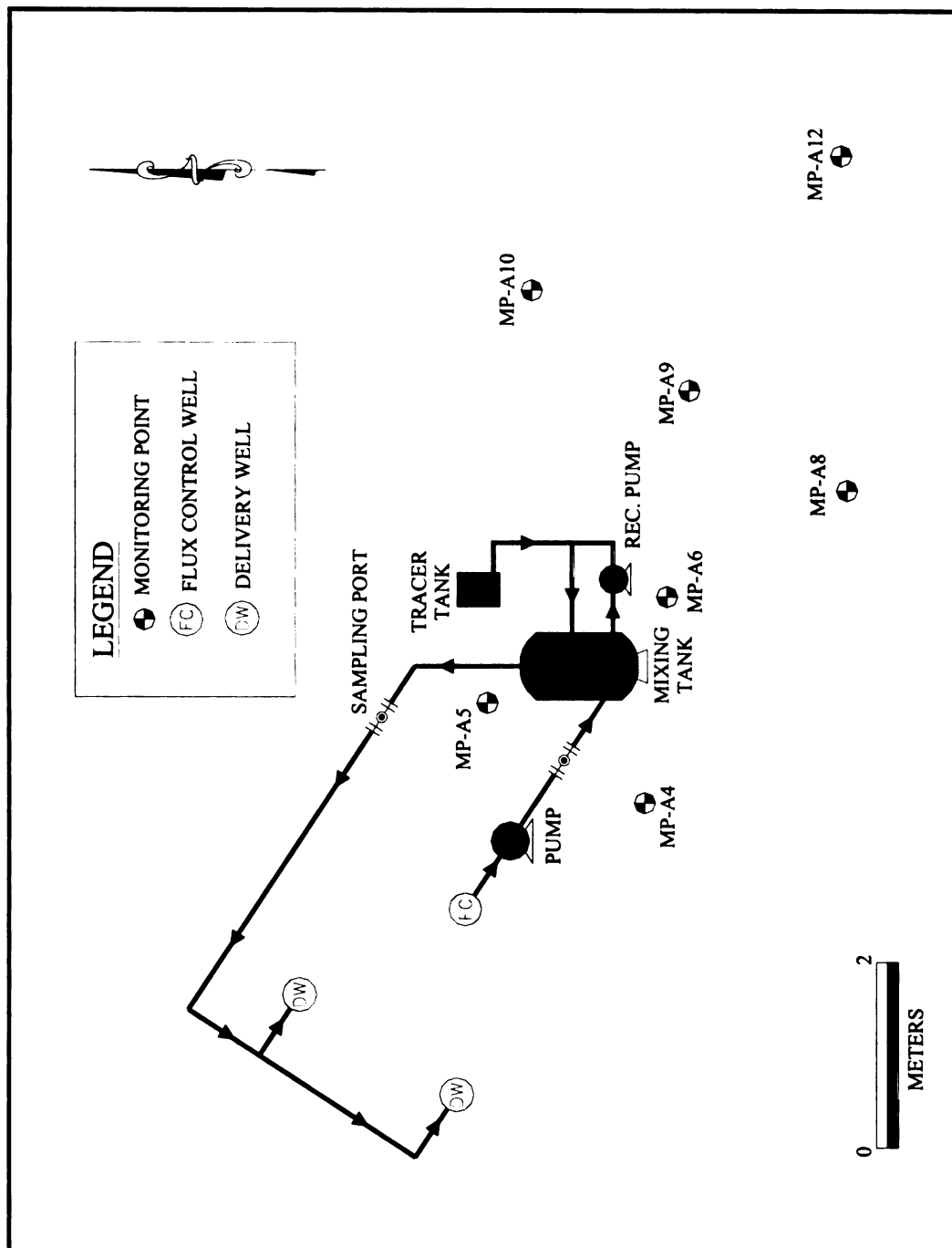
Figure 2.9. Layout of the tracer injection system.

39
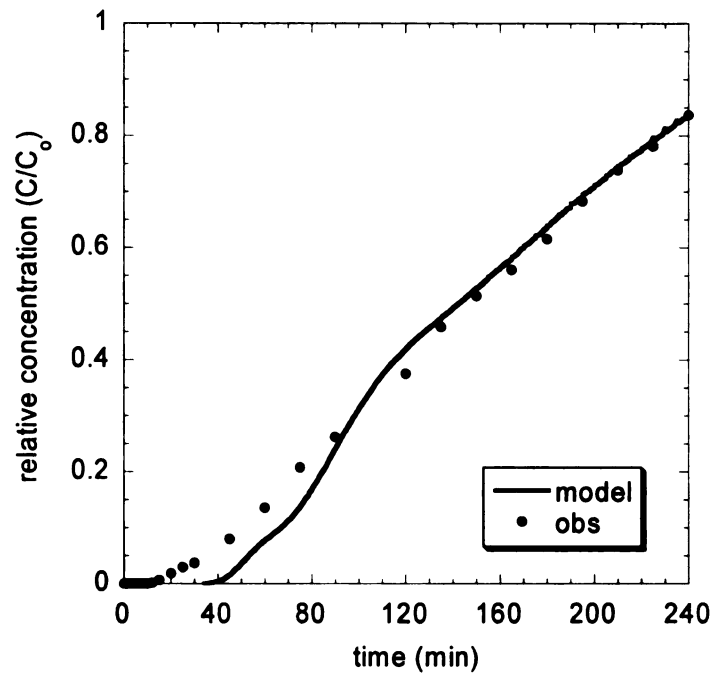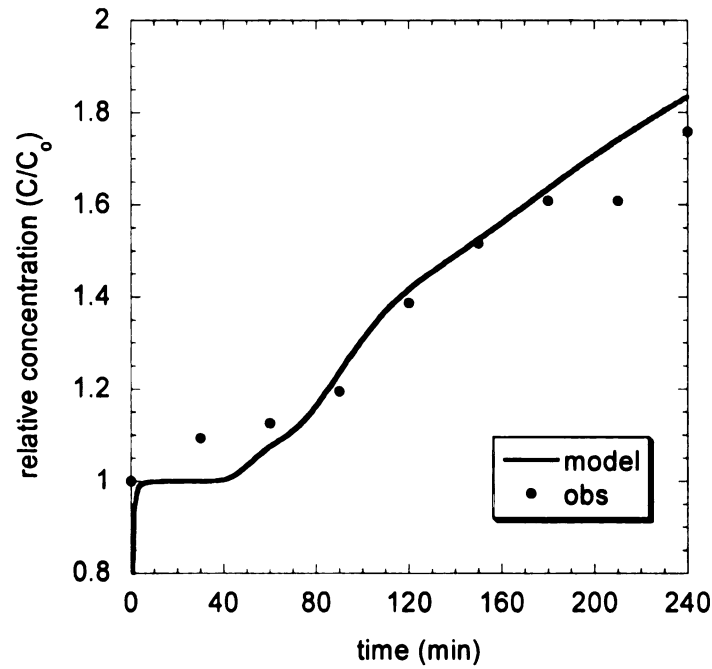
Figure 2.10. Tracer breakthrough curves at (a) flux control well,
and (b) delivery wells.

wells are greater than 1 as soon as tracer breaks through in the flux control well. When this condition occurs, the injected concentration will increase by the relative concentration coming from the flux control well. To model this recirculation system in MT3DMS (Zheng and Wang 1999) a series of additions and modifications were made to the main code and subroutines. Breakthrough results indicate that at least 2.7hrs of pump time at a rate of $2.6\times10^{-3}m^3/s$ is required in order to create a uniform solute distribution region across the well screens.

Heterogeneity effects upon tracer distribution could not be evaluated during tracer injection due to strong hydraulic gradients induced by pump operation. Dispersion effects were more evident during transport under natural gradient conditions.

Two scenarios were simulated with the optimization approach described by Equations 2.4 and 2.5. In the first scenario, depth-specific dispersivity values were estimated. During the second scenario, only one value of dispersivity was used by assuming that a single value was enough to describe the differences seen in tracer breakthrough curves.

Tracer breakthrough curves for the optimized per-layer dispersivity and the grid optimal dispersivity scenarios along with observed data are shown in Figure 2.11. Breakthrough curves obtained in the optimum per-layer scenario closely matched observed tracer concentration for some depth intervals in monitoring points A4 and A5. Dispersivity values assigned on a per-layer basis seems a better representation than a single dispersivity value for the entire model domain. Although dispersivity is a length dependent parameter (Kim *et al.* 2002), one value per model layer was adequate for this simulation. Peak arrival times for the per-layer simulation scenario and observed data
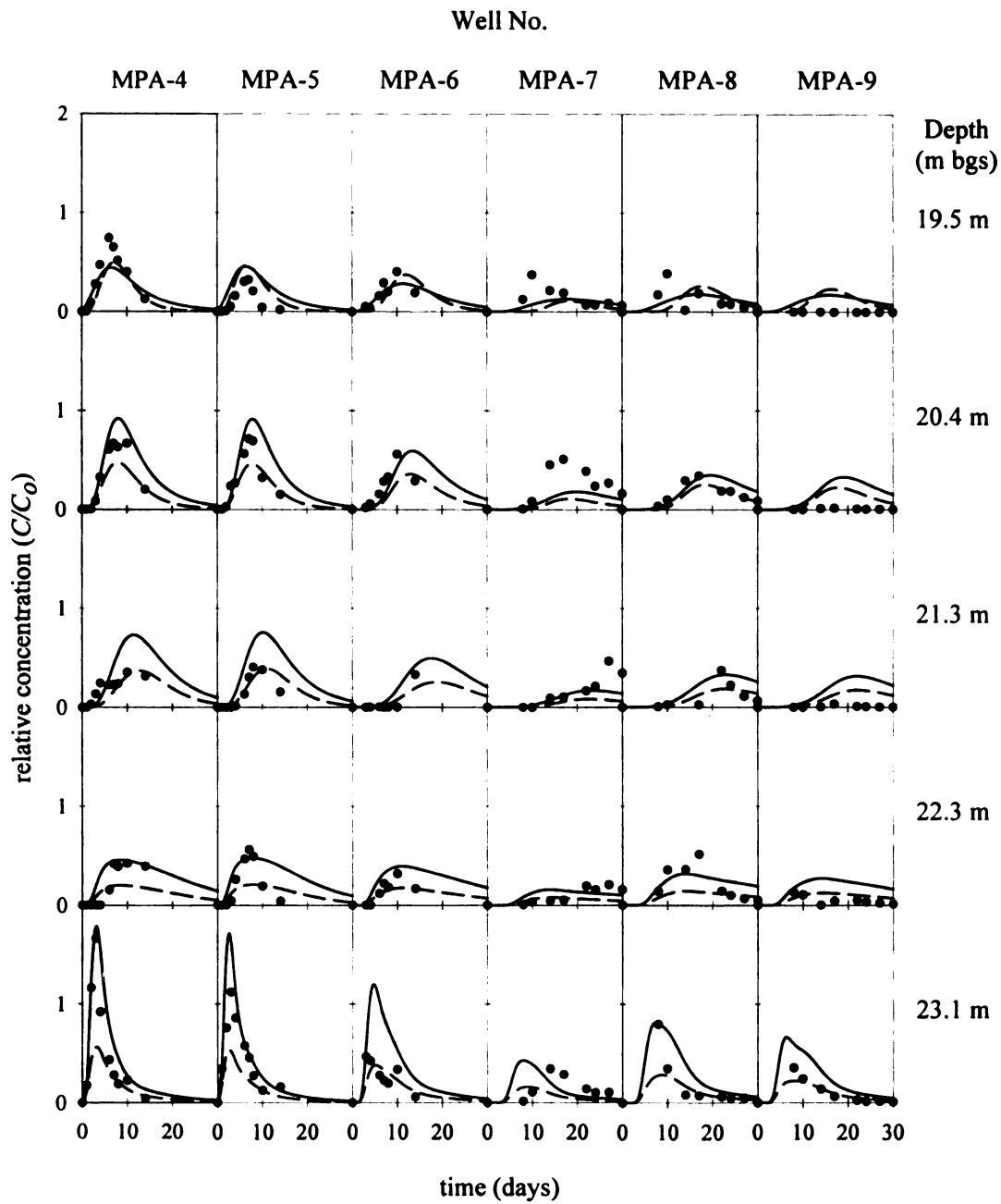
Figure 2.11. Simulated and observed tracer breakthrough curves in downgradient monitoring points: (•) observed, (—) optimum per-layer case, (— —) single optimum value case.

**Table 2.4. Depth-specific dispersivities and corresponding velocities.**

| depth (*m bgs*) | optimal dispersivity, α (*cm*) | Velocity (*cm/day*)[*] | |
| --- | --- | --- | --- |
| | | observed | simulated |
| 19.5 | 15.25 | 57.3 ± 10.7 | 47.7 ± 2.0 |
| 20.4 | 15.24 | 44.9 ± 5.5 | 40.1 ± 1.5 |
| 21.3 | 33.43 | 39.0 ± 10.5 | 33.2 ± 3.00 |
| 22.3 | 15.24 | 49.8 ± 17.3 | 50.1 ± 7.8 |
| 23.2 | 12.19 | 98.4 ± 29.0 | 99.5 ± 9.8 |

[*] Average of multi-level wells at the same depth ± uncertainty in the mean
based on the 95% confidence interval as given by the *t*-distribution.

were used to estimate simulated and observed depth-specific average linear velocity, respectively. Table 2.4 shows optimal dispersivity values and corresponding velocity calculated from observed and simulated tracer breakthrough curves.

Based on these results, the average linear velocity at 23.2m is around two times higher than velocities for other intervals. Similarly, the depth interval with slowest velocity is 21.3m bgs. Results from Table 2.4 indicate that the bottom of this aquifer will serve as a preferential flow path for contaminant migration. This fact can be seen in Figure 2.12, where the concentration contours in a cross through the augmentation grid illustrates the position of the tracer plume at 4hrs, 1 day, and 15 days after tracer injection. From figure 2.12(c), it is evident that the tracer solution is more distributed in the high conductivity zones.

Sensitivity with respect to porosity and dispersivity was evaluated by perturbing these parameters and examining the relative change in the root mean square error between simulated and observed average linear velocity (Anderson and Woessner 1992). This analysis revealed that average linear velocity is more sensitive to changes in porosity than dispersivity. A 10% change in porosity caused approximately a 25% deviation in average linear velocity when compared to optimal values (Figure 2.13). A

3% overall perturbation in the simulated velocity occurred when dispersivity values

changed by 10% from the optimal values.
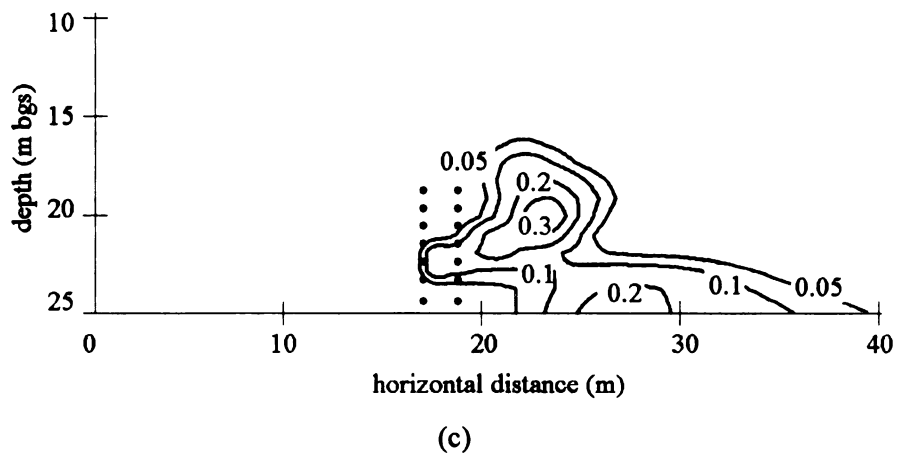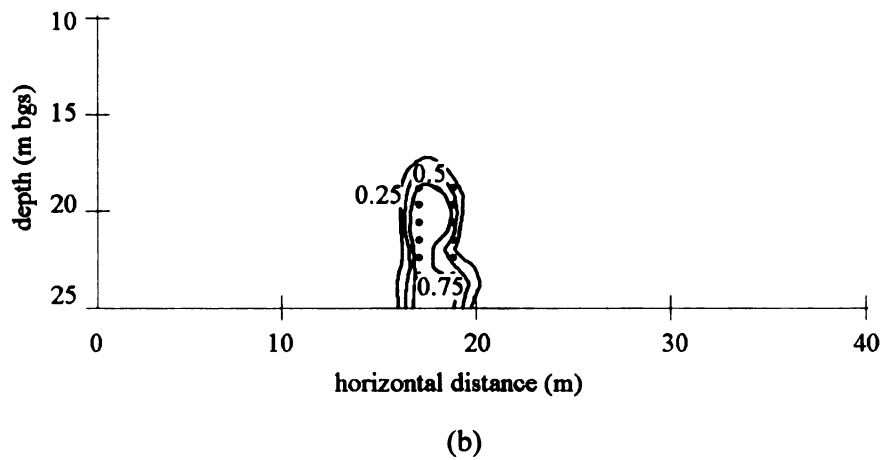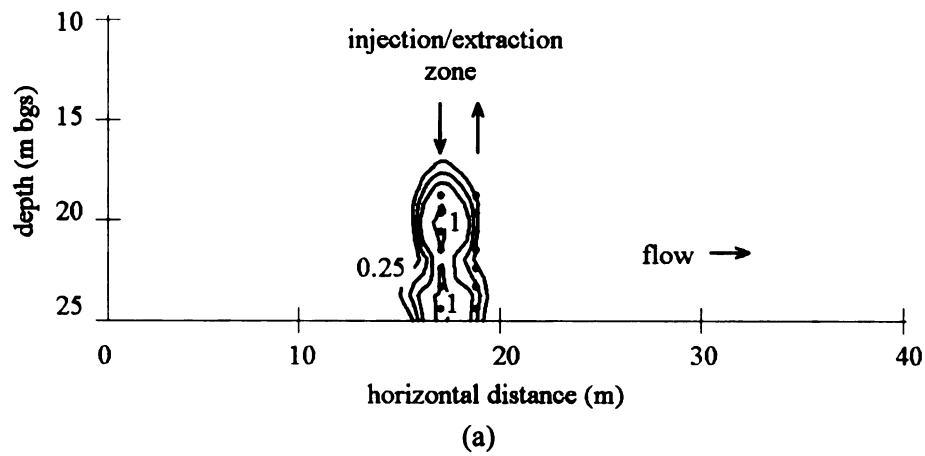
Figure 2.12. Tracer concentration (C/C$_o$) contours at (a) 4 hrs, (b) 1 day, and (c) 15 days after tracer injection. Cross section through augmentation grid.
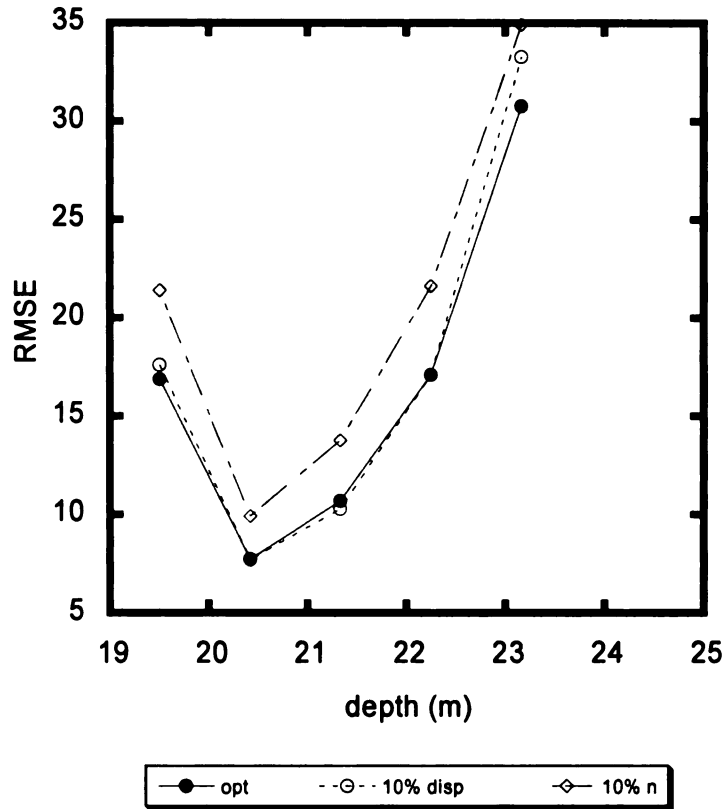
Figure 2.13. Root Mean Square Errors (RMSE) in velocity at each depth interval for a 10% change in porosity, and 10% change in dispersivity (deviation from the optimal values).

## 2.6 Conclusions

A methodology to investigate the influence of local heterogeneity on the distribution of solutes in an unconfined aquifer was evaluated. This methodology coupled laboratory and field tests with optimization techniques for solving the generalized groundwater flow and transport equations. Hydraulic conductivity results revealed the existence of high-energy zones that could act as preferential flow pathways for contaminant migration. This was further confirmed by observations made during

tracer experiments.

Optimal depth-specific dispersivity values for these zones were found by solving the advection-dispersion equation using an inverse modeling approach. This approach yielded dispersivity values that better represent the distribution of tracer as compared to a solution scenario where a single dispersivity value was used for the entire model domain. The values obtained during these simulations were used to estimate depth-specific average linear velocities. The magnitude of the average linear velocity at the 23.2m bgs interval was, in general, two times greater than the rest of the zones.

Simulated tracer concentrations were more sensitive to changes in dispersivity than porosity. One limitation of the methodology developed here is that it does not consider the length scale dependency of the dispersivity parameter. However, since a small study area was selected, a single value per depth interval was adequate to describe the longitudinal dispersivity value in the region. This approach might be adequate in small aquifer areas where a treatment technology is being evaluated for in-situ groundwater remediation. Since laboratory experiments for hydraulic conductivities are tedious, a similar approach can be developed to estimate optimal values for hydraulic conductivity and dispersivity based solely on tracer concentration histories.

This characterization provides the foundation for understanding the impacts that the hydrogeologic environment exert upon the distribution of contaminants and geochemical constituents. This could reveal important information regarding the natural processes that are responsible for changes in concentrations observed in chemically polluted environments.

## 2.7 Acknowledgments

## 2.8 Literature cited

Anderson, M. P., and Woessner, W. W. (1992). *Applied Groundwater Modeling: Simulation of flow and advective transport*, Academic Press, INC., San Diego, Ca.

Bear, J. (1979). *Hydraulics of Groundwater*, McGraw-Hill.

Bower, H., and Rice, R. C. (1976). "A slug test for determining hydraulic conductivity of unconfined aquifers with completely or partially penetrating wells." *Water Resources Research*, 12(3), 423-428.

Cho, J. S., Wilson, J. T., and Beck, F. P. (2000). "Measuring vertical profiles of hydraulic conductivity with in situ direct-push methods." *Journal of Environmental Engineering-ASCE*, 126(8), 775-777.

Coleman, T., Branch, M. A., and Grace, A. (1999). "Optimization Toolbox for use with MATLAB: User's Guide." The Math Works, Inc., Natick, Mass.

Dybas, M. J., Barcelona, M., Bezborodnikov, S., Davies, S., Forney, L., Heuer, H., Kawka, O., Mayotte, T., Sepulveda-Torres, L., Smalla, K., Sneathen, M., Tiedje, J., Voice, T., Wiggert, D. C., Witt, M. E., and Criddle, C. S. (1998). "Pilot-scale evaluation of bioaugmentation for in-situ remediation of a carbon tetrachloride contaminated aquifer." *Environmental Science & Technology*, 32(22), 3598-3611.

Dybas, M. J., Hyndman, D., Heine, R., Tiedje, J., Linning, K., Wiggert, D., Voice, T., Zhao, X., Dybas, L., and Criddle, C. (2002). "Development, operation, and long-term performance of a full-scale biocurtain utilizing bioaugmentation." *Environmental Science & Technology*, 36(16), 3635-3644.

Fetter, C. W. (2001). *Applied Hydrogeology*, Prentice Hall, Upper Saddle River, NJ.

Freeze, R. A., and Cherry, J. A. (1979). *Goundwater*, Prentice Hall, Inc.

Hoard, C. J. (2002). "The influence of detailed aquifer characterization of groundwater flow and transport models at Schoolcraft, Michigan," M.S. thesis, Michigan State University, East Lansing, MI.

Hurt, K. L., Beck, F. P., and Wilson, J. T. (2001). "Implications of subsurface heterogeneity at a potential monitored natural attenuation site." *Ground Water Monitoring and Remediation*, 21(3), 59-63.

Hvorslev, M. J. (1951). "Time lag and soil permeability in groundwater observations." *Bull. 36*, U.S. Army Corps of Engineers Waterways Experimental Station, Vicksburg, Miss.

Hyndman, D., Dybas, M. J., Forney, L., Heine, R., Mayotte, T., Phanikumar, M. S., Tatara, G., Tiedje, J., Voice, T., Wallace, R., Wiggert, D., Zhao, X., and Criddle, C. S. (2000a). "Hydraulic characterization and design of a full-scale biocurtain." *Ground Water*, 38(3), 462-474.

Hyndman, D. W., and Gorelick, S. M. (1996). "Estimating lithologic and transport properties in three dimensions using seismic and tracer data." *Water Resources Research*, 32(9), 2659-2670.

Hyndman, D. W., Harris, J. M., and Gorelick, S. M. (1994). "Coupled seismic and tracer test inversion for aquifer property characterization." *Water Resources Research*, 30(7), 1965-1977.

Hyndman, D. W., Harris, J. M., and Gorelick, S. M. (2000b). "Inferring the relation between seismic slowness and hydraulic conductivity in heterogeneous aquifers." *Water Resources Research*, 36(8), 2121-2132.

Kim, D. J., Kim, J. S., Yun, S. T., and Lee, S. H. (2002). "Determination of longitudinal dispersivity in an unconfined sandy aquifer." *Hydrological Processes*, 16, 1955-1964.

Lee, J. Y., Cheon, J. Y., Lee, K. K., Lee, S. Y., and Lee, M. H. (2001). "Factors affecting the distribution of hydrocarbon contaminants and hydrogeochemical parameters in a shallow sand aquifer." *Journal of Contaminant Hydrology*, 50(1-2), 139-158.

Lewis, M. (2001). "Installing continuous multi-chamber tubing using sonic drilling." *Water Well Journal*, 16-17.

Lipinski, B. A. (2002). "Estimating natural attenuation rates for a chlorinated hydrocarbon plume in a glacio-fluvial aquifer, Schoolcraft, Michigan," M.S. thesis, Michigan State University, East Lansing, MI.

Mayotte, T. J., Dybas, M. J., and Criddle, C. S. (1996). "Bench-scale evaluation of bioaugmentation to remediate carbon tetrachloride-contaminated aquifer materials." *Ground Water*, 34(2), 358-367.

McDonald, M. G., and Harbaugh, A. W. (1988). "A modular three-dimensional finite-difference groundwater flow model." *Book 6, Chapter A1, USGS Open-file Report*.

Phanikumar, M. S., Hyndman, D. W., Wiggert, D. C., Dybas, M. J., Witt, M. E., and Criddle, C. S. (2002). "Simulation of microbial transport and carbon tetrachloride biodegradation in intermittently-fed aquifer columns." *Water Resources Research*, 38(4), 1-13.

Wiedemeier, T. H., Swanson, M. A., Moutoux, D. E., Gordon, E. K., Wilson, J. T., Wilson, B. H., Kampbell, D. H., Haas, P. E., Miller, R. N., Hansen, J. E., and Chapelle, F. H. (1998). "Technical protocol for evaluating natural attenuation of chlorinated solvents in groundwater." *EPA/600/R-98/128*, USEPA, Cincinnati Oh.

Zheng, C., and Wang, P. P. (1999). "MT3DMS: A modular three-dimensional multispecies transport model for simulation of advection, dispersion, and chemical reactions of contaminants in groundwater systems." U.S. Army Corps of Engineers, Washington, DC.

# CHAPTER 3

# EVALUATION OF NATURAL ATTENUATION IN A CONTROL VOLUME OF A VOC CONTAMINATED AQUIFER

## 3.1 Abstract

Natural attenuation was evaluated in a study region of an aquifer located

approximately in the center of mass of VOC contaminant plume. The approach

undertaken in this chapter provides a methodology for evaluating natural attenuation of

chlorinated solvents when both parent and daughter products of dechlorination are

identified in the contaminant source. This study includes solid and liquid phase data

collected over a three year period. Generally, studies of natural attenuation of chlorinated

solvents often emphasize the liquid phase concentration, which downplays the role of

sediment associated constants. In this study, TCE concentrations in the solid phase up to

1,200μg/kg were detected. This value is twice the concentration found in the liquid

phase for the same sampling event. Levels of cis-DCE were similar for solid and liquid

phase concentrations (on a per Kg basis).

The co-existence of high levels of TCE and cis-DCE, with only low

concentrations of the parent PCE, indicates that reductive dechlorination has occurred to

some extent at some point in time. However, VC concentrations were very low

compared to its parent products, and coupled with the accumulation of cis-DCE, indicates

incomplete reductive dechlorination of chlorinated parent products.

Low nitrate concentrations in the deepest zones of this aquifer along with elevated

chloride concentration suggest that dechlorination of VOC has occurred in the anaerobic

51

zones of this aquifer. However this is not strong evidence to support the hypothesis that

dechlorination processes are still taking place within the study region.


## 3.2 Introduction

Over the past few years there has been an increased reliance on natural processes

to clean-up contaminated sites (NRC 2000). Natural attenuation include physical,

chemical, and biological processes that, under favorable circumstances, act upon

contaminants to reduce its mass, toxicity, mobility, volume, or concentration (EPA 1998).

Although natural attenuation has been implemented at a significant number of sites

contaminated with a broad range of organic compounds, concern has been raised in the

scientific community because the behavior of most of these compounds in the

environment is not fully understood.

Natural attenuation has been successfully demonstrated at sites contaminated with

BTEX compounds. Suarez and Rifai (2002) analyzed historical data for a benzene plume

at an industrial facility and found a constant decrease in extent and concentration of

contaminants with time. These results were further confirmed by a geochemical

characterization of the site. Frazmann *et al.* (2002) demonstrated toluene degradation

under sulfate reducing conditions in a coastal plain in Western Australia. However,

degradation of benzene within the plume was not significant. Extensive natural

attenuation of BTEX compounds was observed at a Coast Guard base facility in Traverse

City, MI (NRC 2000). In this aquifer, the presence of breakdown products of BTEX

degradation along with oxygen depleted zones followed by methane and rich Fe(II) zones

where indicative footprints of aerobic and anaerobic decomposition of BTEX

compounds.

Due to their wide spread use during the last few decades perchloroethene (PCE), trichloroethene (TCE), and trichloroethane (1,1,1 TCA) are among the most common contaminants found in groundwater. Attenuation of these compounds presents a major challenge since they are highly recalcitrant in the environment. Although the biodegradability of these compounds have been demonstrated in laboratory (Ferguson and Pietari 2000; Kao and Wang 2001; Maymó-Gatell et al. 1997; Ndon et al. 2000; Vogel et al. 1987; Vogel and McCarty 1987; Witt et al. 1999; Yang and McCarty 1998), attenuation of these compounds in natural environments is mostly attributed to physical mechanisms such as dilution, dispersion, and immobilization. However, sequential biodegradation of these compounds has been observed at some contaminated sites.

Weaver et al. (1996) observed sequential dechlorination of TCE at the St. Joseph, MI, Superfund site. Presence of methanogenic zones evidenced the strongly reducing conditions suitable for sequential dechlorination of TCE to ethene. Data from individual boreholes at the site confirmed that high cis-DCE concentrations correlated with declines in oxygen and sulfate concentrations. Also, high concentrations of ethene and vinyl chloride where found in the most methanogenic zones of this aquifer.

At Area 6, Dover Air Force Base, metabolic byproducts of the degradation of PCE/TCE, and oxygen depleted zones with elevated methane and hydrogen concentration evidenced that natural attenuation processes are acting to reduce the contaminants at this site (Davis et al. 2002; Witt et al. 2002). Similar observations were made at a Superfund hazardous waste site in Louisiana (Clement et al. 2002) where the "lines of evidence" approach suggested by the United States Environmental Protection Agency (EPA 1998)

was employed to demonstrate that natural attenuation processes were responsible for the degradation of PCE and TCE.

In all these cases, the presence of electron donors necessary for the reductive dechlorination process is readily available either as co-contaminants to the chlorinated organics or as naturally occurring organic matter. However, partial dechlorination is frequently encountered due to deficiency or depletion of electron donors (McCarty *et al.* 1998; Richmond *et al.* 2001). This deficiency translates into accumulation of metabolic by-products such as cis-DCE or VC that might be more toxic or are regulated at lower concentrations than their parent compound.

To evaluate the extent to which natural attenuation is occurring at a particular site, several protocols have been developed (NRC 2000). A "lines of evidence" approach is the basis of most of these protocols where evidence of natural attenuation can be provided by: (1) documented loss of contaminants from the site; (2) evidence that the biodegradation potential is actually realized in the field; and (3) laboratory assays showing that microorganisms from site have the potential to transform the contaminants (Röling and van Verseveld 2002). A "scoring system" assigns a numeric value based on the evidence collected and that number is used to reach conclusions about the natural attenuation potential for a particular site. This approach has been criticized for assigning a numerical value to a series of qualitative assessments; an assignment which implies more confidence than justified by field evidence (NRC 2000).

The objective of this study is to analyze geochemical and VOC concentration data in a control volume located within the contaminant plume to determine if natural attenuation is occurring in this particular area. This might be a useful approach to

evaluate natural attenuation of chlorinated organic compounds, especially when both, parent and daughter products are found in the contaminant source area. Clement *et al.* (2002) indicate that the scoring system proposed by the EPA (1998) might result in underestimation of overall attenuation because metabolic by-products from the degradation of parent chlorinated compounds have to be excluded from the evaluation if they are present in the source area. Analysis of data in a control volume might be useful in resolving this conflict.

Also, a detailed hydraulic characterization of the control volume will be used to investigate the influence that variations in geophysical parameters may have upon natural attenuation of these compounds. A control volume approach will be compared to the scoring system used by the EPA to derive conclusions regarding the natural attenuation processes in this area.

## 3.3 Site description

*Site history*

The village of Schoolcraft is a small rural community located in Kalamazoo, MI (Figure 3.1). Several plumes of organic and metal contaminants were discovered in the unconfined aquifer beneath the village approximately two decades ago by the Michigan Department of Environmental Quality (MDEQ). The most extensive of them is a VOC plume, designated by MDEQ as Plume G. It has been estimated that this plume has impacted about $1.3 \times 10^7 m^3$ of aquifer material. ARCO Industries, a former manufacturer of automobile plastic parts, was identified as the source of this contamination. A detailed

study area

VOC Plume (G)

SCALE IN METERS

0  300  600
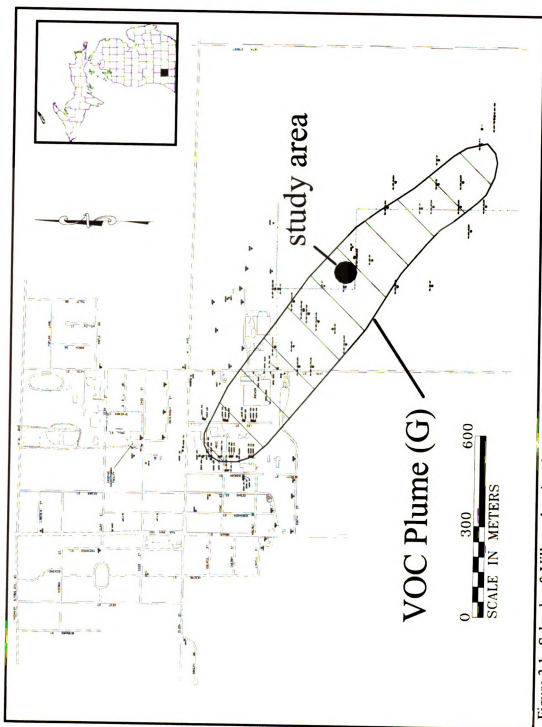
Figure 3.1. Schoolcraft Village showing the extent of the VOC contaminant plume.

investigation conducted in 1986 on the ARCO premises identified five major areas where usage and disposal of chlorinated compounds occurred throughout the history of the facility (Figure 3.2). Table 3.1 shows the major chlorinated compounds and the maximum concentration found in soil samples collected at different locations over the property during the 1986 site investigation. In addition to the compounds listed in Table 3.1, toluene was found in several sediment samples ranging from non-detectable levels to a maximum concentration of 115,000μg/kg. Although there were no historical record of toluene usage in the industrial operations at ARCO, one of the chemical providers admitted that one supplied product was, at least, contaminated with toluene.

Water and bottom sediment samples from the wastewater disposal pond (Figure 3.2) showed low level concentrations of xylene, ethylbenzene, and chlorobenzene in addition to VOC. However, VOC concentration from these sediments and from the pond's water was several orders of magnitude lower than concentrations found at other locations.

The combined effects of the five areas shown in Figure 3.2 resulted in a VOC contaminant plume extending about 2km southeast from the ARCO facility (Figure 3.1). Near the center of mass, the plume is approximately 400m wide.

Table 3.1. Chlorinated compounds and concentrations found in sediment samples at ARCO facilities.

| Compound | concentration, μg/kg |
|----------|----------------------|
| PCE | 300,000 |
| TCE | 280,000 |
| cis + trans-DCE | 520,000[a] |
| VC | N.A.[b] |

[a] estimated based on percent recovery from a pilot vapor extraction system.

[b] not available in historical reports
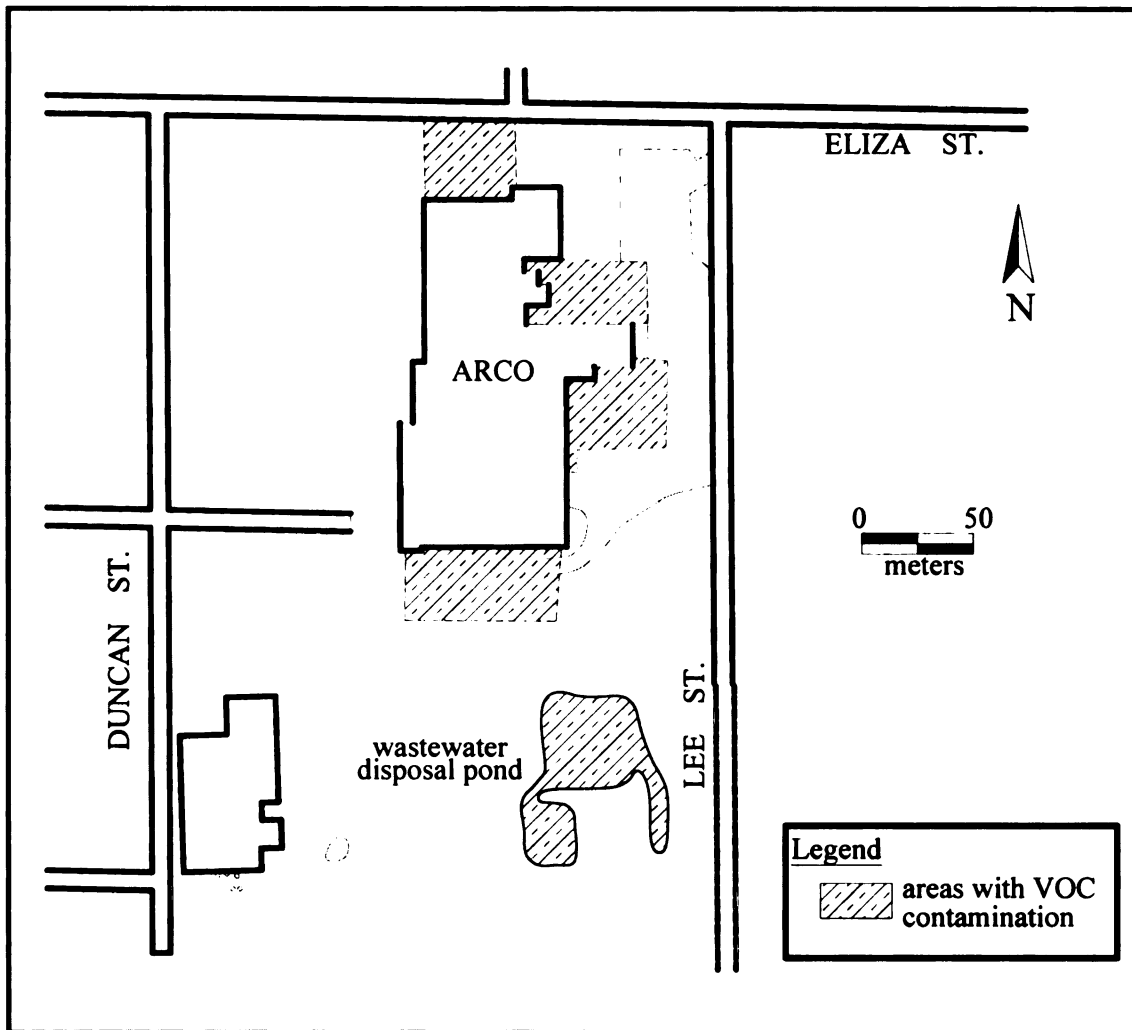
Figure 3.2.   Location of the major source areas of contaminants identified during the
1986 investigation (modified form Lipinsky, 2002).

*Hydrogeological characterization*

The unconfined aquifer beneath the Schoolcraft Village is mostly composed of highly stratified glacial outwash deposits (Lipinski 2002; Mayotte *et al.* 1996). The surficial layer overlaying this outwash sand is a dark brown, silty sandy clay that extends from the ground surface to about 0.6 to 1.2m below ground surface (bgs). Underlying the outwash sediments, a light gray clay deposit was found at depths ranging from 21.3 to 30.5m bgs. It is believed that this layer prevents further contaminant migration to the underlying confined sandy aquifer.

The water table in the unconfined aquifer is, on the average, at 4.6m bgs. General groundwater flow direction is towards the southeast at an average linear velocity of 15cm/day (Dybas *et al.* 2002; Mayotte *et al.* 1996). Hydrogeological features that control the regional groundwater flow are shown in Figure 3.3. Recharge for the entire area is approximately 23.7cm/yr (Lipinski 2002). It is believed that upon further migration, this plume will eventually discharge at the surface water bodies located southeast of the Schoolcraft region.

*Characterization of the control volume for evaluating natural attenuation*

An area located approximately in the center of mass of a VOC contaminated plume was selected to study the natural attenuation processes using a control volume approach. Figure 3.4 shows the control area with all the monitoring wells installed for this study. The approximate dimensions for this area are 30.5m x 30.5m x 24.4m (LxWxD). Groundwater flow direction is approximately perpendicular to the northwest and southeast boundaries and parallel to the other two sides.

59
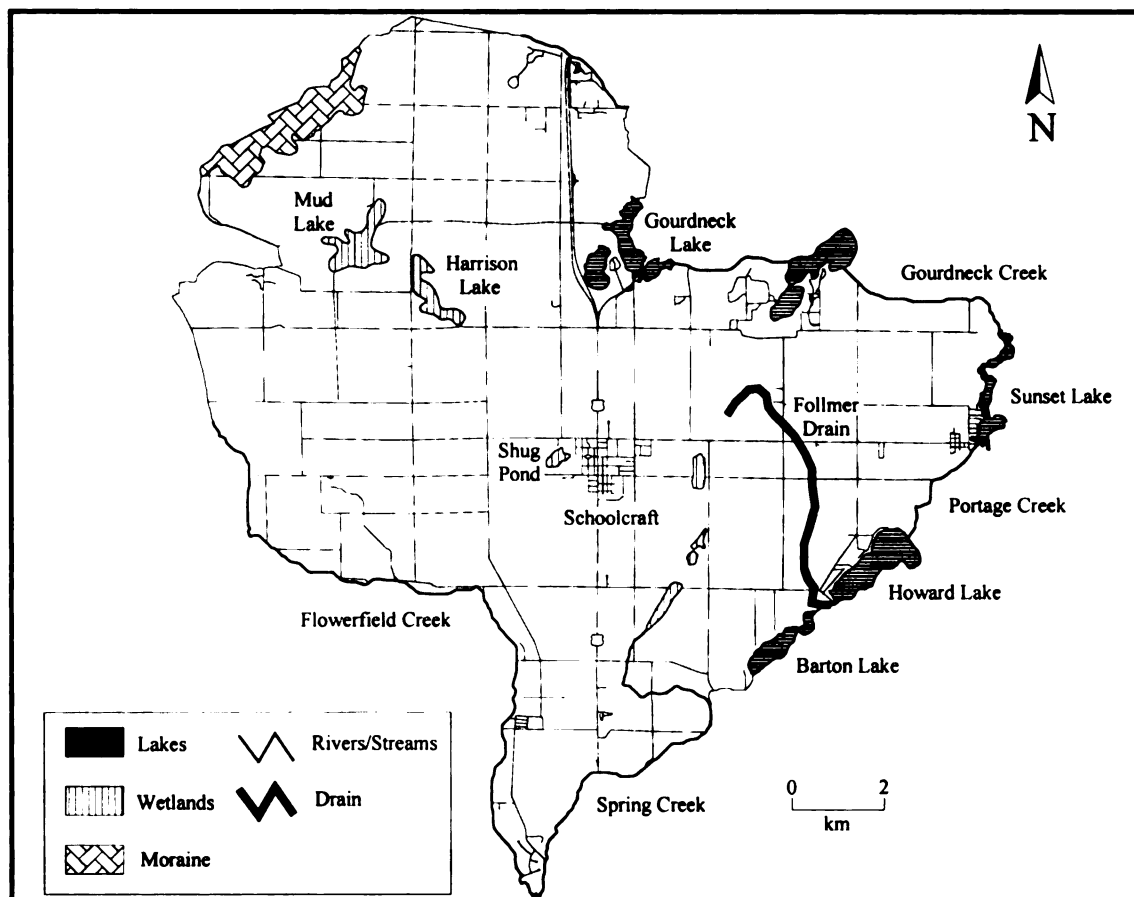
Figure 3.3. Regional hydrologic boundaries that control groundwater flow in the Schoolcraft area (modified from Lipinski, 2002).
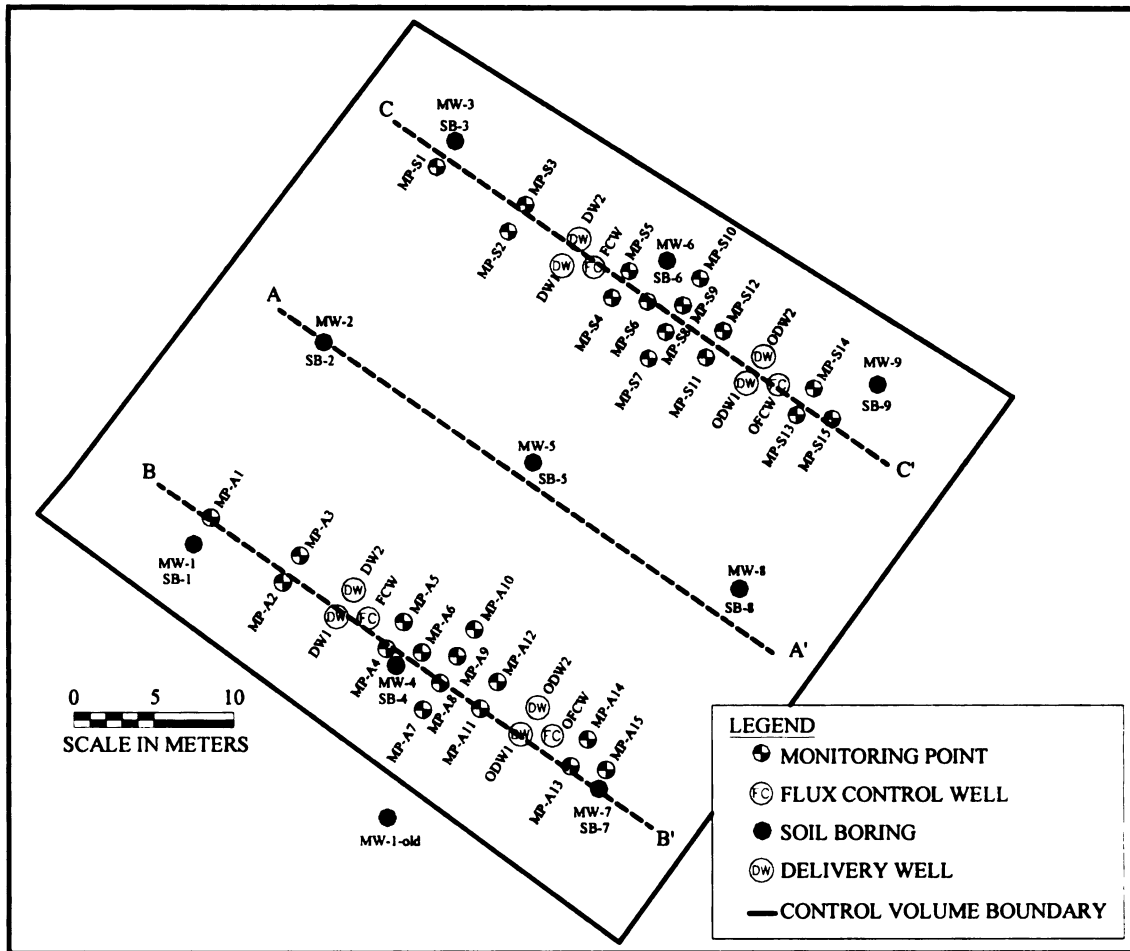
Figure 3.4. Control area with monitoring wells for the natural attenuation study.

All monitoring wells consists of 5cm internal diameter PVC pipes with 8 or 9

multi-level ports attached at different locations for depth specific sampling. Details of

the monitoring wells with the multi-level ports are illustrated in Figure 3.5.

A hydraulic characterization of the control volume using tracer tests coupled to

numerical models and optimization techniques were conducted to estimate relevant flow

and transport parameters. A summary of the depth-specific physical parameters found in

this study is given in Table 3.2. Total porosity based on the bulk density of the sediments

in this region ranged from 0.21 to 0.50 with a mean value of $0.33 \pm 0.006$ (95%

confidence interval). A cross-section through the site (A-A' in Figure 3.4) is shown in

Figure 3.6. Two preferential flow path regions were identified from the soil cores

extracted from the site. These zones are located on the average at 20m, and 23m bgs.

Table 3.2. Depth-specific summary of physical parameters.

| depth (*m bgs*) | hydraulic conductivity, K (*$10^{-2}$) (*cm/s*)[a] | average linear velocity, *v* (*cm/day*)[a] | optimal dispersivity, α (*cm*) | solute retention time (1/day) |
|---|---|---|---|---|
| 19.5 | 8.1 ± 3.4 | 57.3 ± 10.7 | 15.3 | 53.2 |
| 20.4 | 11.6 ± 4.4 | 44.9 ± 5.5 | 15.2 | 67.9 |
| 21.3 | 10.7 ± 4.0 | 39.0 ± 10.5 | 33.4 | 78.1 |
| 22.3 | 9.0 ± 2.9 | 49.8 ± 17.3 | 15.2 | 61.2 |
| 23.2 | 16.6 ± 4.9 | 98.4 ± 29.0 | 12.2 | 31.0 |

[a] mean of samples at the same depth ± uncertainty in the mean at the 95% confidence interval given by a *t*-distribution.

5 cm id PVC well

non-reactive
peristaltic pump
tubing

15.2 cm

0.61 m screen length

8 or 9 @ 0.9 m each
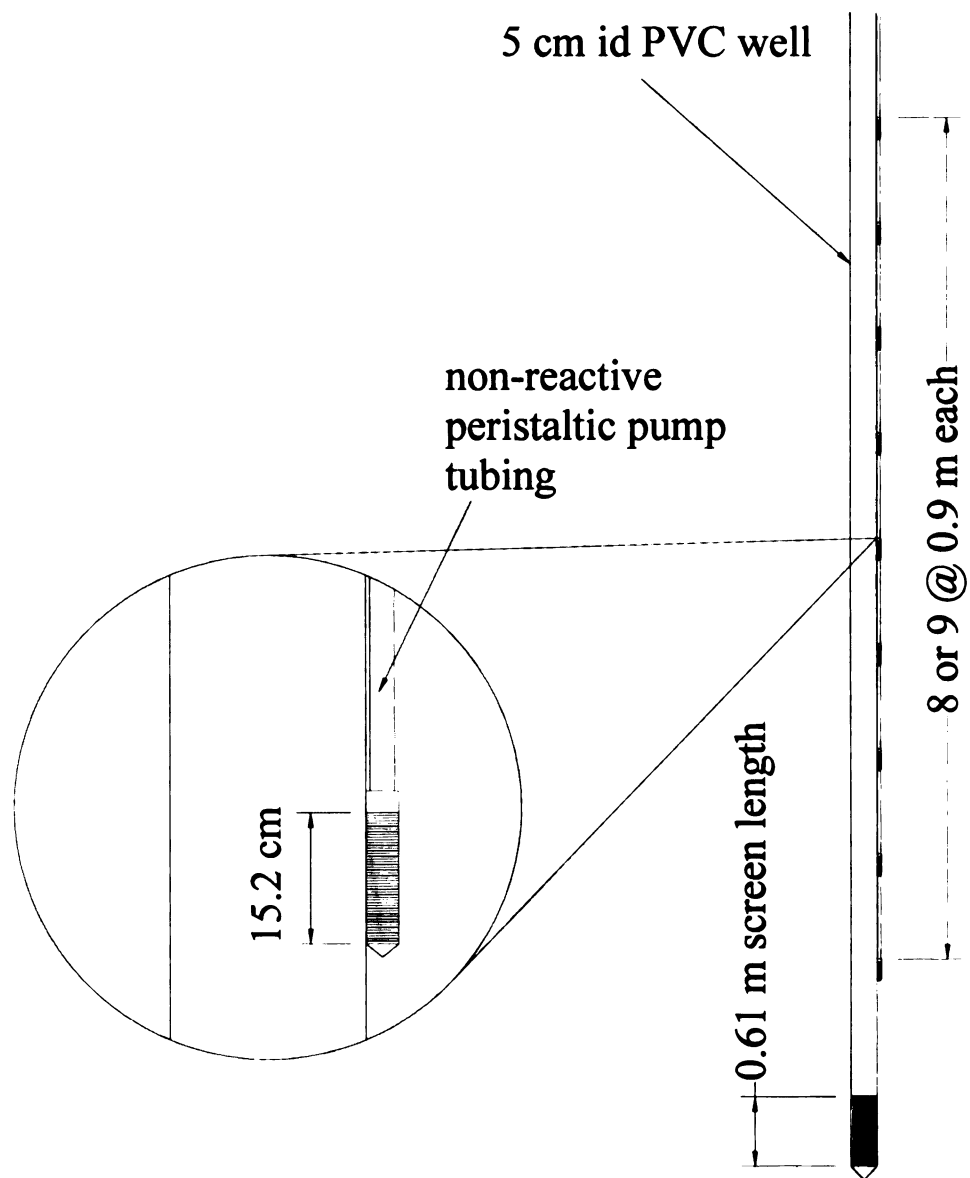
Figure 3.5.   Details of the multi-level wells installed for the natural attenuation study.

63
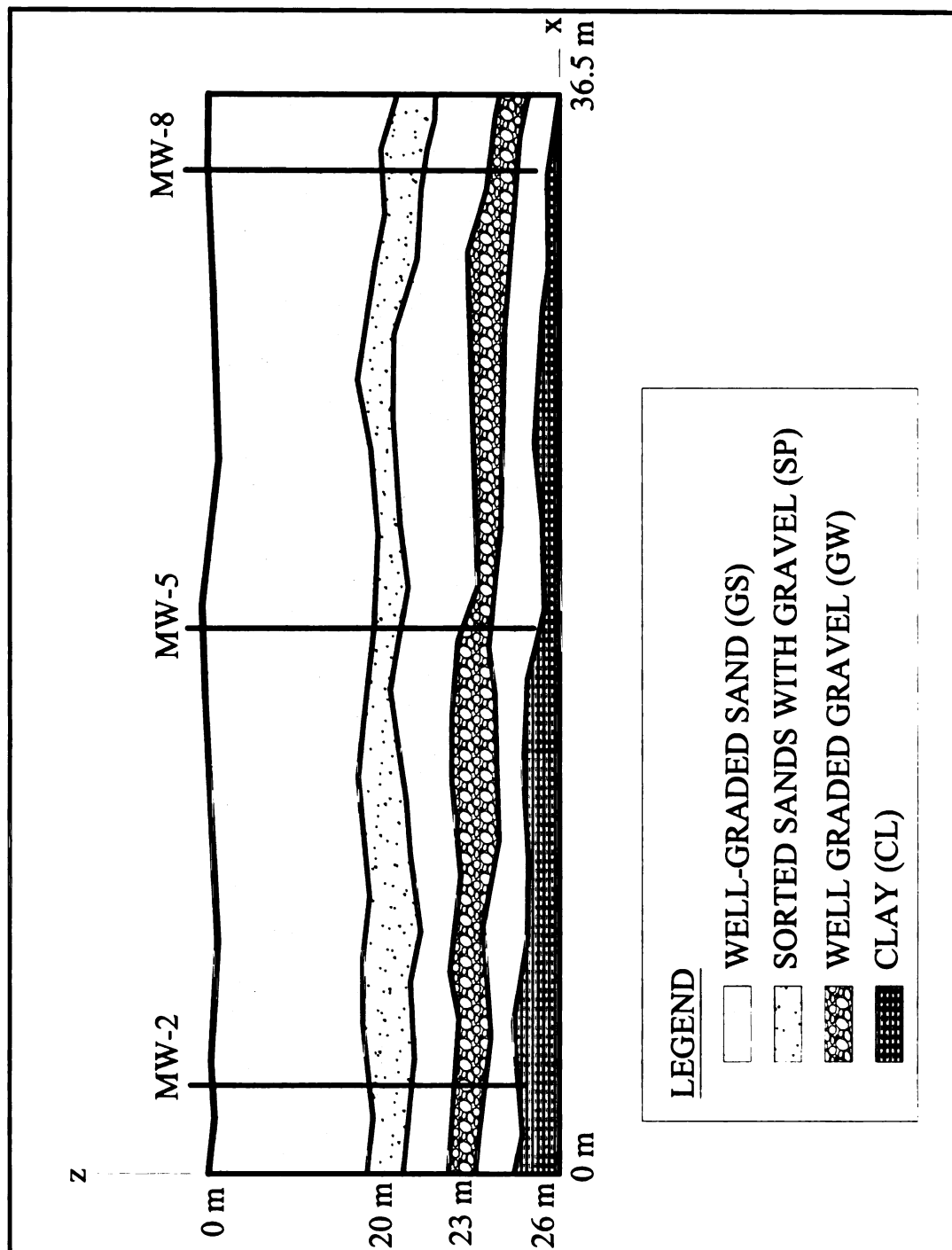
Figure 3.6. Cross section A-A' (Figure 3.4) showing the location of two preferential flow pathways.

LEGEND

WELL-GRADED SAND (GS)

SORTED SANDS WITH GRAVEL (SP)

WELL GRADED GRAVEL (GW)

CLAY (CL)

64

## 3.4 Materials and methods

Samples for geochemical constituents and organic compounds were collected in four sampling events over a three year period. The logistics for the sampling event and the matrix sampled in each one is given in Table 3.3.

*Aquifer sediment sampling*

Aquifer sediment samples were obtained during drilling of the monitoring wells. Cores were extracted from each borehole using the Waterloo cohesionless continuous sand sampler (Dybas *et al.* 1998) from 15.5m to 25.0m bgs in 1.5m intervals or the Rotosonic method, where cores where extracted in 6m intervals. Solid samples from both core types were collected by inserting a syringe-type sampler to extract approximately 2 to 4cm$^3$ of sediment. These samples were place in 40mL headspace vials containing 10mL of 2% (w/v) NaHSO$_4$ solution and were sealed with Teflon-lined septa. Samples were transported in ice to the laboratory for volatile organic analyses.

*Groundwater sampling*

Groundwater samples for organic and inorganic analyses were collected from each port attached to the multi-level wells after purging three well casing volumes. Groundwater was extracted using peristaltic pumps at a rate of 200mL/min. For VOC analyses, samples were collected in 40mL VOA vials containing 1mL of 40% (w/v) NaHSO$_4$ solution and were sealed with Teflon-lined septa. Samples for inorganic analyses were collected in 15mL tubes (0.45μm filtration) with nitric acid (1% final concentration) preservative in the case of soluble metals.

**Table 3.3. Description of the sampling events in the control volume for the three year study.**

| Sampling Event Date | Wells Sampled [a] | Matrix sampled | Description |
|---|---|---|---|
| Fall 2000 | MW-1 – MW-9 | aquifer sediments | Solid phase samples taken during installation of monitoring wells MW-1 through MW-9 |
| Spring 2001 | MW-1 – MW-9 some MDEQ wells | Groundwater groundwater | Liquid phase samples from the wells installed during Fall 2000 and some wells outside the control volume installed by the Michigan Department of Environmental Quality in 1986. |
| Spring 2002 | MW-1 – MW-9 MP-A1 – MP-A15 MP-S1 – MP-S15 FCW's and DW's | Groundwater aquifer sediments & groundwater aquifer sediments & groundwater aquifer sediments | Liquid phase samples from the installed MW wells and from the recently installed multi-level wells (MP-A's and MP-S's). Solid phase samples from the cores extracted during MP-A's, MP-S's, FCW's and DW installation. |
| Summer 2002 | MP-A1 – MP-A15 MP-S1 – MP-S15 | groundwater groundwater | Liquid phase samples from the multi-level wells installed during the Winter 2002. |

[a] see Figure 3.4 for well location

*Volatile organic and inorganic analyses*

Volatile organic compounds were analyzed using a Tekmar Precept II headspace auto sampler interfaced with a sampler and concentrator (Teckmar-Dohrmann 3100) and an Agilent 6890 gas chromatograph system.

A Dionex model 2000i/SP ion chromatograph with suppressed conductivity detection, equipped with a Dionex model AS4-A column was used for anion analyses. The mobile phase was a solution of 1.8mM bicarbonate and 1.7mM carbonate at 3mL/min. Dissolved oxygen, temperature, pH, and oxidation-reduction potential were measured in the field with a Purge-Saver Model FC2000 flow-through cell. Details for these analyses can be found in Dybas *et al.* (1998).

*Hydrogen Analysis*

Hydrogen gas was measured using the bubble strip method (Chapelle *et al.* 1997;

Lovley *et al.* 1994). Groundwater was continuously pumped through a gas sampling bulb

containing a nitrogen or air "bubble" so that hydrogen can partition between the gas and

liquid phases. When an equilibrium between the dissolved and air concentration of

hydrogen was reached, a sample of the air bubble was collected and analyzed for $H_2$ with

RGA-3, a reduced gas analyzer (Trace Analytical, Inc.). The dissolved $H_2$ concentration

was found using the Ideal Gas Law and Henry's Law.

## 3.5 Results and discussion

*Electron acceptor profiles: correlation between geochemical and reductive*
*dechlorination indicators*

Depth specific concentration of chlorinated ethene compounds in aquifer

sediments during the course of this study can be seen in Figures 3.7 and 3.8. Solid phase

samples were collected during drilling activities of MW wells surrounding the multi-level

samplers network (Figure 3.4). VOC concentration profiles in the solid phase showed

highest contamination approximately between 17.4 to 24.4m bgs. TCE concentrations as

high as 1,200μg/kg (MW-6) were found in sediments extracted from this region. Also, a

maximum cis-DCE concentration of 800μg/kg was found at 24.1m bgs in sediments from

MW-8. Vinyl chloride concentrations in the sediments were low compared to

concentrations of TCE and cis-DCE. VC concentrations were, on the average, two orders

of magnitude lower than its parent products.

The general patterns of chlorinated ethene concentrations in the liquid phase

67
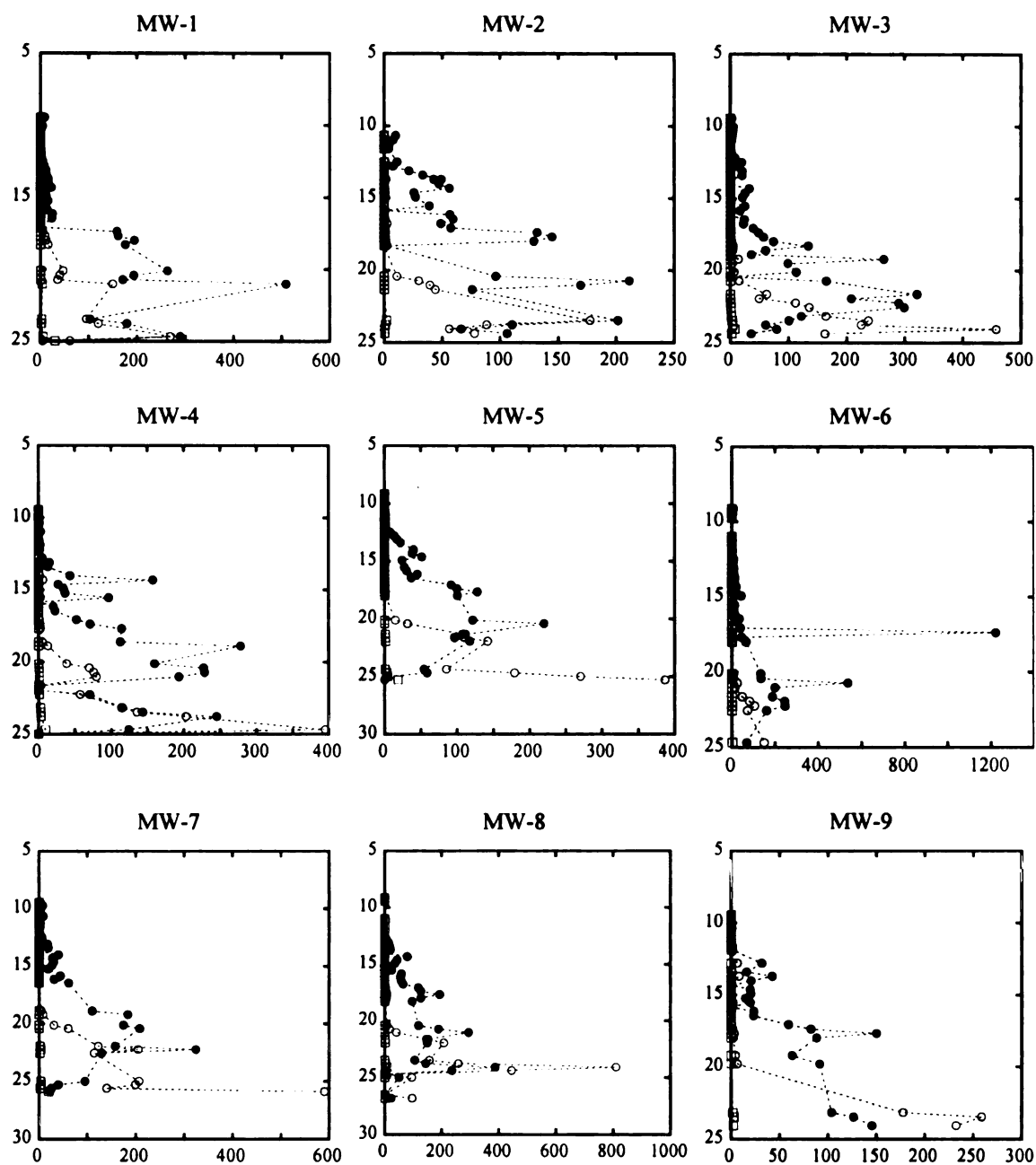
Figure 3.7. Chlorinated ethene concentration in aquifer sediments (Fall 2000 sampling event); TCE(•), cis-DCE(○), and VC(□). Vertical axis represents the depth in meters below the ground surface at which the sample was collected. Horizontal axis is the concentration in μg/kg.
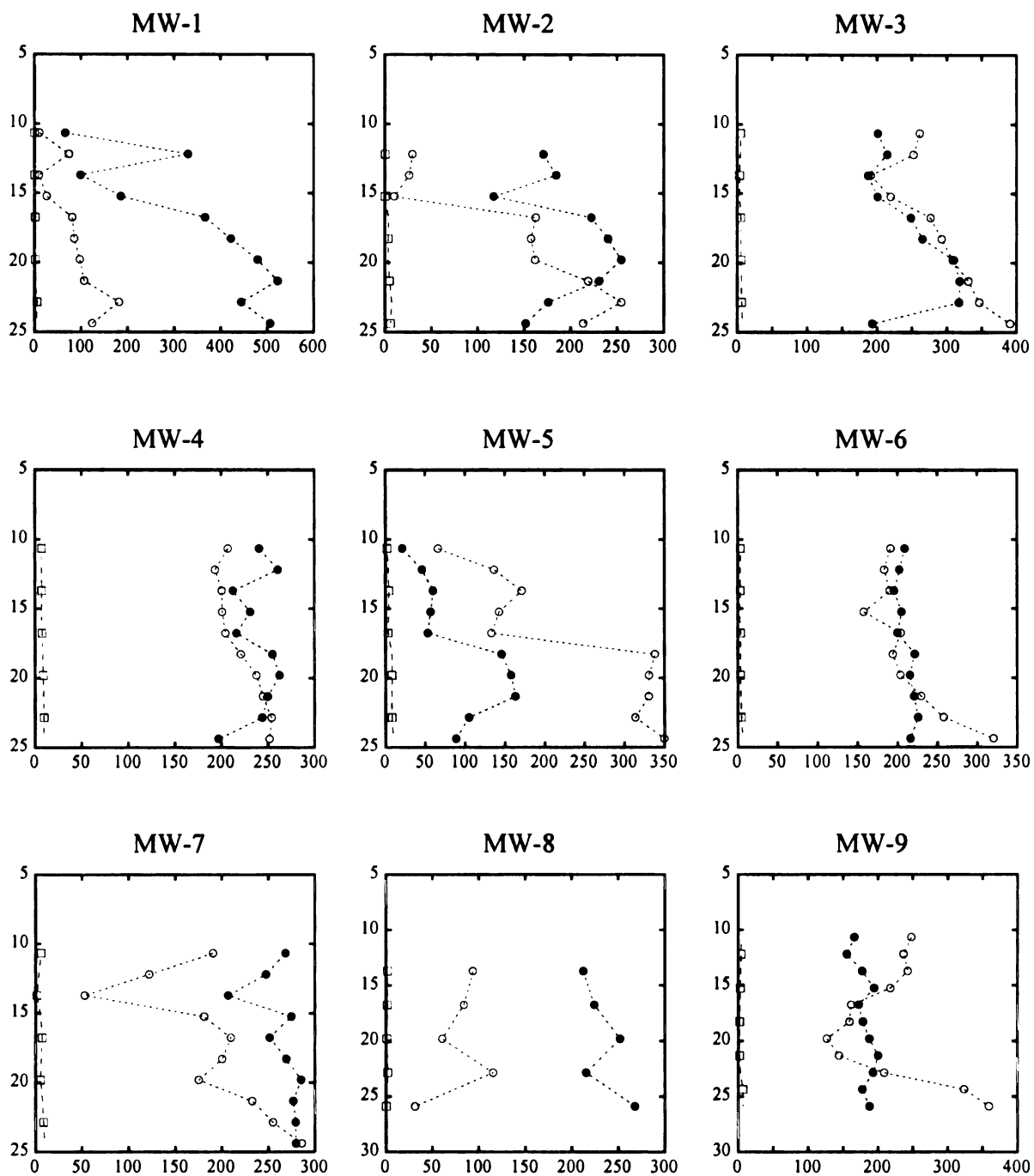
Figure 3.8. Chlorinated ethene compounds in groundwater samples (Spring 2001 sampling event); TCE(●), cis-DCE(○), and VC(□). Vertical axis represents the depth in meters below the ground surface at which the sample was collected. Horizontal axis is the concentration in μg/L.

(Figure 3.8) were similar to the solid-phase concentration profiles on Figure 3.7. Generally, concentrations of TCE ranged from 100 to 300µg/L in most of the wells except for MW-1 where liquid phase concentrations as high as 500µg/L were found. Cis-DCE concentrations ranged from 50 to 350µg/L. A positive correlation between cis-DCE and TCE concentrations is apparent in some of the profiles of Figure 3.8. Vinyl chloride concentrations in the area were low compared to TCE and cis-DCE.

Depth specific concentration of geochemical parameters (Figure 3.9) shows an apparent decrease in nitrate concentrations with depth for some of the wells. The most noticeable concentration change occurs in MW-1 where nitrate drops from 100mg/L at 10m bgs to a concentration of 20mg/L at 23m bgs. However, no trend in nitrate concentration data was observed in the profiles of MW-4, MW-6, MW-8, and MW-9. Sulfate concentrations were between 40 and 80mg/L and although a slight increase in concentration with respect to depth was observed in the wells, generally, the data shows no significant depth related trend for this parameter.

Even though chloride is both a metabolic byproduct of dechlorination processes and a geochemical parameter, it is included in these plots because increases in its concentration could be indicative of microbially mediated dechlorination processes. Chloride concentration ranged from 20 to 85mg/L with no appreciable concentration trends. For most of the wells, chloride concentration was in the range of 60 to 80 mg/L.

Other groundwater parameters measured, such as dissolved oxygen, specific conductivity, pH, and temperature are given in Table 3.4. Dissolved oxygen concentration varies from 1.6mg/L at 9.1m bgs to 0.78mg/L at 24.4m bgs. This suggests that aerobic zones overlay anaerobic zones in this aquifer. The source of oxygen

70
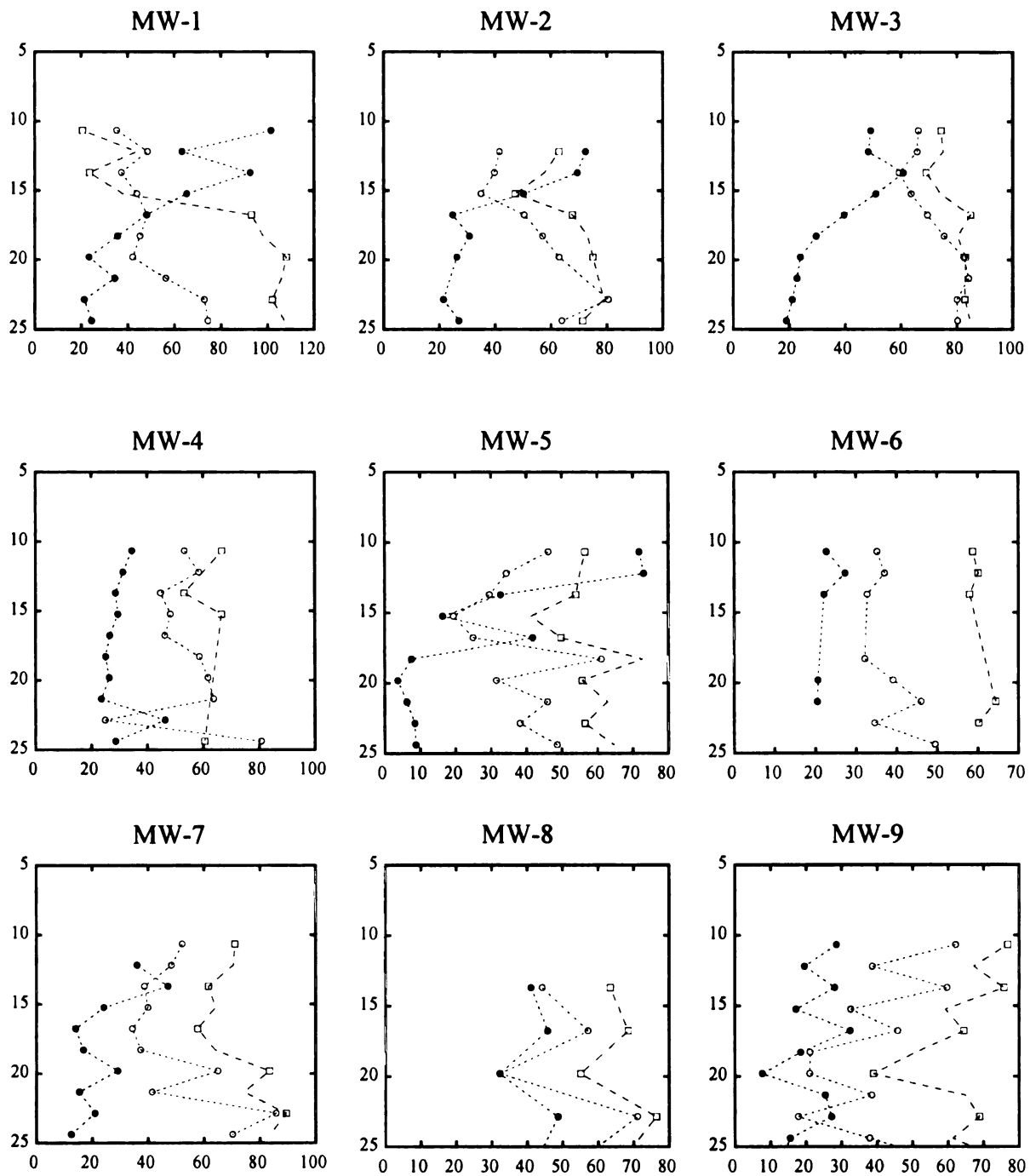
Figure 3.9.    Geochemical constituents concentration in groundwater samples (Spring
2001 sampling event); $NO_3^-$(•), $SO_4^{2-}$(○), and $Cl^-$(□).  Vertical axis
represents the depth in meters below the ground surface at which the sample
was collected.  Horizontal axis is the concentration in mg/L.

**Table 3.4. Flow through cell parameters.**

| depth (m bgs) | specific conductivity (mS/cm)* | dissolved oxygen (mg/L)* | temperature (°C) | pH |
|---|---|---|---|---|
| 9.1 | 0.989 ± 0.032 | 1.62 ± 0.40 | 11.4 | 7.2 |
| 12.2 | 0.991 ± 0.028 | 1.59 ± 0.40 | 11.4 | 7.2 |
| 15.2 | 0.993 ± 0.037 | 1.52 ± 0.42 | 11.4 | 7.2 |
| 18.3 | 0.999 ± 0.042 | 1.33 ± 0.42 | 11.3 | 7.2 |
| 21.3 | 1.011 ± 0.045 | 1.08 ± 0.38 | 11.3 | 7.2 |
| 24.4 | 1.031 ± 0.052 | 0.78 ± 0.51 | 11.3 | 7.2 |

* average ± uncertainty in the average at the 95% confidence interval

in the shallower portion of this aquifer is believed to be recharge from precipitation or

snow melt. The pH for this water was 7.4 on the average and the temperature was

11.4°C.

Comparison of solid and liquid phase concentration data (Figure 3.7 and 3.8)

show a similar pattern in the profiles for the VOC concentrations. Generally,

concentrations are lower in the shallower portion of the aquifer and increase with depth.

Solid phase concentrations in MW-5 show that cis-DCE is higher than TCE

concentrations at 25m bgs. Comparing this panel with the liquid phase concentration for

the same well in Figure 3.8 shows that cis-DCE is also higher that TCE. However, this

relation was not observed in all wells. For example, the solid-phase TCE profile for

MW-8 shows lower TCE concentrations at 25m bgs than cis-DCE. On the other hand,

liquid phase TCE is higher that cis-DCE concentration for the same well at the same

depth interval. The reason for this inconsistency is unknown at this moment. This type

of comparison could be useful in identifying inconsistencies in the analytical data,

collection procedures, and reformulation of conceptual views.

Even though solid and liquid phase samples were not collected at exactly the

same time, this data set can give an insight as to the concentration in the liquid and solid

phases since this data was collected within a 4 month time span and the migration of the contaminants in the zone are not expected to be significant within this time period.

A comparison between Figures 3.8 and 3.9 was made to find patterns indicative of microbial reductive dechlorination processes. The geochemical concentration profile of MW-1 show that nitrate concentration decrease with depth while chloride concentration increases. However, the liquid-phase TCE data for the same well is higher in the deepest portion of the aquifer than cis-DCE. Thus, the increase in chloride concentration cannot be attributed to reductive dechlorination of TCE to cis-DCE. The geochemical profiles in Figure 3.9 and the VOC concentration profiles (Figure 3.8) do not confirm that reductive dechlorination is a significant component of the natural attenuation process at this location.

*Effects of hydrogeology on contaminant distribution and transport*

To evaluate hydrogeological effects on transport and distribution of constituents, data was collected at several depth specific wells located in cross section B-B' (Figure 3.4). Color-coded images of the interpolated data along with observed values are shown in Figures 3.10 through 3.12

The interpolated image for solid-phase VOC concentrations is shown in Figure 3.10. Also, the location where data was collected is indicated by color-coded filled circles. TCE concentrations in the cross section ranged from undetectable levels to 600μg/kg. Soil concentration of cis-DCE was as high as TCE. Maximum areas of cis-DCE concentration are around 300μg/kg (Figure 3.10 b). However, sorbed VC concentration was low compared to TCE and cis-DCE. VC concentration in the solid-
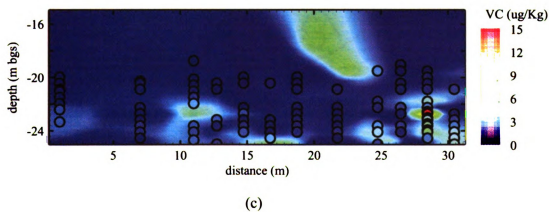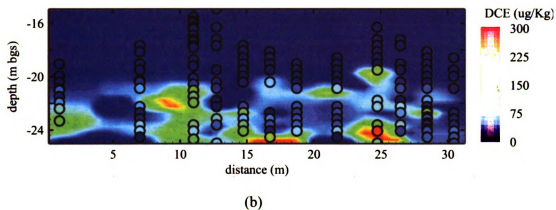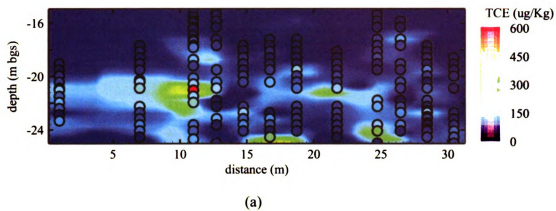
Figure 3.10. Solid phase chlorinated ethene concentration (µg/kg) in B-B' cross section (spring 2002 sampling event). (a) TCE, (b) cis-DCE, and (c) VC.
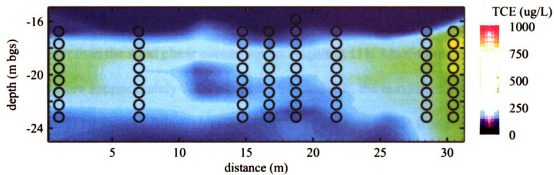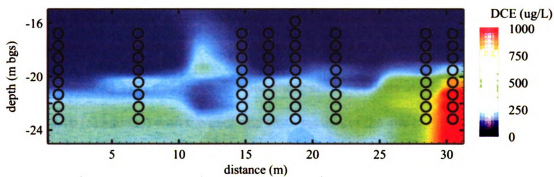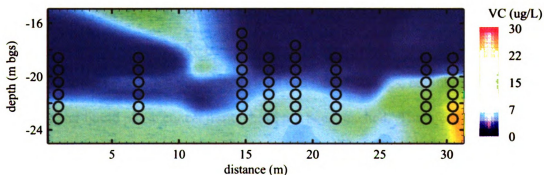
Figure 3.11. Liquid phase chlorinated ethene concentration (µg/L) in B-B' cross section (spring 2002 sampling event). (a) TCE, (b) cis-DCE, and (c) VC.

phase ranged from non-detected levels to 15μg/kg.

Liquid phase concentration images of VOC compounds show a more uniform distribution than the solid phase concentration (Figure 3.11). Maximum concentrations for TCE were approximately 700μg/L while for cis-DCE, the maximum concentrations were around 1000μg/L. Vinyl chloride concentrations were within 0 and 20μg/L.

The geochemical parameters where also interpolated in the B-B' cross section. Figure 3.12 show interpolated images for nitrate, sulfate, and chloride. Nitrate concentration seems to be distributed between 10 and 30mg/L. Sulfate and chloride images show maximum concentrations in this cross section of 130 and 100mg/L, respectively.

Comparing TCE and cis-DCE solid-phase concentrations in cross section B-B' (Figure 3.10 (a) and (b)) with the geologic cross section of the site (Figure 3.6) show that higher concentration areas are located in areas that were identified as preferential flow pathways. VC concentrations, however, do not show a clear trend.

Liquid phase chlorinated ethene concentration (Figure 3.11) shows that for TCE, the maximum concentration contours apparently do not fall within the preferential flow regions identified in Figure 3.6. However, higher vinyl chloride areas are within this region. It could be possible that in these high conductivity zones, equilibrium between the solid and liquid phase concentration have not been reached. Therefore, concentrations of compounds that have a tendency for sorption to the solid phase will be higher in these high conductivity zones than in zones where quiescent water provides more retention time to reach that equilibrium point. A sorption experiment using a layered aquifer system could be helpful in the interpretation of these observations.

76
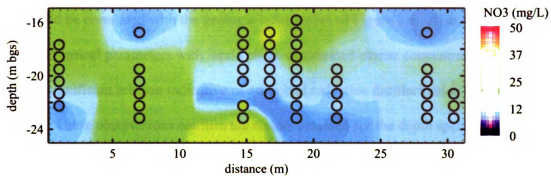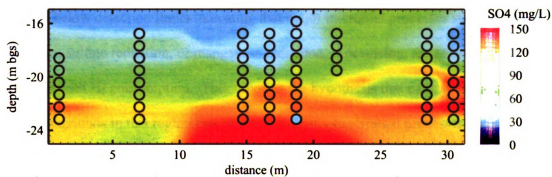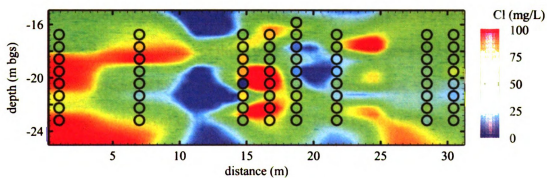
Figure 3.12. Geochemical parameter concentrations (mg/L) in B-B' cross section (spring 2002 sampling event). (a) NO$_3^-$, (b) SO$_4^{2-}$, (c) Cl$^-$.

The geochemical parameter images in Figure 3.12 do not show a significant trend

that could be correlated with the geologic information of Figure 3.6. Also, comparison of

the geochemical parameters with liquid phase chlorinated ethene concentrations do not

show a significant relation indicative of microbial reductive dechlorination in this cross

section. These observations confirm the results obtained for the depth specific data

sampling.

Methane concentrations were measured in selected wells in the area however, no

quantifiable levels of methane were found. Also, hydrogen concentration measurements

were all below detection limits indicating that major microbial processes such as iron

reduction, sulfate reduction, or manganese reduction, if occurring, are at low rates

balanced with $H_2$ consumption. This supports the hypothesis that natural attenuation of

these compounds in this region can be attributed only to physical processes such as

dilution and dispersion.


*Evaluation of natural attenuation by EPA (1998) guidelines*

An analysis of geochemical parameters and VOC compounds based on the EPA

(1998) protocol show that some of these wells will score between 6 to 14 points in the

scoring system proposed by the guidelines. These values indicate, "limited evidence for

anaerobic biodegradation of chlorinated organics" in the control volume area. However,

based on the geochemical and volatile organic analysis, there is no evidence that

reductive dechlorination is occurring in this region. Table 3.5 shows the score obtained

by analyzing geochemical and VOC data collected in a selected well at 20.4m bgs.

**Table 3.5. EPA (1998) screening process applied to a selected aquifer interval (MP-A3 at *20.4m bgs*).**

| Analyte | concentration | points awarded |
|---|---|---|
| dissolved oxygen | 1.08 mg/L | -2 |
| Nitrate | 11.8 mg/L | 0 |
| Iron (II) | ND[a] | 0 |
| Sulfate | 80.8 mg/L | 0 |
| ORP | > 100 mV[b] | 0 |
| Chloride | 121.3 µg/L | 2 |
| TCE | 286.5 µg/L | 0 |
| cis-DCE | 163.3 µg/L | 2 |
| VC | 2.4 µg/L | 2 |
| 1,1,1 TCA | 100.2 µg/L | 0 |
| 1,1 DCA | 24.5 µg/L | 2 |
| | Total | 6 |

[a] not detected in previous sampling events

## 3.6 Conclusions

Data on geochemical and chlorinated organic compounds were collected on a control volume in an area of a VOC contaminant plume to evaluate the extent to which natural attenuation processes are occurring. Solid and liquid phase data show that TCE concentrations in the solids are higher than concentrations found in the liquid phase. In most natural attenuation studies in the literature, solid phase data is not considered or is not evaluated. This can lead to underestimation of the contaminants in the area since sorption increases with degree of chlorination of the compound.

The co-existence of elevated TCE and cis-DCE contaminated zones, both in the liquid and solid phase, indicate that reductive dechlorination took place at certain times within the contaminated area. The lower concentrations of VC and the accumulation of cis-DCE provide evidence that reductive dechlorination is not happening at a significant rate in this area. The absence of an electron donor that can promote biological usage of chlorinated ethenes as electron acceptors could be the main reason for the apparent

accumulation of cis-DCE.

High concentration of solid-phase chlorinated ethene compounds in zones of high conductivity indicates that contaminants in these zones have the potential to migrate faster to downgradient receptors. However, the horizontal extent of these zones is uncertain. Also, retardation with respect to the groundwater flow velocity is expected since all of these compounds sorb to soil particles.

Although the EPA (1998) scoring system indicates that there is limited evidence of reductive dechlorination in this area, the analysis performed in this study indicates that at some point in time, reductive dechlorination was an important process for the degradation of chlorinated compounds in the area, however, there is no evidence that supports the hypothesis that these processes are still occurring in this region.

A conceptual analysis of the historical events for this site could help in identifying all the physical, chemical, and biological processes that lead to the development of this chlorinated solvents plume.


## 3.7 Acknowledgments

## 3.8 Literature cited

Chapelle, F. H., Vroblesky, D. A., Woodward, J. C., and Lovley, D. R. (1997). "Practical considerations for measuring hydrogen concentrations in groundwater." *Environmental Science & Technology*, 31(10), 2873-2877.

Clement, T. P., Truex, M. J., and Lee, P. (2002). "A case study for demonstrating the application of US EPA's monitored natural attenuation screening protocol at a hazardous waste site." *Journal of Contaminant Hydrology*, 59(1-2), 133-162.

Davis, J. W., Odom, J. M., DeWeerd, K. A., Stahl, D. A., Fishbain, S. S., West, R. J., Klecka, G. M., and DeCarolis, J. G. (2002). "Natural attenuation of chlorinated solvents at Area 6, Dover Air Force Base: characterization of microbial community structure." *Journal of Contaminant Hydrology*, 57(1-2), 41-59.

Dybas, M. J., Barcelona, M., Bezborodnikov, S., Davies, S., Forney, L., Heuer, H., Kawka, O., Mayotte, T., Sepulveda-Torres, L., Smalla, K., Sneathen, M., Tiedje, J., Voice, T., Wiggert, D. C., Witt, M. E., and Criddle, C. S. (1998). "Pilot-scale evaluation of bioaugmentation for in-situ remediation of a carbon tetrachloride contaminated aquifer." *Environmental Science & Technology*, 32(22), 3598-3611.

Dybas, M. J., Hyndman, D., Heine, R., Tiedje, J., Linning, K., Wiggert, D., Voice, T., Zhao, X., Dybas, L., and Criddle, C. (2002). "Development, operation, and long-term performance of a full-scale biocurtain utilizing bioaugmentation." *Environmental Science & Technology*, 36(16), 3635-3644.

U.S. Environmental Protection Agency (EPA). (1998). "Technical protocol for evaluating natural attenuation of chlorinated solvents in groundwater." *EPA/600/R-98/128*, USEPA, Cincinnati, OH.

Ferguson, J. F., and Pietari, J. M. H. (2000). "Anaerobic transformations and bioremediation of chlorinated solvents." *Environmental Pollution*, 107(2), 209-215.

Franzmann, P. D., Robertson, W. J., Zappia, L. R., and Davis, G. B. (2002). "The role of microbial populations in the containment of aromatic hydrocarbons in the subsurface." *Biodegradation*, 13(1), 65-78.

Kao, C. M., and Wang, Y. S. (2001). "Field investigation of the natural attenuation and intrinsic biodegradation rates at an underground storage tank site." *Environmental Geology*, 40(4-5), 622-631.

Lipinski, B. A. (2002). "Estimating natural attenuation rates for a chlorinated hydrocarbon plume in a glacio-fluvial aquifer, Schoolcraft, Michigan," M.S. thesis, Michigan State University, East Lansing, MI.

Lovley, D. R., Chapelle, F. H., and Woodward, J. C. (1994). "Use of dissolved H2 concentrations to determine distribution of microbially catalyzed redox reactions in anoxic groundwater." *Environmental Science & Technology*, 28(7), 1205-1210.

Maymó-Gatell, X., Chien, Y., Gossett, J., and Zinder, S. (1997). "Isolation of a bacterium that reductively dechlorinates tetrachloroethene to ethene." *Science*, 276(6), 1568-1571.

Mayotte, T. J., Dybas, M. J., and Criddle, C. S. (1996). "Bench-scale evaluation of bioaugmentation to remediate carbon tetrachloride-contaminated aquifer materials." *Ground Water*, 34(2), 358-367.

McCarty, P. L., Goltz, M. N., Hopkins, G. D., Dolan, M. E., Allan, J. P., Kawakami, B. T., and Carrothers, T. J. (1998). "Full scale evaluation of in situ cometabolic degradation of trichloroethylene in groundwater through toluene injection." *Environmental Science & Technology*, 32(1), 88-100.

Ndon, U. J., Randall, A. A., and Khouri, T. Z. (2000). "Reductive dechlorination of tetrachloroethylene by soil sulfate-reducing microbes under various electron donor conditions." *Environmental Monitoring and Assessment*, 60(3), 329-336.

NRC. (2000). *Natural attenuation for groundwater remediation*, National Academy Press, Washington, D.C.

Richmond, S. A., Lindstrom, J. E., and Braddock, J. F. (2001). "Assessment of natural attenuation of chlorinated aliphatics and BTEX in subarctic groundwater." *Environmental Science & Technology*, 35(20), 4038-4045.

Röling, W. F. M., and van Verseveld, H. W. (2002). "Natural attenuation: What does the subsurface have in store?" *Biodegradation*, 13(1), 53-64.

Suarez, M. P., and Rifai, H. S. (2002). "Evaluation of BTEX remediation by natural attenuation at a coastal facility." *Ground Water Monitoring and Remediation*, 22(1), 62-77.

Vogel, T. M., Criddle, C., and McCarty, P. L. (1987). "Transformation of halogenated aliphatic compounds." *Environmental Science & Technology*, 21, 722-736.

Vogel, T. M., and McCarty, P. L. (1987). "Abiotic and biotic transformation of 1,1,1-trichloroethane under methanogenic conditions." *Environmental Science & Technology*, 21, 1208-1213.

Weaver, J. W., Wilson, J. T., and Kampbell, D. H. "Case study of natural attenuation of trichloroethene at St. Joseph, Michigan." *Proceedings of the symposium on natural attenuation of chlorinated organics in ground water*, Dallas, TX, 67-70.

Witt, M. E., Dybas, M. J., Worden, R. M., and Criddle, C. S. (1999). "Motility-enhanced bioremediation of carbon tetrachloride- contaminated aquifer sediments." *Environmental Science & Technology*, 33(17), 2958-2964.

Witt, M. E., Klecka, G. M., Lutz, E. J., Ei, T. A., Grosso, N. R., and Chapelle, F. H. (2002). "Natural attenuation of chlorinated solvents at Area 6, Dover Air Force Base: groundwater biogeochemistry." *Journal of Contaminant Hydrology*, 57(1-2), 61-80.

Yang, Y. R., and McCarty, P. L. (1998). "Competition for hydrogen within a chlorinated solvent dehalogenating anaerobic mixed culture." *Environmental Science & Technology*, 32(22), 3591-3597.

# CHAPTER 4

## DEVELOPMENT AND APPLICATION OF A NATURAL ATTENUATION MODEL FOR A VOC CONTAMINATED AQUIFER UNDER LIMITED ELECTRON DONOR CONDITIONS

### 4.1 Abstract

A reductive dechlorination model considering the bioavailability and of electron donors was develop to be included in the mathematical formulation of natural attenuation. This model was first tested in a hypothetical batch reactor to evaluate the behavior of the mathematical expression and evaluate mass conservation at the end of the simulation. Toluene was modeled as the electron donor with an initial concentration of 100μg/L. This concentration was not in stoichiometric excess for complete degradation of the VOC in the reactor. It was assumed that PCE and TCE were initially present in the reactor in equilibrium with the solid-phase. Liquid-phase concentration of PCE and TCE were 100 and 50μg/L, respectively. Results showed incomplete degradation of PCE due to a lack of electron donors capable to sustain an active population of dehalogenators. Also, accumulation of cis-DCE and VC was observed at the end of the modeling period.

The developed model was applied to a VOC contaminated aquifer in Schoolcraft, MI to evaluate the relative importance of reductive dechlorination in the natural attenuation process occurring at this site. Based on the plume distributions at two different time periods it was concluded that reductive dechlorination will not play a significant role in the natural attenuation process due to the lack of electron donor sources capable of maintaining reduced conditions. The use of Monod-type kinetics in the

mathematical formulation of reductive dechlorination makes the model difficult to apply because of the significant number of constant parameters involved.

## 4.2 Introduction

Chlorinated aliphatic hydrocarbons are the most frequent detected contaminants in groundwater due to their widespread use in chemical dry cleaning and as metal degreasing agents (Ferguson and Pietari 2000; Middledorp *et al.* 1999; Shouakar-Stash *et al.* 2003). Once in the groundwater, these contaminants tend to dissolve in the groundwater contaminating large volumes of soil and water. Due to their resistance to chemical and biological breakdown, they tend to persist in groundwaters for long periods of time posing a risk to the human health and the environment.

Monitored natural attenuation has emerged as a potential remedy for chlorinated solvent contamination because it is less expensive and in some cases more practical than engineered cleanup solutions (Richmond *et al.* 2001). Natural attenuation of chlorinated solvents has been successfully demonstrated in field and laboratory microcosm studies (Delvin *et al.* 2002; Kao and Wang 2001; Ndon *et al.* 2000).

Witt *et al.* (2002) used the "lines of evidence" approach adopted by the US Environmental Protection Agency (1998) to document the occurrence of natural attenuation of chlorinated solvents at the Dover Air Force Base in Delaware. Biological and geochemical data collected over a two-year period support the hypothesis that sequential anaerobic and aerobic degradation of chlorinated solvents are occurring at this site. Biological destruction of PCE and TCE was most likely due to reductive dechlorination processes; however, the bioavailability of potential electron donors was

not evaluated in this study.

The same protocol was implemented at a Brooklawn hazardous waste site in Baton Rouge, LO (USA) to evaluate the extent to which natural attenuation is responsible for the observed decline in contaminant mass (Clement *et al.* 2002). The hazardous waste plume generated from the source contained around twelve different chlorinated organic compounds. Site-specific data indicated that chlorinated ethene and ethane compounds are being attenuated within 300m downgradient from the source. A swamp located upstream of the contaminated site is believed to provide the organic carbon necessary for the biological destruction of the chlorinated compounds. Based on the site's conceptual model, it was concluded that reductive dechlorination process is occurring with excess of electron donor. Although the carbon source in this study seems to be adequate to support reductive dechlorination for a long period of time, an analysis of the potential to rely on natural attenuation as a sole treatment technique to reduce contaminants to regulatory standards was not conducted.

To assess potential future extent of plume migration and the sustainability of the natural attenuation process it is necessary to include in the conceptual model all the physical, chemical, and biological processes that play a key role in transport and degradation of the contaminants. Of those mechanisms, biological destruction has received broader attention since it is not a reversible process such as sorption and does not involve a contaminant phase transfer such as volatilization.

Under natural conditions, it has been recognized that reductive dechlorination is the biological mechanism responsible for the observed degradation of chlorinated compounds (McCarty 1997) although cis-DCE and VC are susceptible to aerobic

degradation (Klier *et al.* 1999; Vogel *et al.* 1987). The complete destruction of PCE and TCE to ethene requires, among other things, a supply of electron donors that microorganisms can use for growth and maintenance. Conceptual and numerical models usually ignore the presence of a carbon source needed for reductive dechlorination.

To date, most models of natural attenuation of chlorinated solvents do not assess the bioavailability of carbon sources to sustain complete depletion of VOC compounds. Fennell and Gossett (1998) pointed out that the complex nature of reductive dechlorination has not been addressed in fate and transport models applied to natural attenuation and demonstrated that the inclusion of a bio-kinetic term for hydrogen utilization in the mathematical expression for reductive dechlorination closely matched data collected in batch reactors. Another study by Haston and McCarty (1999) suggested that zero-order or Monod kinetics were more appropriate than first-order kinetics to model reductive dechlorination processes occurring in microcosms amended with PCE as the electron acceptor and hydrogen as the electron donor. In this study, however, the electron donor was in excess to ensure complete dechlorination of PCE to ethene.

The objective of this study is to develop a reductive dechlorination numerical model coupled to oxidation of a carbon source and assess if availability of the electron donor is limiting the biological component of natural attenuation in a contaminated aquifer. Toluene was used as the electron donor for the microbial population and PCE and TCE were used as electron acceptors according to the redox stoichiometry presented. The model was initially tested in a hypothetical batch reactor to evaluate the behavior of the mathematical expressions. The model was applied to a VOC contaminated site to study the natural attenuation process occurring. It is believed that this approach to model

natural attenuation will help to assess the sustainability of biological destruction of VOC

compounds at other sites where reductive dechlorination is occurring.

## 4.3 Model development and methodology

*Reductive dechlorination stoichiometry with toluene as electron donor*

The stoichiometric equations describing reductive dechlorination with toluene as

the electron donor can be obtained by combining appropriate half-reaction expressions.

The following equations were combined and represent the conceptual model for reductive

dechlorination with toluene as the electron donor:

$$\underset{\text{PCE}}{18C_2Cl_4} + 14H_2O + \underset{\text{toluene}}{C_6H_5CH_3} \xrightarrow{\text{microbes}} \underset{\text{TCE}}{18C_2HCl_3} + 7CO_2 + 18H^+ + 18Cl^- \quad (4.1)$$

$$\underset{\text{TCE}}{18C_2HCl_3} + 14H_2O + C_6H_5CH_3 \xrightarrow{\text{microbes}} \underset{\text{cisDCE}}{18C_2H_2Cl_2} + 7CO_2 + 18H^+ + 18Cl^- \quad (4.2)$$

$$\underset{\text{cisDCE}}{18C_2H_2Cl_2} + 14H_2O + C_6H_5CH_3 \xrightarrow{\text{microbes}} \underset{\text{VC}}{18C_2H_3Cl} + 7CO_2 + 18H^+ + 18Cl^- \quad (4.3)$$

$$\underset{\text{VC}}{18C_2H_3Cl} + 14H_2O + C_6H_5CH_3 \xrightarrow{\text{microbes}} \underset{\text{ethene}}{18C_2H_4} + 7CO_2 + 18H^+ + 18Cl^- \quad (4.4)$$
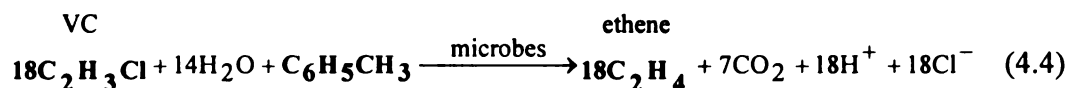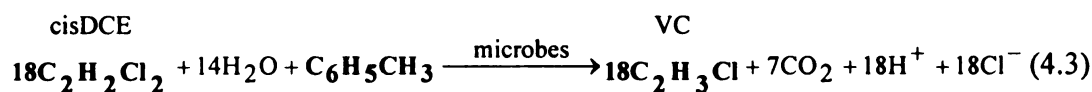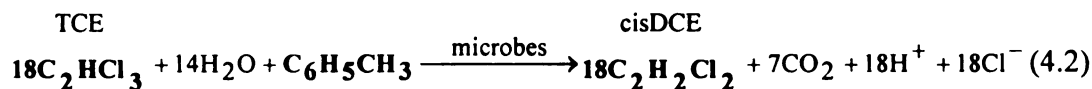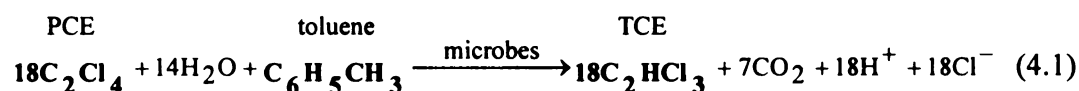
A general pathway showing the sequence of degradation of the chlorinated

compounds catalyzed by microbial activity is given in Figure 4.1. Gibbs free energy
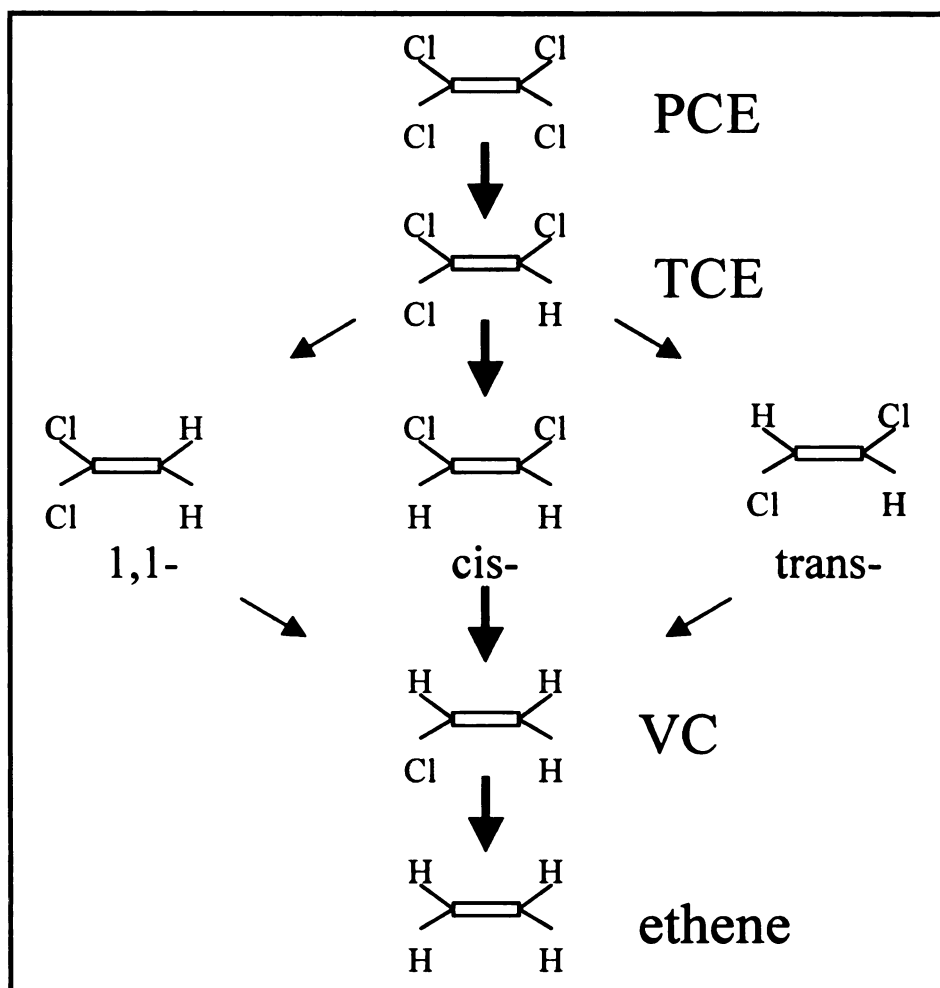
Figure 4.1. General pathway for the reductive dechlorination process of PCE to ethene. Bold arrows indicate the most likely pathway under the influence of microbial processes (Garant & Lynd, 1998).

calculations show that all these reactions are feasible at standard temperature and

pressure (Table 4.1). However, the reductive dechlorination pathway is a step-by-step

process in a series that is generally; but not always, catalyzed by more than one organism

that ultimately leads to the formation of ethene (Dolfing 2000).

The simplified stoichiometric reactions presented here ignore intermediate steps

in the reductive dechlorination process. It is important to emphasize that those

Table 4.1. Gibbs free energy for reductive dechlorination
with toluene as the electron donor.

| Electron Acceptor | $\Delta G^{\circ\prime}$ kcal/mole [a] |
|---|---|
| PCE | -425.6 |
| TCE | -404.9 |
| cis-DCE | -340.1 |
| VC | -331.5 |

[a] at 298 K and 1 atm

intermediate steps determine what type of electron accepting process will ultimately take place in a contaminated environment and consequently certain microbial populations will outcompete others for preferential consumption of those intermediate metabolites. Such is the case for hydrogen. Research has shown that anaerobic hydrogen production in natural environments determines the type of electron accepting processes that will be favored (Lovley *et al.* 1994; Lovley and Goodwin 1988). Researchers have tried to correlate hydrogen concentration with specific reductive dechlorination process (Fennell and Gossett 1998; Haston and McCarty 1999; Yang and McCarty 1998). In general, it has been found that hydrogen concentrations above 5 nm produced favorable conditions for chloroethene dechlorination (Meer *et al.* 2001).

*Kinetic model for electron donor*

Reductive dechlorination kinetics is coupled to toluene degradation using Monod expressions. Although different microbial populations can be involved in this complex process (McCarty 1997), it was assumed that a single population growing on toluene was capable of using the chlorinated ethenes as electron acceptors. Competitive inhibition was not modeled here since those kinetic expressions would tend to complicate further the application of the model to the aquifer environment and there is no evidence that such

a formulation will improve model predictions in natural environments.

Based on Monod kinetics, the rate of toluene utilization by the dehalogenators would be:

$$\frac{d[tol]}{dt} = -q_{max}[X]\left(\frac{[tol]}{[tol]+K_{s[tol]}}\right) - \xi_{[tol]}\left([tol] - \frac{[tol]_{soil}}{K_{d[tol]}}\right) \qquad (4.5)$$

where $[tol]$ is the concentration of toluene [M L$^{-3}$]; $q_{max}$ is the maximum specific toluene utilization rate [M M$^{-1}$ T$^{-1}$]; $[X]$ is the biomass concentration [M L$^{-3}$]; $K_{s[tol]}$ is the half-velocity coefficient for toluene consumption [M L$^{-3}$]; $[tol]_{soil}$ is the solid-phase toluene concentration [M M$^{-1}$]; $\xi_{[tol]}$ is the first-order mass transfer coefficient between liquid and solid phase; $K_{d[tol]}$ is the toluene partitioning coefficient [L$^{3}$ M$^{-1}$]; and t is the time [T].

Transfer of toluene between solid and liquid phase is modeled assuming first order mass transfer kinetics. Solid-phase concentration of toluene is given by:

$$\frac{d[tol]_{soil}}{dt} = \frac{\phi\,\xi_{[tol]}}{\rho}\left([tol] - \frac{[tol]_{soil}}{K_{d[tol]}}\right) \qquad (4.6)$$

where $\phi$ is the soil porosity [L$^{3}$ L$^{-3}$]; and $\rho$ is the bulk density of the soil matrix [M L$^{-3}$];

The net rate of active biomass growing on the dissolved toluene using chlorinated ethene compounds as electron acceptors can be written as:

$$\frac{d[X]}{dt} = \mu_{max}[X]\left(\frac{[tol]}{[tol]+K_{s[tol]}}\right) - b[X] \qquad (4.7)$$

where $\mu_{max}$ is the maximum specific growth rate of dehalogenators [$T^{-1}$], and b is the

cell endogenous decay coefficient [$T^{-1}$]. Limitation on growth with respect to electron

acceptors was not considered since it was assumed that VOC compounds are in excess

and the reductive dechlorination process is controlled by the bioavailability of electron

donors.

The relation between biomass growth rate and substrate utilization is given by:

$$\mu_{max} = q_{max} Y_{[X]/[tol]} \qquad (4.8)$$

where $Y_{[X]/[tol]}$ is the yield coefficient for cell synthesis [$M M^{-1}$].

*Kinetic model for reductive dechlorination*

Chlorinated compounds are modeled as a kinetic limited liquid-solid phase with

biological degradation in the liquid phase. The concentration of the PCE on the liquid

phase is given by:

$$\frac{d[PCE]}{dt} = -\hat{q}_{[PCE]}[X]\left(\frac{[PCE]}{[PCE]+K_{s[PCE]}}\right) - \xi_{[PCE]}\left([PCE] - \frac{[PCE]_{soil}}{K_{d[PCE]}}\right) \qquad (4.9)$$

where [PCE ] is the liquid phase PCE concentration [$M L^{-3}$]; $\hat{q}_{[PCE]}$ is the maximum

92

specific utilization rate of PCE [M $M^{-1}$ $T^{-1}$]; $K_{s[PCE]}$ is the PCE half-velocity coefficient

[M $L^{-3}$]; $\xi_{[PCE]}$ is the first-order mass transfer rate coefficient [$T^{-1}$]; $[PCE]_{soil}$ is the

sorbed PCE concentration [M $M^{-1}$]; and $K_{d[PCE]}$ is the PCE partitioning coefficient

between the solid and the liquid phase [L-3 M-1]. The first term on right hand side of

Equation 4.9 represents the utilization of PCE by dehalogenators and the second term is

the kinetic limited sorption-desorption. A mass balance of PCE on the solid phase yields:

$$\frac{d[PCE]_{soil}}{dt} = \frac{\phi \, \xi_{[PCE]}}{\rho} \left( [PCE] - \frac{[PCE]_{soil}}{K_{d[PCE]}} \right) \qquad (4.10)$$

Utilization of PCE as the electron acceptor during toluene degradation will yield a

stoichiometric amount of TCE (Equation 4.1). The utilization rate of TCE can be found

by:

$$\frac{d[TCE]}{dt} = Y_{[TCE]/[PCE]} \, \hat{q}_{[PCE]} [X] \left( \frac{[PCE]}{[PCE] + K_{s[PCE]}} \right) -$$

$$\hat{q}_{[TCE]} [X] \left( \frac{[TCE]}{[TCE] + K_{s[TCE]}} \right) - \xi_{[TCE]} \left( [TCE] - \frac{[TCE]_{soil}}{K_{d[TCE]}} \right) \qquad (4.11)$$

where $Y_{[TCE]/[PCE]}$ is the stoichiometric yield of PCE to TCE [M $M^{-1}$]; [TCE ] is the

liquid phase TCE concentration [M $L^{-3}$]; $\hat{q}_{[TCE]}$ is the maximum specific utilization rate

of TCE [M $M^{-1}$ $T^{-1}$]; $K_{s[TCE]}$ is the TCE half-velocity coefficient [M $L^{-3}$]; $\xi_{[TCE]}$ is the

TCE first-order mass transfer rate coefficient $[T^{-1}]$; $[TCE]_{soil}$ is the sorbed TCE

concentration $[M\ M^{-1}]$; and $K_{d[TCE]}$ is the TCE partitioning coefficient between solid

and liquid phase. The first term on the right hand side of Equation 4.11 is the metabolic

production of TCE due to PCE degradation. The second and third terms represents

biodegradation and sorption-desorption processes, respectively. Solid-phase TCE

concentration is given by:

$$\frac{d[TCE]_{soil}}{dt} = \frac{\phi\ \xi[TCE]}{\rho}\left([TCE] - \frac{[TCE]_{soil}}{K_{d[TCE]}}\right) \tag{4.12}$$

Similarly, expressions for the rate of production and consumption for DCE, VC,

and ethene can be obtained. A mass balance on the liquid and solid phase for DCE, VC,

and ethene will give:

$$\frac{d[DCE]}{dt} = Y_{[DCE]/[TCE]}\,\hat{q}_{[TCE]}\,[X]\left(\frac{[TCE]}{[TCE]+K_{s[TCE]}}\right)$$
$$-\hat{q}_{[DCE]}\,[X]\left(\frac{[DCE]}{[DCE]+K_{s[DCE]}}\right) - \xi_{[DCE]}\left([DCE] - \frac{[DCE]_{soil}}{K_{d[DCE]}}\right) \tag{4.13}$$

$$\frac{d[DCE]_{soil}}{dt} = \frac{\phi\ \xi[DCE]}{\rho}\left([DCE] - \frac{[DCE]_{soil}}{K_{d[DCE]}}\right) \tag{4.14}$$

94

$$\frac{d[VC]}{dt} = Y_{[VC]/[DCE]} \hat{q}_{[DCE]} [X] \left( \frac{[DCE]}{[DCE] + K_s [DCE]} \right)$$

$$- \hat{q}_{[VC]} [X] \left( \frac{[VC]}{[VCE] + K_s [VC]} \right) - \xi_{[VC]} \left( [VC] - \frac{[VC]_{soil}}{K_{d[VC]}} \right) \tag{4.15}$$

$$\frac{d[VC]_{soil}}{dt} = \frac{\phi \, \xi_{[VC]}}{\rho} \left( [DCE] - \frac{[VC]_{soil}}{K_{d[VC]}} \right) \tag{4.16}$$

$$\frac{d[ethene]}{dt} = Y_{[ethene]/[VC]} \hat{q}_{[VC]} [X] \left( \frac{[VC]}{[VC] + K_s [VC]} \right)$$

$$- \xi_{[VC]} \left( [VC] - \frac{[VC]_{soil}}{K_{d[VC]}} \right) \tag{4.17}$$

$$\frac{d[ethene]_{soil}}{dt} = \frac{\phi \, \xi_{[ethene]}}{\rho} \left( [ethene] - \frac{[ethene]_{soil}}{K_{d[ethene]}} \right) \tag{4.18}$$

Reaction terms for DCE, VC, and ethene are analogous to the terms in the PCE and TCE equations.

*Batch mode testing*

Equations 4.5 to 4.18 were coded in FORTRAN and solved for a hypothetical batch reactor using RT3D (Clement 1997). For this experiment, a batch reactor with a toluene concentration of $100\mu g/L$ was used. This concentration was not in stoichiometric excess with respect to PCE or TCE. Starting concentrations of liquid-phase PCE and

**Table 4.2. Parameters for the reductive dechlorination model.**

| Parameter | Definition | Value | Model Value | Source |
|---|---|---|---|---|
| $K_s \, [\text{tol}]$ | half-velocity coefficient for toluene, $\text{mg L}^{-1}$ | 35.0 − 59.0 | 35.0 | Elmen *et al.* (1997) |
| $K_d \, [\text{tol}]$ | toluene partitioning coefficient, $\text{L mg}^{-1}$ | $6.6 \times 10^{-7}$ − $2.28 \times 10^{-6}$ | | calculated based on $f_{oc}$ (Zhao *et al.*, 1999) |
| $q_{max}$ | maximum toluene utilization rate, $\text{d}^{-1}$ | 0.2 − 3.97 | 0.3 | Elmen *et al.* (1997) |
| $\mu_{max}$ | maximum biomass specific growth rate, $\text{d}^{-1}$ | 0.1 − 6.03 | 0.46 | Elmen *et al.* (1997) |
| $Y \, [\text{x}]/[\text{tol}]$ | yield coefficient for toluene degraders, $\text{mg VSS mg tol}^{-1}$ | 0.64 | 0.64 | Reardon *et al.* (2000) |
| $b$ | endogenous cell decay coefficient, $\text{d}^{-1}$ | 0.001 − 0.3 | 0.1 | Assumed |
| $\hat{q}[\text{PCE}]$ | maximum specific PCE utilization rate, $\text{d}^{-1}$ | 0.0035 − 0.0046 | 0.004 | EPA (1999) |
| $K_s \, [\text{PCE}]$ | half velocity coefficient for PCE , $\text{mg L}^{-1}$ | 0.008 − 32.8 | 0.008 | Rittman & McCarty (2001) |
| $\xi[\text{PCE}]$ | mass transfer rate coefficient for PCE, $\text{d}^{-1}$ | 0.0001 − 0.1 | 0.1 | Clement & Jones (1998) |
| $K_d \, [\text{PCE}]$ | PCE partitioning coefficient, $\text{L mg}^{-1}$ | $1.25 \times 10^{-6}$ − $2.15 \times 10^{-6}$ | $1.3 \times 10^{-6}$ | calculated based on $f_{oc}$ (Zhao *et al.*, 1999) |
| $\phi$ | soil porosity | 0.2 − 0.4 | 0.35 | measured from laboratory re-packed columns |
| $\rho$ | bulk density of soil matrix, $\text{mg L}^{-1}$ | $1.59 \times 10^6$ | $1.59 \times 10^6$ | Zhao *et al.* (1999) |
| $\hat{q}[\text{TCE}]$ | maximum TCE utilization rate, $\text{d}^{-1}$ | 0.006 − 0.008 | 0.007 | EPA (1999) |
| $Y \, [\text{TCE}]/[\text{PCE}]$ | PCE to TCE stoichiometric yield coefficient, $\text{mg TCE mg PCE}^{-1}$ | 0.79 | 0.79 | from stoichiometric equations |
| $K_s \, [\text{TCE}]$ | half velocity coefficient for TCE, $\text{mg L}^{-1}$ | 0.18 − 31.2 | 0.18 | Rittman & McCarty (2001) |
| $\xi[\text{TCE}]$ | mass transfer rate coefficient for TCE, $\text{d}^{-1}$ | 0.0001 − 0.1 | 0.1 | Clement & Jones (1998) |
| $K_d \, [\text{TCE}]$ | TCE partitioning coefficient, $\text{L mg}^{-1}$ | $0.52 \times 10^{-6}$ − $0.9 \times 10^{-6}$ | $0.7 \times 10^{-6}$ | calculated based on $f_{oc}$ (Zhao *et al.*, 1999) |
| $\hat{q}[\text{DCE}]$ | maximum DCE utilization rate, $\text{d}^{-1}$ | 0.058 − 0.547 | 0.09 | Rittman & McCarty (2001) |
| $Y \, [\text{DCE}]/[\text{TCE}]$ | TCE to DCE stoichiometric yield coefficient, $\text{mg DCE mg TCE}^{-1}$ | 0.57 | 0.57 | from stoichiometric equations |
| $K_s \, [\text{DCE}]$ | half velocity coefficient for DCE, $\text{mg L}^{-1}$ | 0.288 − 0.371 | 0.290 | Rittman & McCarty (2001) |
| $\xi[\text{DCE}]$ | mass transfer rate coefficient for DCE, $\text{d}^{-1}$ | 0.0001 − 0.1 | 0.1 | Clement & Jones (1998) |

**Table 4.2. (continued)**

| Parameter | Definition | Value | Model Value | Source |
|---|---|---|---|---|
| $K_{d\,[DCE]}$ | TCE partitioning coefficient, L mg$^{-1}$ | $0.29 \times 10^{-6} - 0.48 \times 10^{-6}$ | $0.4 \times 10^{-6}$ | calculated based on $f_{oc}$ (Zhao et al., 1999) |
| $\hat{q}_{[VC]}$ | maximum VC utilization rate, d$^{-1}$ | $0.037 - 0.285$ | $0.05$ | Rittman & McCarty (2001) |
| $Y_{[VC]/[DCE]}$ | DCE to VC stoichiometric yield coefficient, mg VC mg DCE$^{-1}$ | $0.65$ | $0.65$ | from stoichiometric equations |
| $K_{s\,[VC]}$ | half velocity coefficient for VC , mg L$^{-1}$ | $0.161 - 22.3$ | $0.161$ | Rittman & McCarty (2001) |
| $\xi_{[VC]}$ | mass transfer rate coefficient for VC, d$^{-1}$ | $0.0001 - 0.1$ | $0.1$ | Clement & Jones (1998) |
| $K_{d\,[VC]}$ | VC partitioning coefficient, L mg$^{-1}$ | $2.0 \times 10^{-9} - 3.4 \times 10^{-7}$ | $2.0 \times 10^{-9}$ | calculated based on $f_{oc}$ (Zhao et al., 1999) |
| $Y_{[ethene]/[VC]}$ | VC to ethene stoichiometric yield coefficient, mg VC mg DCE$^{-1}$ | $0.45$ | $0.45$ | from stoichiometric equations |
| $\xi_{[ethene]}$ | mass transfer rate coefficient for ethene, d$^{-1}$ | $0.0001 - 0.1$ | $0.1$ | Clement & Jones (1998) |
| $K_{d\,[ethene]}$ | ethene partitioning coefficient, L mg$^{-1}$ | $1.0 \times 10^{-9} - 3.6 \times 10^{-7}$ | $1.0 \times 10^{-9}$ | calculated based on $f_{oc}$ (Zhao et al., 1999) |

TCE were 100 and 50μg/L, respectively. An initial concentration of toluene degraders equal to 0.001 mg VSS/L was assumed to be present in the reactor. Total porosity in the reactor was 0.30 and the soil bulk density was $1.6 \times 10^{-6}$ mg/L. Constant parameters for the equations were extracted from laboratory and field studies in the literature and are listed in Table 4.2.

To evaluate mass conservation of the numerical scheme an equivalent PCE concentration computed on the basis of all chlorinated ethene compounds was compared at any two selected time steps. Equation 4.19 was used to calculate the equivalent PCE concentration at any time, $t$:

$$[PCE]_{eq} = \left\{ [PCE] + \frac{[PCE]_{soil}\,\rho}{\phi} + \left( [TCE] + \frac{[TCE]_{soil}\,\rho}{\phi} \right) \left( \frac{1}{Y_{[TCE]/[PCE]}} \right) \right.$$

$$+ \left( [DCE] + \frac{[DCE]_{soil}\,\rho}{\phi} \right) \left( \frac{1}{Y_{[DCE]/[TCE]}\, Y_{[TCE]/[PCE]}} \right)$$

$$+ \left( [VC] + \frac{[VC]_{soil}\,\rho}{\phi} \right) \left( \frac{1}{Y_{[VC]/[DCE]}\, Y_{[DCE]/[TCE]}\, Y_{[TCE]/[PCE]}} \right) \quad (4.19)$$

$$+ \left( [ethene] + \frac{[ethene]_{soil}\,\rho}{\phi} \right)$$

$$\left. \times \left( \frac{1}{Y_{[ethene]/[VC]}\, Y_{[VC]/[DCE]}\, Y_{[DCE]/[TCE]}\, Y_{[TCE]/[PCE]}} \right) \right\}_t$$

*Model application to a VOC contaminated aquifer*

The developed model was applied to a VOC contaminated aquifer located in Schoolcraft, MI (USA). Regional and local hydrogeologic conditions for this site have been described elsewhere (Lipinski 2002; Dybas *et al.* 1998; Mayotte *et al.* 1996). The unconfined aquifer has been contaminated with organic and heavy metal compounds as result of previous industrial activities (Figure 4.2). A VOC plume extending approximately 2 km southeast of the suspected source has developed. ARCO Industries, a former manufacturer of automobile plastic parts was identified as the source of this contamination, which impacts an estimated $1.3 \times 10^7 m^3$ aquifer materials.

The existence of metabolic by-products of degradation of PCE and TCE confirm that biological destruction of these compounds have occurred in the past. However, data collected over the last 2 years reveal that reductive dechlorination is not a major component of the current natural attenuation process. Initial soil contamination reports revealed that not only PCE and TCE were handled at this facility but also toluene and

other BTEX compounds. However, none of these compounds have been detected in recent groundwater and soil samples. It is believed that once the electron donors were depleted, reductive dechlorination ceased and only physical processes are responsible for the natural attenuation of VOC compounds at this site. The reductive dechlorination model developed in this study will be used to gain an understanding of the processes that lead to the transport and spread of these contaminants.

*Reactive transport model for the Plume G site*

The following expression (Bear 1979) was used to simulate groundwater flow in the area of interest:

$$\frac{\partial}{\partial x_i}\left(K_i \frac{\partial h}{\partial x_i}\right) + q_s = S_y \frac{\partial h}{\partial t} \qquad (4.20)$$

where $x_i$ is distance along the respective Cartesian coordinate [L]; $K_i$ is the principal component of the hydraulic conductivity tensor [L $T^{-1}$]; h is the hydraulic head [L]; $q_s$ is the fluid source-sink term [L $T^{-1}$]; $S_y$ is the specific storage of the aquifer [$L^{-1}$]; and t is the time, [T].

The concentration of each chlorinated ethene compounds along with toluene and dehalogenators can be found by (Clement *et al.* 1998):

$$\frac{\partial C_k}{\partial t} + \frac{\rho}{\phi}\frac{\partial \tilde{C}_k}{\partial t} = \frac{\partial}{\partial x_i}\left(D_{ij}\frac{\partial}{\partial x_j}\right) - \frac{\partial}{\partial x_i}(v_i C_k) + \frac{q_s}{\phi}C_k' + R_k \qquad (4.21)$$

where $C_k$ is the dissolved concentration of the $k^{th}$ specie [M L$^{-3}$]; $\tilde{C}_k$ is concentration of

the $k^{th}$ species sorbed on the subsurface solids [M M$^{-1}$]; $D_{ij}$ is the hydrodynamic

dispersion coefficient tensor [L$^2$ T$^{-1}$]; $C'_k$ is the source-sink flux term concentration for

the $k^{th}$ species [M·L$^{-3}$]; and $R_k$ is the reaction term for the $k^{th}$ specie. The reaction terms

for the dissolved species and the solid-phase concentrations are defined by Equations 4.5

through 4.18.

Figure 4.2 shows the model domain and the wells where pump tests were

conducted to define the hydraulic conductivity field of the unconfined contaminated

aquifer. The constant head boundaries surrounding the area were defined by telescopic

grid refinement (Anderson and Woessner 1992) from a regional groundwater flow model

developed by Lipinski (2002). The regional model considers all the major hydrogeologic

features of the area and extends the boundaries to lakes, rivers, and aquifer no-flow

boundaries that control groundwater movement in the vicinity.

The flow and transport models were solved numerically using MODFLOW 2000

(Harbaugh *et al.* 2000) and RT3D (Clement 1997), respectively. The "user-defined

reactions" module was used for the partial differential equations describing the reductive

dechlorination process. The FORTRAN code for the reactions is given in Appendix III.

Model parameters and initial conditions for the species involved are given in Table 4.3.
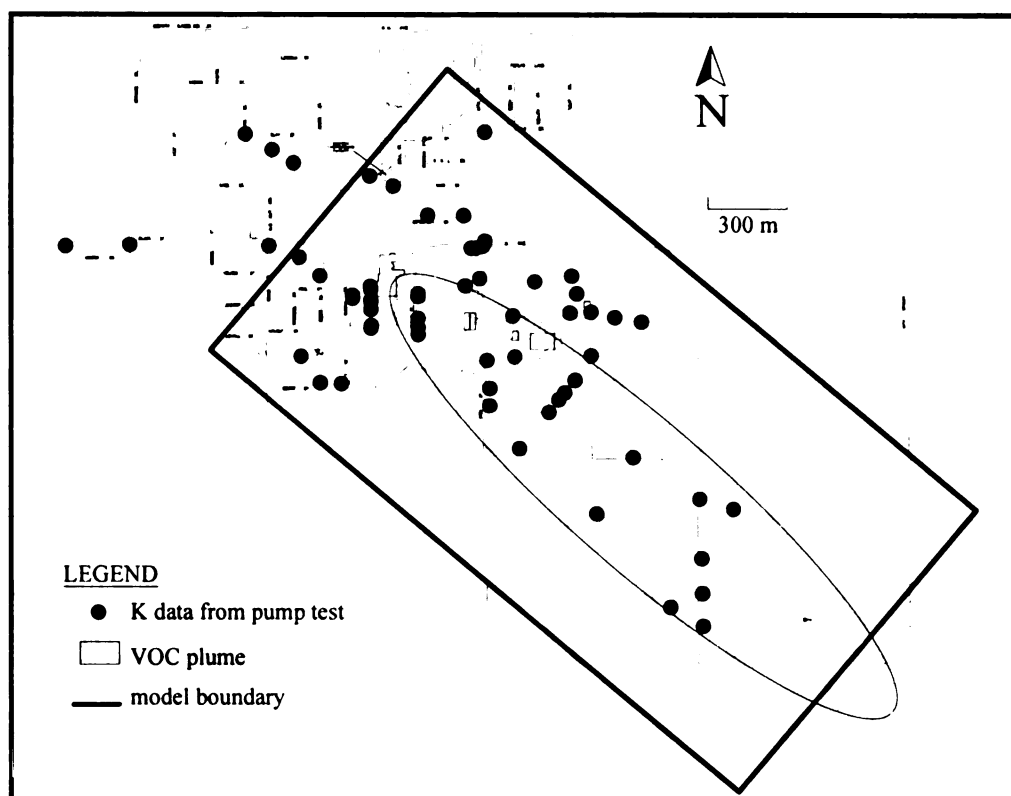
Figure 4.2. Site location and model boundaries for reactive transport simulation.

Table 4.3. Flow model parameters and initial conditions for the natural attenuation simulation of the VOC contaminated site.

| Model parameter | Value |
|---|---|
| *Flow Model (steady state)* | |
| hydraulic conductivity, cm s$^{-1}$ | values kriged from 89 pump tests |
| effective porosity | 0.2 – 0.3 |
| boundary conditions | from Lipinski (2002) |
| recharge, m day$^{-1}$ | 6.1x10$^{-4}$ |
| *Reactive Transport Model* | |
| stress periods | Loading period: 1953 ~ 1988 (35 yrs) |
| | no loads: 1988 ~ 2003 (15 yrs) |
| *Starting concentrations* | |
| Toluene, μg L$^{-1}$ | 500 |
| Toluene sorb, μg Kg$^{-1}$ | 330 |
| PCE, μg L$^{-1}$ | 150 |
| PCE sorb, μg Kg$^{-1}$ | 190 |
| TCE, μg L$^{-1}$ | 1000 |
| TCE sorb, μg Kg$^{-1}$ | 520 |
| cis-DCE, μg L$^{-1}$ | 0.0 |
| cis-DCE sorb, μg Kg$^{-1}$ | 0.0 |
| VC, μg L$^{-1}$ | 0.0 |
| VC sorb, μg Kg$^{-1}$ | 0.0 |
| dehalogenators, mg VSS L$^{-1}$ | 0.001 |

## 4.4 Results and discussion

*Reactions batch mode testing*

Initial liquid-phase concentrations of toluene, PCE, and TCE in the batch reactor were 100, 100, and 50µg/L, respectively. Concentration of cis-DCE, VC, and ethene were assumed equal to zero since these two compounds were expected by-products of the utilization of PCE and TCE.

The relation between toluene degradation and growth of dehalogenators is shown in Figure 4.3. An initial acclimation period of 40 days is required to develop a biomass concentration that can degrade the available toluene in the theoretical reactor. Biomass concentration reaches a maximum of 80mg VSS/L at approximately 50 days following toluene addition. These reactions were modeled for a total of 150 days with a time step
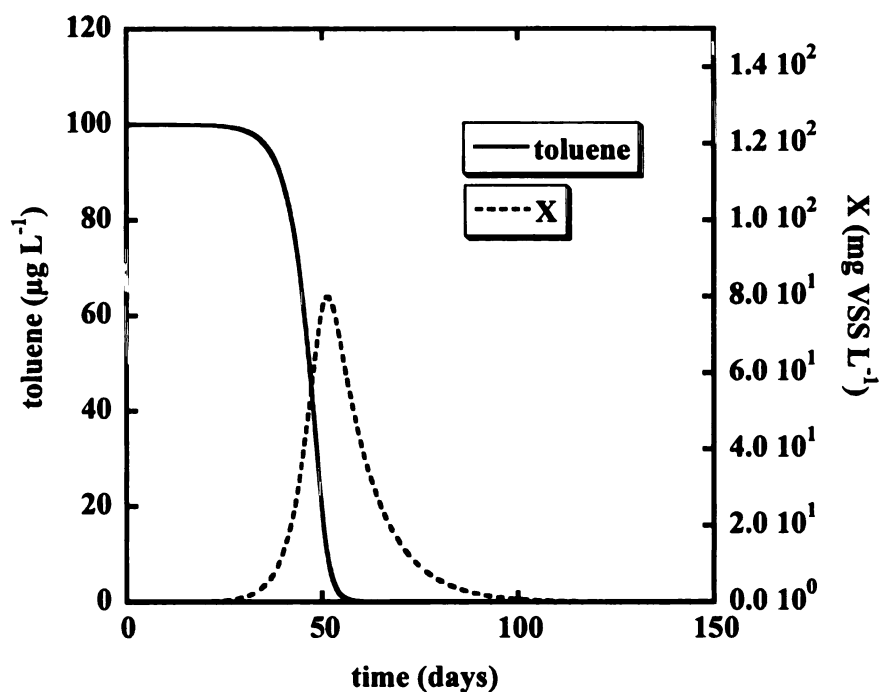
Figure 4.3. Toluene and biomass concentration in the hypothetical batch reactor simulation.

of 2.4 hours. Total utilization of toluene is achieved in approximately 60 days. The specific toluene utilization rate was $0.3d^{-1}$ and the maximum growth rate used was $0.456d^{-1}$.

Figure 4.4 shows the PCE concentration in the liquid and the solid phase. Utilization of the PCE as the electron acceptor starts approximately at the same time of toluene utilization. Complete degradation of PCE is not achieved since activity of dehalogenators decrease when toluene is utilized and there is no alternate substrate that can promote its growth. At the end of the simulation period, a liquid phase PCE concentration of $42\mu g/L$ is still present in the reactor.

The solid phase PCE concentration starts desorbing from the solid particles as soon as the concentration in the liquid phase decreases. This desorption process occur to maintain equilibrium between the solid and the liquid phase. However, the slope of the liquid-phase PCE degradation curve in the interval where PCE is being utilized is steeper than its solid counterpart due to a kinetically controlled mass transfer mechanism between the two phases. At the end of the simulation period, a solid-phase PCE concentration of approximately $4 \times 10^{-6}\mu g/mg$ will remain attached to the solid particles.

PCE degradation will yield a TCE amount according to the stoichiometry given in Equation 4.1. An initial $50\mu g/L$ of TCE was added to the model reactor. Figure 4.5 shows that TCE remains unchanged for approximately 50 days until a decrease in concentration is observed. An increase in the liquid TCE concentration due to the utilization of PCE was not observed. The reason could be the slightly higher TCE utilization rate (Table 4.2) used in the simulation. This model predicts that approximately $15\mu g/L$ of TCE will remain in the reactor at the end of 150 days.
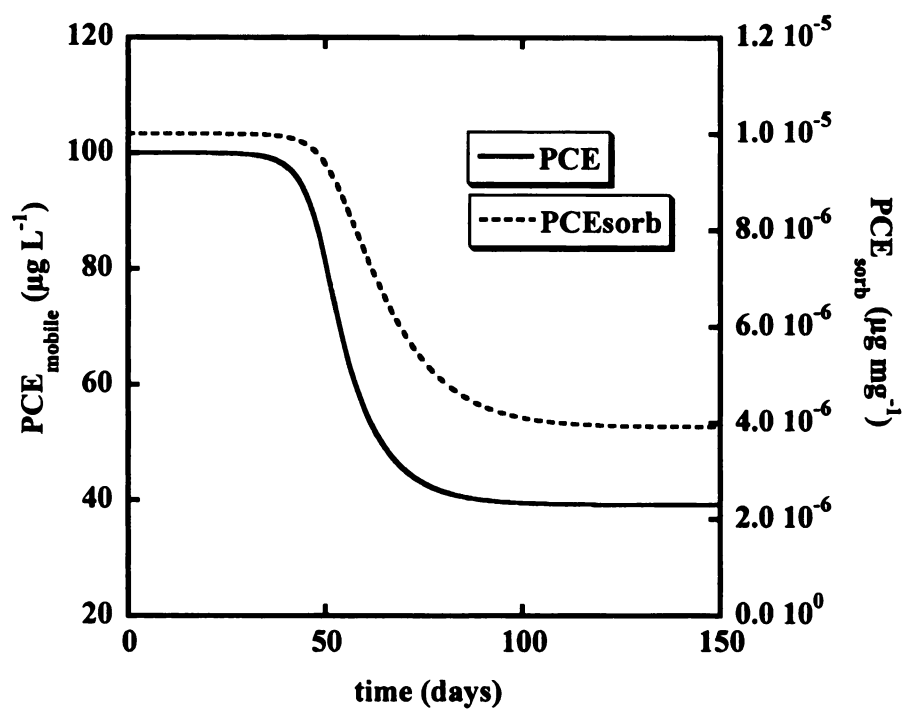
Figure 4.4. Liquid and solid phase PCE concentration for the hypothetical batch reactor simulation.
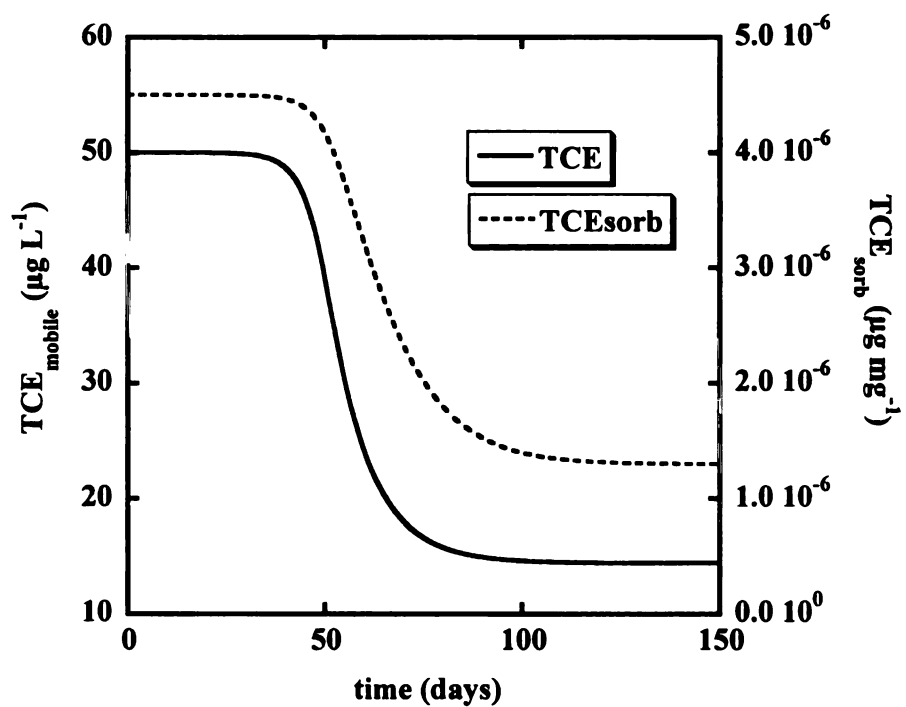


Figure 4.5. Liquid and solid phase TCE concentration in the batch reactor.

Complete degradation of TCE is not achieved since the biomass concentration declines when there is no more toluene to support its growth (Figure 4.3). TCE equilibrium concentration in the solid phase at the end of the simulation is $1.5 \times 10^{-6} \mu g$ TCE/mg soil.

Concentrations of metabolic by-products from the PCE and TCE degradation are shown in Figures 4.6, 4.7, and 4.8. TCE degradation results in the production of cis-DCE, cis-DCE degradation results in the production of vinyl chloride, which consequently degrades to produce ethene. At this stage, the biomass concentration has declined substantially and the metabolic chlorinated by products start accumulating in the hypothetical reactor. At the end of the simulation the concentrations in the liquid phase of cis-DCE, VC, and ethene are 35, 2.1, and $2.8 \mu g/L$, respectively. Solid-phase concentrations of these three compounds are $1.7 \times 10^{-6} \mu g$ cis-DCE/mg soil, $4.5 \times 10^{-9} \mu g$ VC/ mg soil, and $2.8 \times 10^{-9} \mu g$ ethene/mg soil. Accumulation of these byproducts occurs due to the lack of electron donors capable of supporting a microbial population that can perform complete degradation of the chlorinated compounds and its by-products.

An equivalent PCE concentration was computed with Equation 4.19 at 0 and 50 days to ensure mass conservation throughout the simulation period. PCE equivalent concentration at 0 days was $247 \mu g/L$, which compares reasonable well with $244 \mu g/L$ at 50 days. The equivalent PCE concentration at 50 days yields a 1.3% error with respect to the initial equivalent PCE concentration. The difference between these values could be attributed to small numerical errors introduced by the algorithm.

The model showed high sensitivity to several parameters. For example, an order of magnitude change in the biomass decay coefficient $b$, resulted in a dramatic change in concentration profiles for all organic compounds. Also, each particular equation showed

105
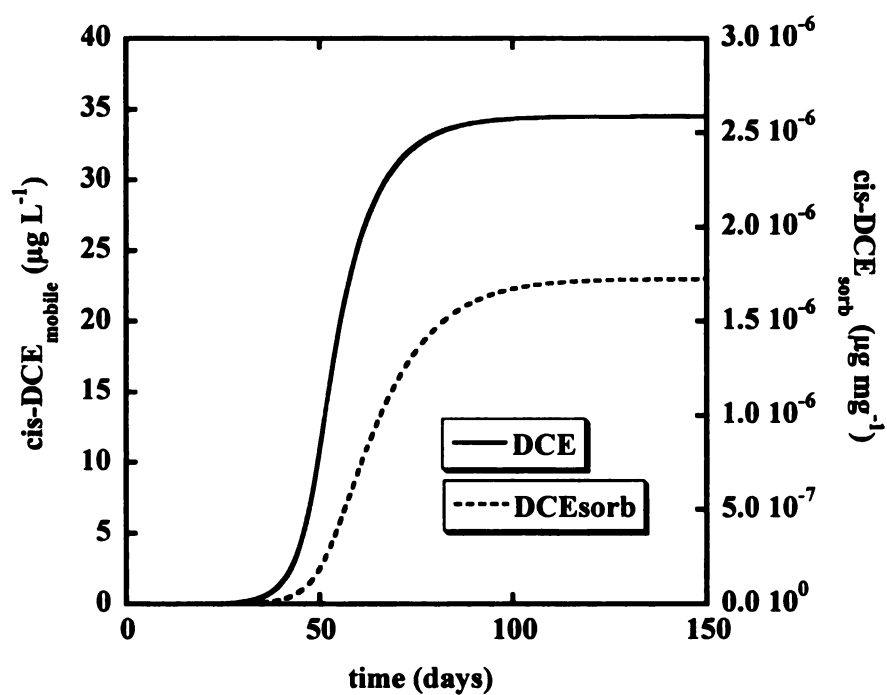
Figure 4.6. Liquid and solid phase DCE concentration in the batch reactor.
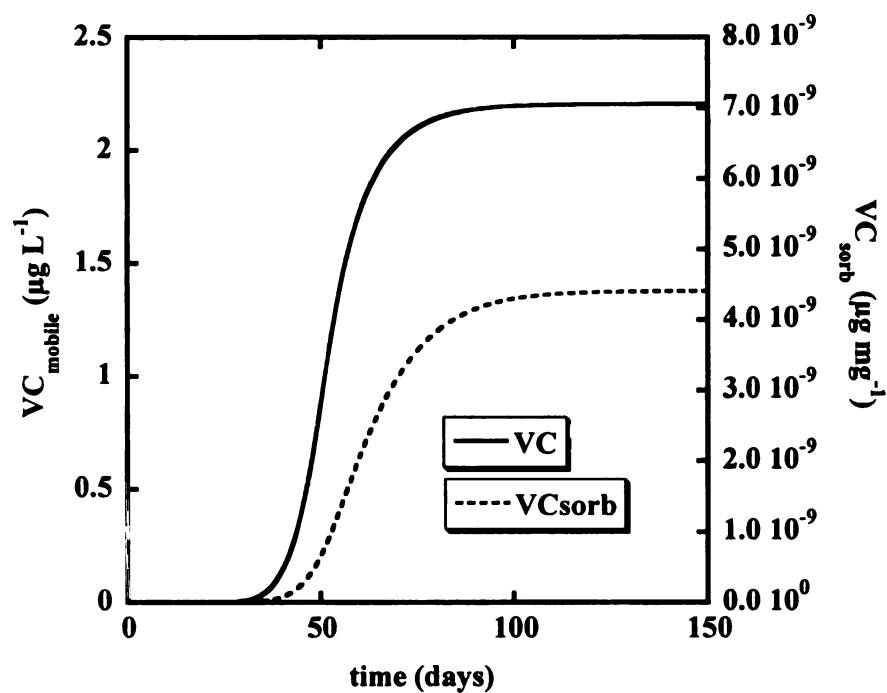


Figure 4.7. Liquid and solid phase VC concentration in the batch reactor.
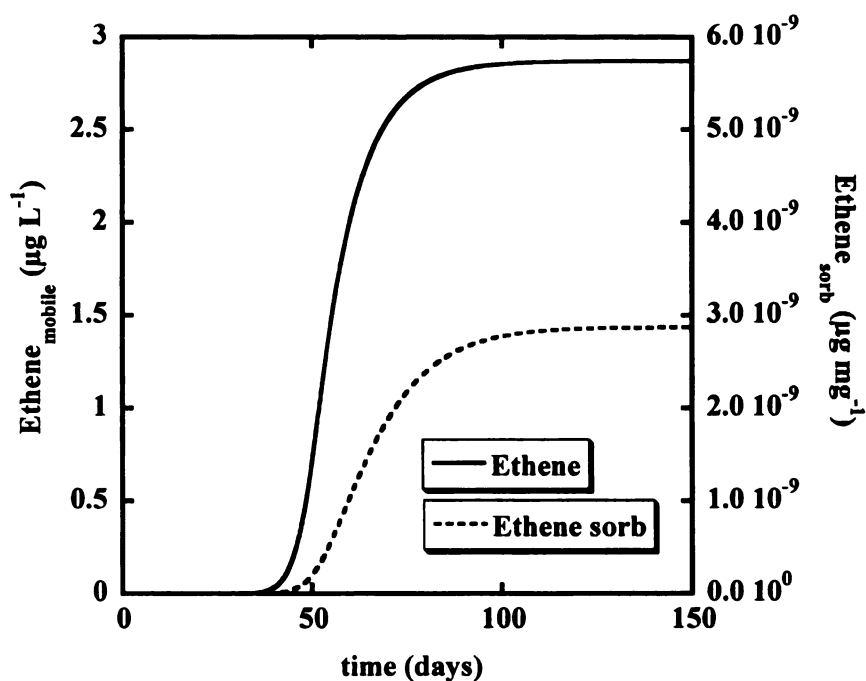
Figure 4.8. Liquid and solid phase ethene concentration in the batch reactor.

high sensitivity to the maximum substrate utilization rate coefficient. This model has a total of 27 different reaction parameters of which only the stoichiometric yield coefficients can be easily determined. Also, field values for all of these parameters are expected to be different from those determined in the laboratory. Similar Monod type kinetic models have accurately predicted reductive dechlorination processes in laboratory reactors; however, the application of these models to field conditions becomes complicated because measurement of constant parameters is not possible.

These modeling results are representative of what may occur at sites where a steady supply of electron donors is not available to support complete reductive dechlorination. It is believed that this condition occurred in a VOC contaminated aquifer in Schoolcraft, MI where partial reductive dechlorination was observed.

*Flow model for Schoolcraft VOC plume site*

A regular 2-dimensional finite difference numerical grid was constructed for the model region shown in Figure 4.2. Details of the model domain are given in Table 4.4. The spatial discretization resulted in 98,900 finite difference cells. A small grid size was used to minimize artificial (numerical) dispersion effects.

Mean log(K) from 89 pump tests on selected wells (Figure 4.2) across the site was -1.48 ($10^{-1.48}$cm/s), which is a typical value for outwash sediments composed of medium to coarse sands and gravel. The parameters were used to solve Equation 4.20 numerically using MODFLOW 2000 (Harbaugh *et al.* 2000).

Figure 4.9 shows the solution of the calibrated steady-state flow model for the domain. Groundwater flows towards the southeast with a hydraulic gradient of 0.001m/m. This compares reasonably well with previously reported values obtained in the vicinity of the contaminated aquifer (Dybas *et al.* 2002; Hyndman *et al.* 2000). Head data collected across the site was used in the model calibration. A plot of the final observed vs. computed heads is shown in Figure 4.10. Comparison of these results with the ones presented by Lipinski (2002) confirms the accuracy of the flow model.

**Table 4.4. Details of the numerical model domain.**

| Model Area Parameter | Value |
|---|---|
| domain | 1400 m x 2630 m |
| no. of columns | 230 |
| no. of rows | 430 |
| no. of layers | 1 |
| cell dimensions | |
| $\Delta x$, m | 6.1 |
| $\Delta y$, m | 6.1 |
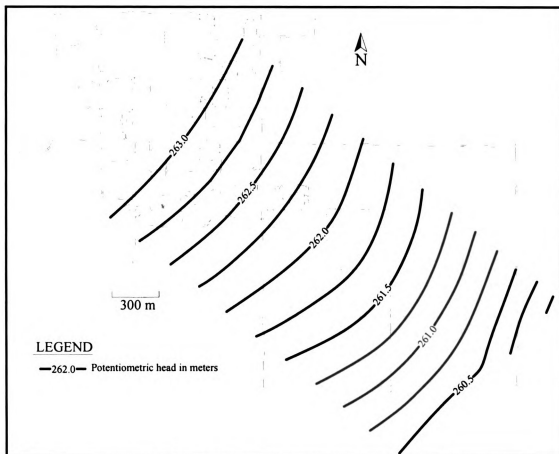
Figure 4.9. Groundwater contour map in the VOC contaminated region.

*Reactive transport model results for the chemical loading period between 1953 and 1988.*

The reductive dechlorination model was coupled to a transport model to simulate the VOC plume in Schoolcraft, MI. Previous reports indicate that industrial activities at the facility started approximately in 1953. This VOC plume was discovered in 1986 during a soil and groundwater contamination investigation conducted by personnel of the Michigan Department of Environmental Quality (formerly Michigan Department of Natural Resources). Sources of contamination were removed during late 1980's to early 1990's.

Figure 4.10. Comparison between observed and computed heads
for several wells in the region.

Based on the historical release of VOC compounds from the ARCO facility, two

major stress periods were assumed for modeling purposes. The first stress period

considers a constant loading of chemicals from 1953 to 1988. The second stress period

considers removal of the suspected source of contamination and no further loadings of

chemicals into the aquifer. This corresponds to the years of 1988 to 2003. The total

simulation time was 50 years.

Although suspected sources of contamination within the ARCO facility have been

identified in previous studies (Lipinski 2002), the entire facility was assumed as a source

due to the lack of information on the spatial and temporal distribution of contaminant

releases in those sub-areas. An approximate surface area of 10,000 $m^2$ was used as the

contaminant handling area for the 35 years of loading.

Figure 4.11 show the simulated and observed 5μg/L iso-concentration line for the chlorinated compounds at the end of the 35 year loading period. This concentration value was chosen because it is the maximum concentration level (MCL) of PCE and TCE in drinking water in the US (EPA 2003). The model predicts the front of the 5μg/L PCE contour to be located approximately 1000m southeast from the source at 35 year (Figure 4.11(a)). Comparison with the delineated contour using data from monitoring wells shows a reasonable agreement between both contours lines. The longitudinal extension of the observed PCE plume is 960m, a difference only of 40m compared with the model calculated. Aerial extent of the observed PCE plume is 177,600 m$^2$ and the model predicted contour is 323,000 m$^2$. The predicted PCE plume covers almost twice the area of the observed plume. A longitudinal dispersion coefficient of 0.20m was used in this model. This value was selected based on previous tracer studies in an area inside the plume. However, the longitudinal scale of the tracer study was 1.5% of the total plume scale. This suggests that dispersivity values for the plume should be larger than the estimated dispersivity for the tracer studies as this parameter varies with the length sale.

The modeled TCE plume has traveled 200m more than the modeled PCE plume for the same period (Figure 4.11(b)). This was expected since a lower partitioning coefficient was used for TCE; and PCE sorbs strongly to the soil compared to TCE. The longitudinal extent of the modeled TCE plume is in close agreement with the observed plume at the end of the loading period. The aerial extent of the observed TCE plume is 262,000 m$^2$ and the extent of the simulated plume is 335,000 m$^2$
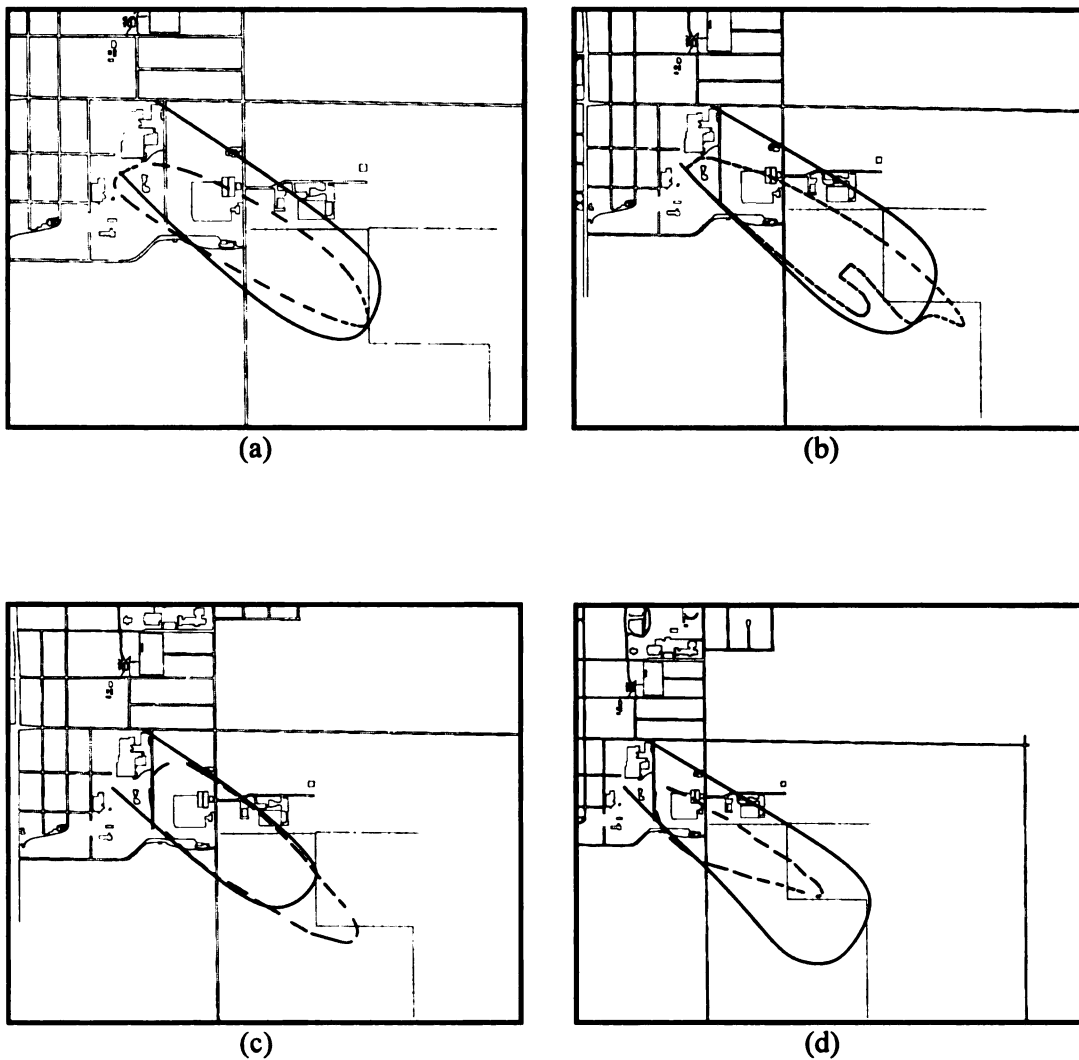
Figure 4.11. Simulated (solid) and observed (dashed) 5μg/L isoconcentration line for (a) PCE, (b) TCE, (c)cis-DCE, and (d) VC at the end of the loading period (35 years).

The front of the 5μg/L cis-DCE contour has not traveled as far as TCE (about 100m less than DCE) in both the modeled and the observed plumes (Figure 4.11(c)). A reason for this could be that TCE was initially present at the source and was not subjected to biodegradation until an active biomass capable of TCE utilization developed. This can be seen in both, the modeled and the observed cis-DCE plume. The longitudinal extent

of the observed cis-DCE plume is approximately 10% longer than the modeled cis-DCE plume. The front of the predicted 5µg/L cis-DCE contour is located 927m from the facility and the observed front is located at an approximate distance of 1190m. However, the areas covered by these plumes are very similar, i.e. 223,150 m$^2$ for the model plume and 221,400 m$^2$ for the delineated.

A discrepancy between the model and the observed contours is revealed in the VC plume for this period (Figure 4.11(d)). The model predicts the VC plume to extend 1,433m from the source whereas the observed front of the 5µg/L VC contour is located 1,150m from the suspected source. The areas covered by these plume are 167,630 m$^2$ and 537,700 m$^2$ for the observed and simulated plumes, respectively. Most likely, the partitioning coefficient used in the simulation was higher than the real field value. Also, a higher dispersion coefficient could produce an elongated VC plume similar to the observed plume.

*Model results for the period of 1988 to 2000.*

Results from the loading period were used as starting concentrations for a reactive transport model considering removal of the contaminant sources. Figure 4.12 shows the simulated and delineated 5µg/L contour line for all VOC compounds for the year 2000. Panel (a) of Figure 4.12 shows the size of the PCE plume to be significantly reduced as compared to Figure 4.11(a). The extent of the observed plume is smaller than the simulated one. Possibly, the PCE specific utilization rate for field conditions is higher than the value used in the model. Also, it might be possible that other carbon sources such as naturally occurring organic matter served as an electron donor after depletion of

113

toluene since measured concentrations of this compound in 2000 were all below detection limits. Areas of the PCE plumes for the year 2000 are 150,000 $m^2$ and 23,200 $m^2$ for model predicted and observed plumes, respectively.

Figure 4.12(b) shows 5µg/L TCE contour lines for the year 2000. The predicted contour is delayed by 150m; however, the areas covered by the plumes are very similar, 247,000 $m^2$ for the simulated vs. 214,000 $m^2$ for the observed plume. Comparison of this panel with that of Figure 4.11 reveal that although some biological attenuation of TCE has occurred, the magnitude is small compared to PCE degradation.

The longitudinal extent of the observed cis-DCE plume for this time period is approximately 1110m (Figure 4.12(c)), which is about the same size it has at the end of the loading time period. This indicates that no major biodegradation of cis-DCE has occurred during the last 15 years and the only attenuation mechanisms that could be taking place are dilution and dispersion. The model simulated contour for cis-DCE shows a different shape as compared to the observed one. However, the areas are very similar; 280,000 $m^2$ for the observed vs. 300,280 $m^2$ for the model predicted plume.

Similarly, in Figure 4.12(d) the model predicts a VC plume different than the observed one. The observed VC plume is elongated and extends through an approximate area of 206,000 $m^2$ with a longitudinal extension of 1040 m. The model simulated plume has an approximate area of 194,340 $m^2$ with a length of 440 m. As with the cis-DCE plume, the aerial extension is reasonable, but the longitudinal extension of the observed
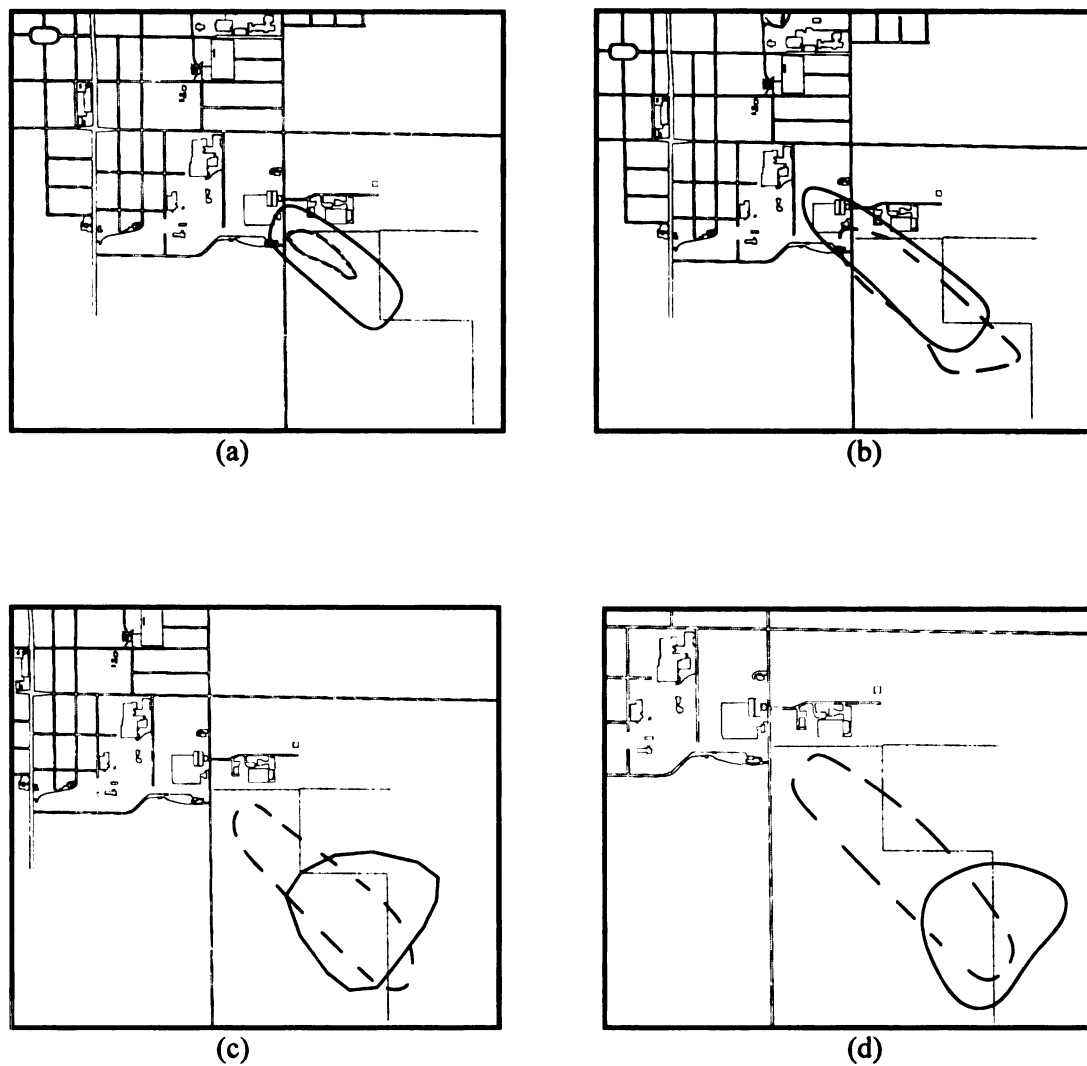
Figure 4.12. Simulated (solid) and delineated (dashed) 5µg/L isoconcentration line for (a) PCE, (b) TCE, (c)cis-DCE, and (d) VC at 47 years.

plume is about two times what the model predicted. The reason could be that the length dependency of the dispersion coefficient was not considered in these simulations

*Assessment of risk to downgradient groundwater receptors*

The impact of the contaminant plume on potential groundwater receptors was

evaluated with the calibrated model. This plume has the potential to discharge into a series of surface water bodies located approximately 4 km southeast of the Schoolcraft village. The results for a predictive model run are shown in Figure 4.13. The 5μg/L PCE contour has not changed significantly from the results obtained for the year 2000. The reason could be that this plume is at "steady-state" where the rates of attenuation are comparable to the travel times in this sandy aquifer. Also, since PCE tends to sorb to soil particles, its migration could be subjected to a significant retardation compared to the groundwater velocity.

The model predicts the TCE plume; delineated by the 5μg/L contour, slightly downgradient as compared to the 2000 yr position. The behavior of this plume is similar to the PCE plume.

The 2050 yr cis-DCE plume has migrated considerably as compared to the results at 2000. However, it has not reach yet the surface water bodies and apparently, dilution and dispersion mechanisms are sufficient to ensure that concentrations above regulatory limits do not reach receiving surface water bodies. This simulation shows that these three plumes, i.e. (PCE, TCE, and cis-DCE), do not represent a risk to the receiving surface water bodies for the modeling period of 1953 to 2050.

The simulated vinyl chloride plume; however appears to reach the lake and start discharging into it at concentrations higher than regulatory limits. The fact that vinyl chloride has migrated significantly more than its parent products is consistent with the sorption characteristics of this compound.
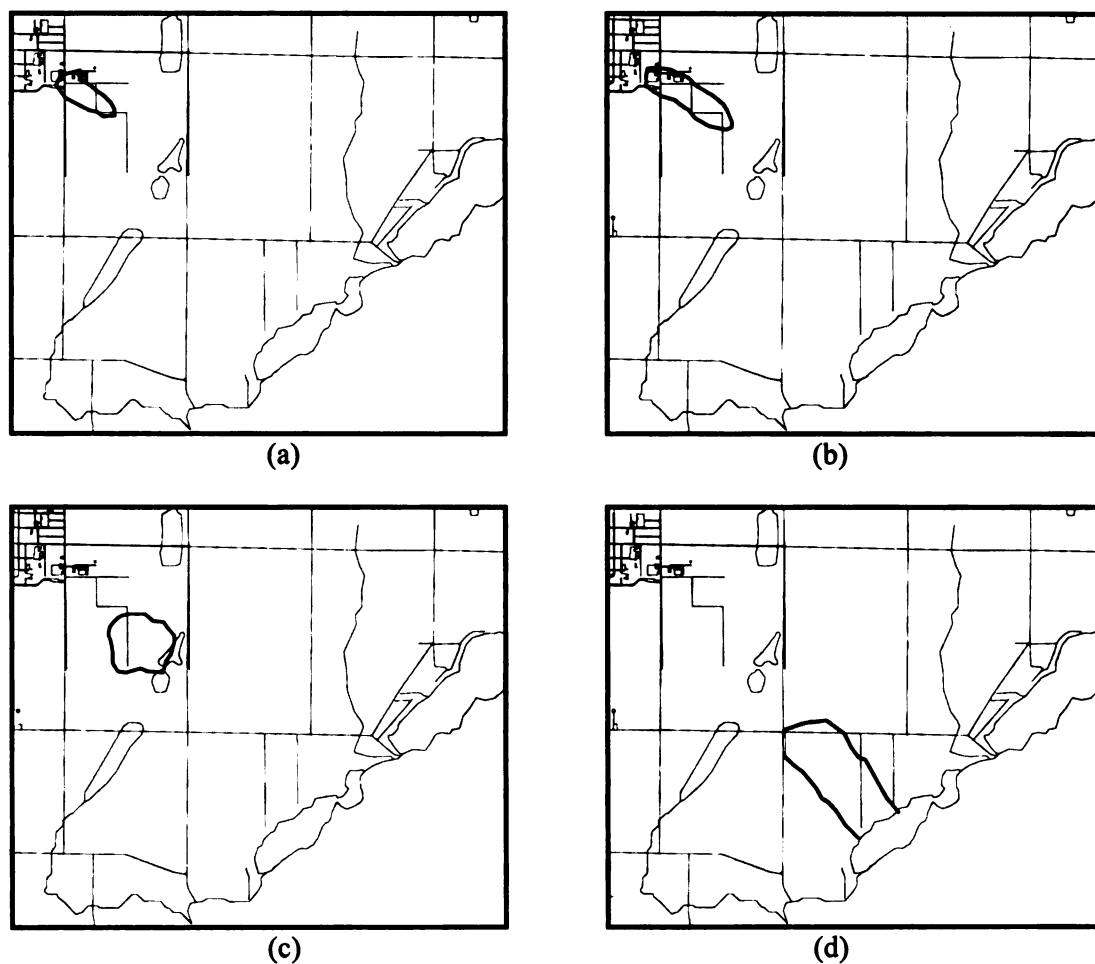
Figure 4.13.  Simulated 5µg/L isoconcentration line for (a) PCE, (b) TCE, (c)cis-DCE, and (d) VC for the year 2050.

This results show that of the VOC compounds most likely to be produced in this aquifer, higher risks are associated with VC production.  However, based on analytical data collected on a previous study, production of VC is not significant and the reductive dechlorination process does not seem to have the electron donor requirements for the conversion of cis-DCE to VC.

## 4.5 Summary and conclusions

Results from this study show that the VOC plume at Schoolcraft Plume G site is not currently undergoing a significant biological attenuation due to depletion of substrates that can support an active population of dehalogenators. The developed numerical model showed a reasonable agreement with the observed plumes for PCE, TCE and cis-DCE. The VC plume was over-predicted by the model; however, not all wells in Figure 4.2 were analyzed for chlorinated compounds during the sampling events conducted on 1988 through 1989 and 2000.

Results from Figure 4.12 show a reduction in aerial extent of PCE plumes. Most likely this reduction is caused by biological degradation processes. The TCE plumes are similar in shape but the simulated plume is spatially delayed for about 200m. The computed cis-DCE and VC contour deviates significantly from contours delineated using the 2000 data. However, this data set is limited and not all the wells were sampled during this sampling event.

Predictive modeling results show that only vinyl chloride has the potential to migrate, threatening to discharge in the lakes located at the southeast hydrological boundary. The other VOC plumes apparent to be in "steady-state" and do not represent a risk to the surface water bodies in this area.

An important feature of this approach to model natural attenuation is the inclusion of the electron donor in the mathematical formulation of reductive dechlorination. Reductive dechlorination has been successfully modeled in laboratory reactors using Monod-type kinetics (Fennell and Gossett 1998; Garant and Lynd 1998; Haston and McCarty 1999); however this type of approach has not been used to model sites where

reductive dechlorination is occurring. An evaluation of the concentration of electron donor compounds support the hypothesis that no major biological activity is occurring in the absence of those sources. This information is important to assess the sustainability of the natural attenuation process and ultimately will benefit decision makers when selecting the appropriate remediation strategy for contaminated sites.

This study shows that although reductive dechlorination was a major component of natural attenuation in the past, most likely it is not a major contributor to the overall process due to the lack of electron donor sources to create a reduced environment capable of sustaining a reductive dechlorination process that could result in complete depletion of the chlorinated ethene compounds.

One potential limitation of this approach is the number of constant parameters involved in the mathematical expressions for reductive dechlorination. Methods for measuring those parameters in the laboratory are well established; however, these values cannot be applied to field conditions. A systematic approach to measure them has not yet been developed.

## 4.6 Acknowledgments

## 4.7 Literature Cited

Anderson, M. P., and Woessner, W. W. (1992). *Applied Groundwater Modeling: Simulation of flow and advective transport*, Academic Press, INC., San Diego, Ca.

Bear, J. (1979). *Hydraulics of Groundwater*, McGraw-Hill.

Clement, T. B., and Jones, N. L. (1998). "RT3D tutorials for GMS users." *PNNL-11805*, Pacific Northwest National Laboratory, Richland, WA.

Clement, T. P. (1997). "A modular computer model for simulating reactive multi-species transport in three-dimensional ground water systems." *PNNL-SA-11720*, PNNL, Richland, Washington.

Clement, T. P., Sun, Y., Hooker, B. S., and Petersen, J. N. (1998). "Modeling multi-species reactive transport in ground water." *Ground Water Monitoring & Remediation*, 18(2), 79-92.

Clement, T. P., Truex, M. J., and Lee, P. (2002). "A case study for demonstrating the application of US EPA's monitored natural attenuation screening protocol at a hazardous waste site." *Journal of Contaminant Hydrology*, 59(1-2), 133-162.

Delvin, J. F., McMaster, M., and Barker, J. F. (2002). "Hydrogeologic assessment on in situ natural attenuation in a controlled field experiment." *Water Resources Research*, 38(1), 1 -11.

Dolfing, J. (2000). "Energetics of anaerobic degradation pathways of chlorinated aliphatic compounds." *Microbial Ecology*, 40(1), 2-7.

Dybas, M. J., Barcelona, M., Bezborodnikov, S., Davies, S., Forney, L., Heuer, H., Kawka, O., Mayotte, T., Sepulveda-Torres, L., Smalla, K., Sneathen, M., Tiedje, J., Voice, T., Wiggert, D. C., Witt, M. E., and Criddle, C. S. (1998). "Pilot-scale evaluation of bioaugmentation for in-situ remediation of a carbon tetrachloride contaminated aquifer." *Environmental Science & Technology*, 32(22), 3598-3611.

Dybas, M. J., Hyndman, D., Heine, R., Tiedje, J., Linning, K., Wiggert, D., Voice, T., Zhao, X., Dybas, L., and Criddle, C. (2002). "Development, operation, and long-term performance of a full-scale biocurtain utilizing bioaugmentation." *Environmental Science & Technology*, 36(16), 3635-3644.

Elmen, J., Pan, W., Leung, S. Y., Magyarosy, A., and Keasling, J. D. (1997). "Kinetics of toluene degradation by a nitrate-reducing bacterium isolated from a groundwater aquifer." *Biotechnology and Bioengineering*, 55(1), 82-90.

U.S. Environmental Protection Agency (EPA). (1998). "Technical protocol for evaluating natural attenuation of chlorinated solvents in groundwater." *EPA/600/R-98/128*, USEPA, Cincinnati, OH.

U.S. Environmental Protection Agency (EPA). (1999). "Anaerobic biodegradation rates of organic chemicals in groundwater: A summary of field and laboratory studies." U.S. Environmental Protection Agency, Washington, DC.

U.S. Environmental Protection Agency (EPA). (2003). "National primary drinking water standards." *EPA 816-F-03-016*, EPA, Washington, DC.

Fennell, D. E., and Gossett, J. M. (1998). "Modeling the production of and competition for hydrogen in a dechlorinating culture." *Environmental Science & Technology*, 32(16), 2450-2460.

Ferguson, J. F., and Pietari, J. M. H. (2000). "Anaerobic transformations and bioremediation of chlorinated solvents." *Environmental Pollution*, 107(2), 209-215.

Garant, H., and Lynd, L. (1998). "Applicability of competitive and noncompetitive kinetics to the reductive dechlorination of chlorinated ethenes." *Biotechnology and Bioengineering*, 57(6), 751-755.

Harbaugh, A. W., Banta, E. R., Hill, M. C., and McDonald, M. G. (2000). "Modflow-2000, The U.S. Geological Survey modular ground-water model-User guide to modularization concepts and the ground-water flow process." *ofr00-92*, United States Geological Survey, Reston, VA.

Haston, Z. C., and McCarty, P. L. (1999). "Chlorinated ethene half-velocity coefficients (K-s) for reductive dehalogenation." *Environmental Science & Technology*, 33(2), 223-226.

Hyndman, D., Dybas, M. J., Forney, L., Heine, R., Mayotte, T., Phanikumar, M. S., Tatara, G., Tiedje, J., Voice, T., Wallace, R., Wiggert, D., Zhao, X., and Criddle, C. S. (2000). "Hydraulic characterization and design of a full-scale biocurtain." *Ground Water*, 38(3), 462-474.

Kao, C. M., and Wang, Y. S. (2001). "Field investigation of the natural attenuation and intrinsic biodegradation rates at an underground storage tank site." *Environmental Geology*, 40(4-5), 622-631.

Klier, N. J., West, R. J., and Donberg, P. A. (1999). "Aerobic biodegradation of dichloroethylenes in surface and subsurface soils." *Chemosphere*, 38, 1175-1188.

Lipinski, B. A. (2002). "Estimating natural attenuation rates for a chlorinated hydrocarbon plume in a glacio-fluvial aquifer, Schoolcraft, Michigan," M.S. thesis, Michigan State University, East Lansing, MI.

Lovley, D. R., Chapelle, F. H., and Woodward, J. C. (1994). "Use of dissolved H2 concentrations to determine distribution of microbially catalyzed redox reactions in anoxic groundwater." *Environmental Science & Technology*, 28(7), 1205-1210.

Lovley, D. R., and Goodwin, S. (1988). "Hydrogen concentrations as an indicator of the predominant terminal electron-accepting reaction in aquatic sediments." *Geochimica Cosmochimica Acta*, 52, 2993-3003.

Mayotte, T. J., Dybas, M. J., and Criddle, C. S. (1996). "Bench-scale evaluation of bioaugmentation to remediate carbon tetrachloride-contaminated aquifer materials." *Ground Water*, 34(2), 358-367.

McCarty, P. L. (1997). "Breathing with chlorinated solvents." *Science*, 166, 1521-1522.

Meer, J. T., Eekert, M., Gerritse, J., and Rijnaarts, H. (2001). "Hydrogen as indicator for redox conditions and dechlorination." Natural attenuation of environmental contaminants: The sixth international in situ and on-site bioremediation symposium, A. Leeson, M. E. Kelly, H. S. Rifai, and V. S. Magar, eds., Battelle Press, San Diego, CA.

Middledorp, P. J., Luijten, M. L. G. C., van de Pas, B. A., van Eekert, M. H. A., Kengen, S. W. M., Schraa, G., and Stams, A. J. M. (1999). "Anaerobic microbial reductive dehalogenation of chlorinated ethenes." *Bioremediation Journal*, 3(3), 151-169.

Ndon, U. J., Randall, A. A., and Khouri, T. Z. (2000). "Reductive dechlorination of tetrachloroethylene by soil sulfate-reducing microbes under various electron donor conditions." *Environmental Monitoring and Assessment*, 60(3), 329-336.

Richmond, S. A., Lindstrom, J. E., and Braddock, J. F. (2001). "Assessment of natural attenuation of chlorinated aliphatics and BTEX in subarctic groundwater." *Environmental Science & Technology*, 35(20), 4038-4045.

Reardon, K. F., Mosteller, D. C., and Bull Rogers, J. D. (2000). " Biodegradation kinetics of benzene, toluene, and phenol as single and mixed substrates for *pseudomonas putida F1*." *Biotechnology and Bioengineering*, 69(4), 385-400.

Rittman, B. E., and McCarty, P. L. (2001). *Environmental Biotechnology: Principles and Applications*, McGraw-Hill, San Francisco, CA.

Shouakar-Stash, O., Frape, S. K., and Drimmie, R. J. (2003). "Stable hydrogen, carbon and chlorine isotope measurements of selected chlorinated organic solvents." *Journal of Contaminant Hydrology*, 60(3-4), 211-228.

Vogel, T. M., Criddle, C., and McCarty, P. L. (1987). "Transformation of halogenated aliphatic compounds." *Environmental Science & Technology*, 21, 722-736.

Witt, M. E., Klecka, G. M., Lutz, E. J., Ei, T. A., Grosso, N. R., and Chapelle, F. H. (2002). "Natural attenuation of chlorinated solvents at Area 6, Dover Air Force Base: groundwater biogeochemistry." *Journal of Contaminant Hydrology*, 57(1-2), 61-80.

Yang, Y. R., and McCarty, P. L. (1998). "Competition for hydrogen within a chlorinated solvent dehalogenating anaerobic mixed culture." *Environmental Science & Technology*, 32(22), 3591-3597.

Zhao, X., Szafranski, M. J., Maraqa, M. A., and Voice, T. C. (1999). "Sorption and bioavailability of carbon tetrachloride in a low organic content sandy soil." *Environmental Toxicology and Chemistry*, 18(8), 1755-1762.

# CHAPTER 5

# SUMMARY AND CONCLUSIONS

## 5.1 Introduction

In recent years natural attenuation has been widely applied, either in conjunction with engineered technologies, or as a sole remediation strategy to clean up contaminated sites. According to EPA data, natural attenuation use in the Superfund program developed during 1990's from application at 6% to more than 25% of groundwater contamination sites (Macdonald 2000). At some sites natural attenuation is being used as a sole remediation technology while at other sites, a combination with engineered treatment technologies has being adopted.

Scientists have demonstrated that natural attenuation can destroy certain contaminants, primarily fuel hydrocarbons (NRC 2000). However, it has been recognized, that the surge in use of natural attenuation has outpaced the development of adequate guidelines for its use (Renner 2000). Yet, this treatment technology has been approved as a formal remedy, despite the limitations in scientific understanding.

Chlorinated compounds are among the most detected contaminants in soil and groundwaters. Their presence in the environment poses a high risk to the human health and the environment due to their high toxicity and mobility. Treatment sites contaminated with chlorinated solvents by natural attenuation has been a focus of intensive research during the last decade. However, the current level of understanding of the process leading to their destruction has been described as moderate (Macdonald

2000), in part because an agreement among researchers on how to evaluate and document natural attenuation of chlorinated solvents does not exist.

Guidelines for documenting natural attenuation of chlorinated solvents are evolving rapidly as the scientific understanding of the processes progress. These guidelines have been used to document natural attenuation at several contaminated sites (Alleman and Leeson 1999; Eganhouse *et al.* 2001; Witt *et al.* 2002). However, it has been recognized that these protocols are oftentimes misused, leading to wrong conclusions about the natural attenuation process at contaminated sites.

In general, it has been recognized that natural attenuation protocols should be replaced by methods (NRC 2000) which assign more weight to the specific conditions of the site being investigated. The goal of this research was to evaluate natural attenuation of chlorinated solvents by studying the processes that most likely influence this treatment strategy. This chapter summarizes, in a systematic way, the process employed during this research to understand and document the natural attenuation process occurring at Schoolcraft Plume G site.

## 5.2 Hydrogeological characterization of the VOC contaminated area

*Conceptual hydrogeological model development*

It is widely recognized that a site's hydrogeological characteristics influence dramatically the transport and distribution of compounds in aquifer systems (Hyndman *et al.* 2000). The characterization of the plume G site groundwater flow was accomplished through a study of the general regional groundwater flow (Lipinski 2002) and developing a local conceptual model for the chemically impacted regions. However, local

hydrogeological characteristics at the plume's scale resolution were not derived from this analysis. A series of cores were drilled in a location impacted by the VOC plume and the extracted material was analyzed to identify local heterogeneities in the saturated aquifer zone that could have influence the migration of VOC compounds. From this analysis two distinctive preferential flow zones were discovered.

A series of tracer tests were used to test the hypothesis that contaminants in this region have a tendency to migrate to downstream groundwater receptors through the zones identified in the soil core analysis. Breakthrough curves generated from the data collected at downstream monitoring wells confirmed the influence that these zones exert on migration patterns of contaminants in this aquifer region. Figure 5.1 show the stratigraphy of the site with typical tracer breakthrough curves obtained in each zone.
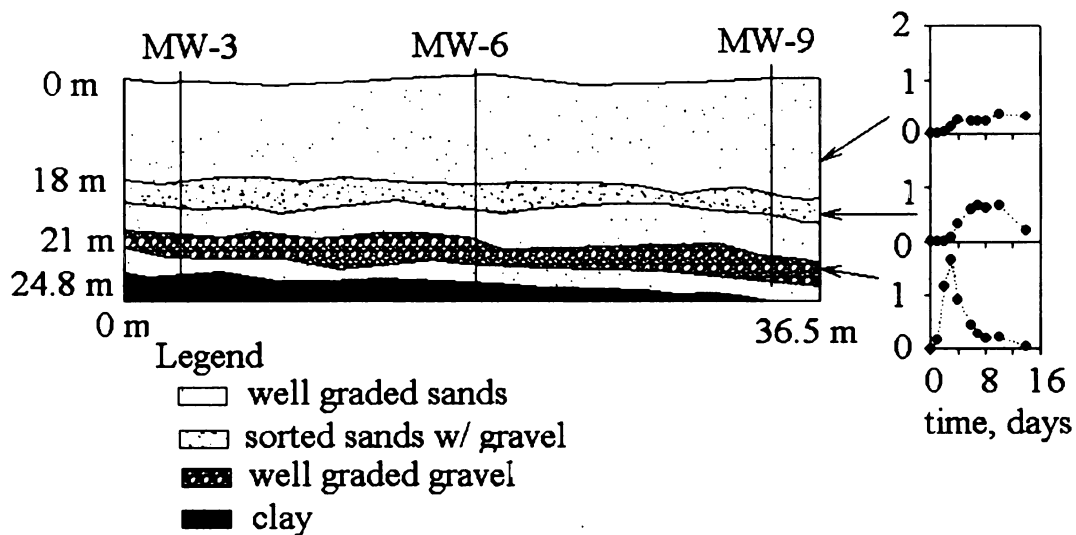


Figure 5.1. Cross section of the Plume G site with distinctive stratigraphic tracer breakthrough curve.

*Hydrogeological Characterization: quantitative description*

A quantitative description of the hydrogeologic features identified in the conceptual model was obtained by the methods described in Chapter 2. Field and laboratory hydraulic conductivity experiments revealed that samples with the higher conductivity values correlate well with the conceptual model description of the site. In general, outwash sediments composing the upper unconfined aquifer have hydraulic conductivity values ranging from $1 \times 10^{-3}$ to $4 \times 10^{-1}$ cm/s.

The hydraulic conductivity and tracer experiments revealed a different transport behavior among the stratigraphic units. To quantitatively describe those differences, a methodology to optimize the estimate of dispersion parameters using all possible collected data was developed. Estimates of depth-specific average linear velocity using this procedure revealed that for high conductivity zones, the average linear velocity was considerably higher than the rest of the aquifer. For example, the average linear velocity at 23.2m bgs was $99.5 \pm 9.81$ cm/day, and at 21.3m bgs was $33.12 \pm 2.99$ cm/day. The model developed showed that optimization on a depth-specific basis validates the observations better than using a single dispersivity value for the entire model domain. Figure 5.2 shows two simulation scenarios; one with the layer optimum dispersivity and one with the entire grid domain optimum dispersivity.
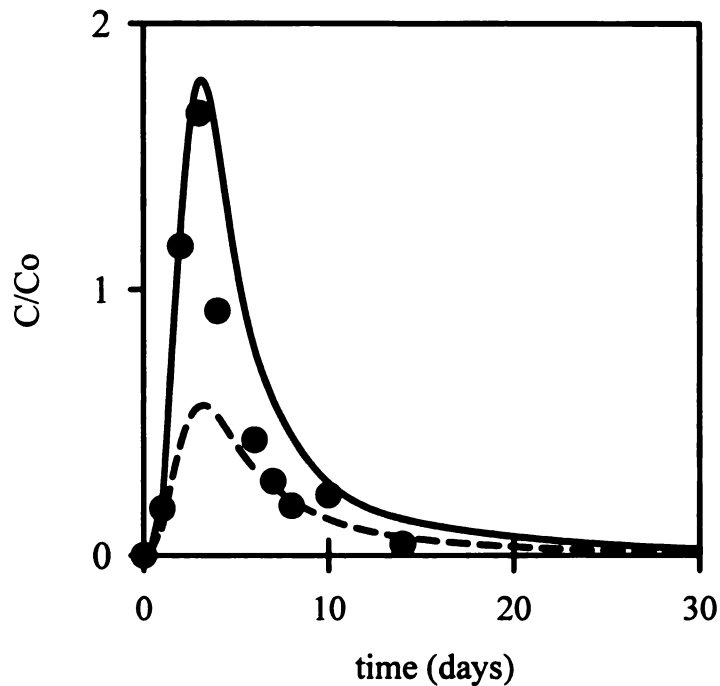
Figure 5.2. Tracer breakthrough curves for the simulated
scenarios. The solid line represents the depth specific
case, the dashed line represents the entire model grid
case, and the solid circles are the observed data.

## 5.3 Geochemical analyses: insight into the natural attenuation process

Generally, footprints of chemical reactions are used as indicators of processes

leading to natural attenuation of contaminants. Measurements of footprints give a

preliminary indication whether or not contaminants at a particular site are being

attenuated.

The most widely accepted destruction mechanism for chlorinated solvents is

reductive dechlorination (McCarty 1997). Figure 5.3 illustrates a conceptual model of

the breakdown of perchloroethene via reductive dechlorination (PCE). A supply of an

electron donor capable of maintaining reduced conditions in the aquifer is an essential

$$
\text{PCE} \xrightarrow[\text{anaerobic}]{\overset{\text{Cl}^-}{\text{\Huge\}}}} \text{TCE} \xrightarrow[\text{anaerobic}]{\overset{\text{Cl}^-}{\text{\Huge\}}}} \text{cis-DCE} \xrightarrow[\text{anaerobic}]{\overset{\text{Cl}^-}{\text{\Huge\}}}} \text{VC} \xrightarrow[\text{anaerobic}]{\overset{\text{Cl}^-}{\text{\Huge\}}}} \text{ETH}
$$
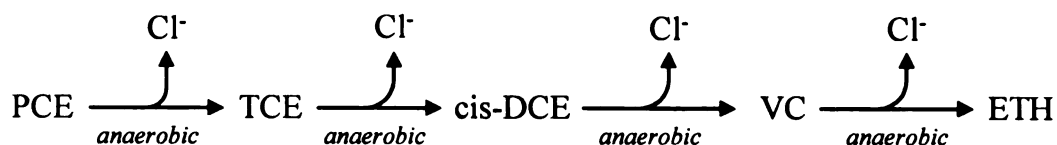
Figure 5.3. PCE to ethene breakdown through reductive dechlorination (Clement *et al.* 2000).

component of reductive dechlorination.

Analysis of geochemical and biological indicators performed during this investigation revealed that biological attenuation at this site has occurred in the past. The presence of metabolic by-products form the PCE and TCE degradation confirm that reductive dechlorination processes have occurred. However, environmental conditions that will ensure complete destruction of PCE, TCE and their metabolic by-products are not favorable. Analysis of geochemical and biological parameters led to the conclusion that reductive dechlorination occurred at this site up to the point where all sources of electron donors were depleted. From that point on, the attenuation that is occurring can be attributed only to physical processes.

Complete destruction of chlorinated solvents has been observed in places where co-contaminant plumes of fuel hydrocarbons exist. Typically, the necessary reduced environment is provided by the degradation of the compounds associated with these co-contaminants. Figure 5.4 shows a typical scenario where different levels of chlorinated solvent attenuation can be achieved based on the location and distribution of the petroleum hydrocarbon plume. Panel (c) of figure 5.4 could have been the scenario that occurred at the Plume G site. However, the co-contaminant plume was not sufficient for complete degradation of the chlorinated compounds.
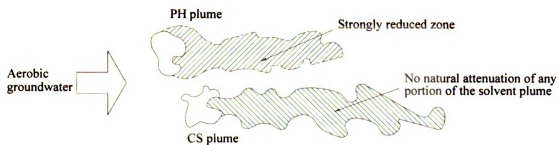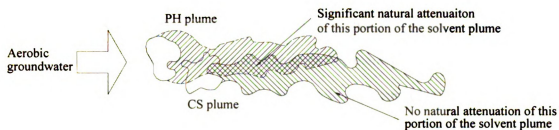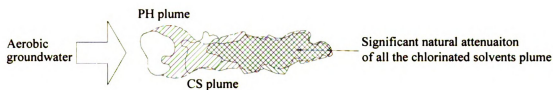
Figure 5.4. Illustration of three different scenarios that can be found in co-contaminated environments. (a) Non-interacting petroleum and chlorinated solvents plumes, (b) partly interacting plumes, and (c) completely interacting plumes. PH = petroleum hydrocarbon, CS = chlorinated solvents. (NRC 2000)

## 5.4 Reductive dechlorination model for the VOC contaminants plume

Numerical computer-based models can be useful when the complexity of the hydrogeology and the bio-geochemistry need to be capture in solute transport models. Based on the analysis of the geochemical and biological indicators at the Plume G site, a reactive transport model incorporating Monod kinetics in reactions terms for chlorinated solvents was developed. It has been recognized that there is a need for models of natural attenuation of chlorinated solvents to address the complex nature of reductive dechlorination (Fennell and Gossett 1998; Haston and McCarty 1999). However, this type of model should be developed only when the underlying processes are studied and understood well enough that they can be represented by mathematical formulations and when data is available to generate a reasonable matrix of parameter estimates.

The numerical model developed during this research simulated the plumes of each of the VOC compounds. Reasonable agreement was found between observed and simulated plumes. A predictive model run showed that only VC has the potential to migrate and contaminate a series of surface water bodies located at the southeast by the year 2050.

## 5.5 Summary

This research explores a methodology for evaluating natural attenuation of chlorinated solvents using conceptual and numerical models considering the hydrogeology and biogeochemistry intrinsic to the contaminated environment. A hydraulic characterization of the site revealed the existence of geologic features that influence dramatically the transport and distribution of solutes in a particular region.

131

Footprints of natural attenuation identified that biological destruction of the VOC compounds occurred in the past. However, biogeochemistry of the aquifer confirms that these mechanisms are not contributing significantly to the natural attenuation process at this site.

A numerical model was developed incorporating Monod type kinetics in the description of the reaction terms for the chlorinated compounds found in this aquifer. This model incorporated all the information collected at the site. Two different loading periods were simulated and the results showed reasonable agreement with plumes delineated with observed data.

Natural attenuation processes of chlorinated solvents at Plume G site methodology were evaluated by means of site specific data coupled with the development of conceptual and numerical models. This novel approach deviates from the traditional screening systems employed in most technical protocols to date, criticized for overestimating the magnitude of natural attenuation processes. Also, the series of experiments in this dissertation could serve as the basis for new protocols and guidelines for evaluating natural attenuation of chlorinated solvents.

## 5.6 Conclusions

1. Field tracer experiments coupled with numerical methods and optimization techniques proved to be effective in the hydrogeologic characterization of contaminated environments. The existence of preferential flow pathways was revealed by the characterization study performed.

2. Solid and liquid phase analysis of biogeochemical parameters revealed the importance of considering both phases when evaluating the extent of naturally occurring degradation processes. This experiment revealed that biological components of the natural attenuation process do not contribute significantly to reduce the contaminant mass and concentration at this site.

3. A model coupling the bioavailability of electron donors in reductive dechlorination processes was successfully employed to describe natural attenuation of chlorinated solvents in a contaminated aquifer. This evaluation confirmed that reductive dechlorination was important as some point in the plume's life-time. However, due to the lack of electron donor sources, reductive dechlorination does not appear to be a major contributor for the natural attenuation process at this site. Also, the predictive model showed that only vinyl chloride represents a risk to downgradient groundwater receptors during the simulated time period.

4. The methodology used in this research could be the foundation for a new approach to evaluate natural attenuation of chlorinated solvents using techniques that deviate from traditional approaches.

**5.7 Literature cited**

Alleman, B. C., and Leeson, A. (1999). *Natural attenuation of chlorinated solvents, petroleum hydrocarbons, and other organic compounds*, Battelle Press, Columbus, OH.

Eganhouse, R. P., Cozzarelli, I. M., Scholl, M. A., and Matthews, L. L. (2001). "Natural attenuation of volatile organic compounds (VOCs) in the leachate plume of a municipal landfill: Using alkylbenzenes as process probes." *Ground Water*, 39(2), 192-202.

Fennell, D. E., and Gossett, J. M. (1998). "Modeling the production of and competition for hydrogen in a dechlorinating culture." *Environmental Science & Technology*, 32(16), 2450-2460.

Haston, Z. C., and McCarty, P. L. (1999). "Chlorinated ethene half-velocity coefficients (K-s) for reductive dehalogenation." *Environmental Science & Technology*, 33(2), 223-226.

Hyndman, D., Dybas, M. J., Forney, L., Heine, R., Mayotte, T., Phanikumar, M. S., Tatara, G., Tiedje, J., Voice, T., Wallace, R., Wiggert, D., Zhao, X., and Criddle, C. S. (2000). "Hydraulic characterization and design of a full-scale biocurtain." *Ground Water*, 38(3), 462-474.

Lipinski, B. A. (2002). "Estimating natural attenuation rates for a chlorinated hydrocarbon plume in a glacio-fluvial aquifer, Schoolcraft, Michigan," M.S. thesis, Michigan State University, East Lansing, MI.

Macdonald, J. A. (2000). "Evaluating natural attenuation for groundwater cleanup." *Environmental Science & Technology*, 34(15), 346A-353A.

McCarty, P. L. (1997). "Breathing with chlorinated solvents." *Science*, 166, 1521-1522.

NRC. (2000). *Natural attenuation for groundwater remediation*, National Academy Press, Washington, D.C.

Renner, R. (2000). "Natural attenuation's popularity outpaces scientific support, NRC finds." *Environmental Science & Technology*, 34(9), 203A-204A.

Witt, M. E., Klecka, G. M., Lutz, E. J., Ei, T. A., Grosso, N. R., and Chapelle, F. H. (2002). "Natural attenuation of chlorinated solvents at Area 6, Dover Air Force Base: groundwater biogeochemistry." *Journal of Contaminant Hydrology*, 57(1-2), 61-80.

**APPENDICES**

# APPENDIX A - BORING LOGS FOR THE WELLS INSTALLED FOR THE PILOT SCALE STUDY

**Well id: MPA-1**

| Depth (m) From | To | Description | Classification |
|---|---|---|---|
| 0.0 | 14.6 | Blind drill to 14.9m | |
| 14.6 | 14.9 | Blind drill to 14.9m | |
| 14.9 | 18.9 | No recovery | |
| 18.9 | 20.9 | Medium to Coarse Sand w/ Fine Gravels | SW |
| 20.9 | 21.0 | Graded Gravels, Mixtures of Medium and Fine Gravels w/ Little or no Fines | Conglomerate |
| 21.0 | 22.3 | No recovery | |
| 22.3 | 22.6 | Medium Sands | SP |
| 22.6 | 24.4 | Medium to Coarse sands with big pebbles and cobbles | GP |
| 24.4 | 25.6 | Gray clay, stiff, dry, cohesive | CL |

**Well id: MPA-2**

| Depth (m) From | To | Description | Classification |
|---|---|---|---|
| 0.0 | 14.6 | Blind drill to 14.6m | |
| 14.6 | 14.9 | Blind drill to 14.6m | |
| 14.9 | 15.8 | Medium to Coarse sands/ Well Graded Sand | SW |
| 15.8 | 16.8 | Graded Gravels, Mixtures of Medium and Fine gravels w/ little or no fines | Conglomerate |
| 16.8 | 22.4 | No recovery | |
| 22.4 | 23.0 | Medium to Coarse Sands/ well graded sands | SW |
| 23.0 | 23.6 | Graded Gravels, Mixtures of Medium and fine gravels w/ little or no fines | Conglomerate |
| 23.6 | 25.1 | Medium to Coarse Sands w/ big pebbles and Cobbles | GP |
| 25.1 | 25.6 | Gray clay, stiff, dry, cohesive | CL |

**Well id: MPA-3**

| Depth (m) | | Description | Classification |
|---|---|---|---|
| From | To | | |
| 0.0 | 14.6 | Blind drill to 14.9m | |
| 14.6 | 14.9 | Blind drill to 14.9m | |
| 14.9 | 17.1 | No recovery | |
| 17.1 | 19.4 | Medium to coarse sands/ well graded sands | SW |
| 19.4 | 21.0 | Gravel-Sand Mixtures/ Poorly graded Gravels | GW |
| 21.0 | 21.9 | No recovery | |
| 21.9 | 24.6 | Medium to Coarse Sand w/ big pebbles and cobbles | GP |
| 24.6 | 25.6 | Gray clay, stiff, dry, cohesive | CL |

**Well id: MPA-4**

| Depth (m) | | Description | Classification |
|---|---|---|---|
| From | To | | |
| 0.0 | 14.6 | Blind drill to 14.9m | |
| 14.6 | 14.9 | Blind drill to 14.9m | |
| 14.9 | 17.4 | No recovery | |
| 17.4 | 20.1 | Medium to coarse sands/ more medium | SW |
| 20.1 | 23.5 | Gravel-Sand Mixtures/ Poorly graded gravels | GW |
| 23.5 | 24.4 | No recovery | |
| 24.4 | 25.6 | Gray clay, stiff, dry, cohesive | CL |

**Well id: MPA-5**

| Depth (m) | | Description | Classification |
|---|---|---|---|
| From | To | | |
| 0.0 | 14.6 | Blind drill to 14.9m | |
| 14.6 | 14.9 | Blind drill to 14.9m | |
| 14.9 | 17.1 | No recovery | |
| 17.1 | 19.5 | Medium to Coarse Sands, more medium | SW |
| 19.5 | 21.0 | Gravel-Sand Mixtures/ Poorly Graded Gravels | GW |
| 21.0 | 22.6 | No recovery | |
| 22.6 | 24.5 | Medium to Coarse Sands w/ big pebbles and cobbles | GP |
| 24.5 | 25.6 | Clay | CL |

**Well id: MPA-6**

| Depth (m) | | Description | Classification |
|---|---|---|---|
| From | To | | |
| 0.0 | 14.6 | Blind drill to 14.9m | |
| 14.6 | 14.9 | Blind drill to 14.9m | |
| 14.9 | 17.1 | Medium to Coarse Sand/ more medium | SW |
| 17.1 | 18.6 | Gravel-Sand Mixtures/ poorly graded gravel | GW |
| 18.6 | 22.6 | No recovery | |
| 22.6 | 23.2 | Medium to coarse sands | SW |
| 23.2 | 25.0 | Medium to coarse sands w/ big pebbles and cobbles | GP |
| 25.0 | 25.6 | Clay | CL |

**Well id: MPA-7**

| Depth (m) | | Description | Classification |
|---|---|---|---|
| From | To | | |
| 0.0 | 14.6 | Blind drill to 14.9m | |
| 14.6 | 14.9 | Blind drill to 14.9m | |
| 14.9 | 19.7 | Brown fine sand, saturated | SW |
| 19.7 | 20.9 | Medium to coarse sand/ more medium | SW |
| 20.9 | 24.4 | Brown medium to coarse sand, saturated | SW |
| 24.4 | 25.6 | Gray clay, stiff, dry, cohesive | CL |

**Well id: MPA-8**

| Depth (m) | | Description | Classification |
|---|---|---|---|
| From | To | | |
| 0.0 | 14.6 | Blind drill to 14.9m | |
| 14.6 | 14.9 | Blind drill to 14.9m | |
| 14.9 | 17.7 | No recovery | |
| 17.7 | 19.4 | Medium to coarse sand/ more medium | SW |
| 19.4 | 21.0 | Gravel-Sand Mixtures/ poorly graded gravel | GW |
| 21.0 | 22.6 | No recovery | |
| 22.6 | 25.0 | Medium to coarse sands w/ bib pebbles and cobbles | GP |
| 25.0 | 25.6 | Clay | CL |

**Well id: MPA-9**

| Depth (m) | | Description | Classification |
|---|---|---|---|
| From | To | | |
| 0.0 | 14.6 | Blind drill to 14.9m | |
| 14.6 | 14.9 | Blind drill to 14.9m | |
| 14.9 | 18.0 | No recovery | |
| 18.0 | 20.1 | Medium to coarse sand/ more medium | SW |
| 20.1 | 21.0 | Gravel-Sand mixtures/ poorly graded gravel | GW |
| 21.0 | 22.3 | No recovery | |
| 22.3 | 24.4 | Medium to coarse sand w/ big pebbles and cobbles | GP |
| 24.4 | 25.6 | Gray clay, stiff, dry, cohesive | CL |

**Well id: MPA-10**

| Depth (m) | | Description | Classification |
|---|---|---|---|
| From | To | | |
| 0.0 | 14.6 | Blind drill to 14.9m | |
| 14.6 | 14.9 | Blind drill to 14.9m | |
| 14.9 | 16.8 | No recovery | |
| 16.8 | 19.8 | Medium to coarse sand/ more medium | SW |
| 19.8 | 21.0 | Gravel-Sand Mixtures/ poorly graded gravel | GW |
| 21.0 | 22.3 | No recovery | |
| 22.3 | 24.4 | Medium to coarse sand/ w big pebbles and cobbles | GP |
| 24.4 | 25.6 | Gray clay, stiff, dry, cohesive | CL |

**Well id: MPA-11**

| Depth (m) | | Description | Classification |
|---|---|---|---|
| From | To | | |
| 0.0 | 14.6 | Blind drill to 14.9m | |
| 14.6 | 14.9 | Blind drill to 14.9m | |
| 14.9 | 17.7 | No recovery | |
| 17.7 | 19.8 | Medium to coarse sand/ more medium | SW |
| 19.8 | 21.0 | Gravel-Sand mixtures/ poorly graded gravel | GW |
| 21.0 | 21.6 | No recovery | |
| 21.6 | 22.7 | Medium to coarse sand w/ gravel and pebbles and cobbles / more coarse sand w/ fine gravel | GP |
| 22.7 | 24.4 | Medium to coarse sand w/ pebbles and cobbles | GP |
| 24.4 | 25.6 | Gray clay, stiff, dry, cohesive | CL |

**Well id: MPA-12**

| Depth (m) | | Description | Classification |
|---|---|---|---|
| From | To | | |
| 0.0 | 14.6 | Blind drill to 14.9m | |
| 14.6 | 14.9 | Blind drill to 14.9m | |
| 14.9 | 18.6 | No recovery | |
| 18.6 | 20.1 | Medium to coarse sand/ more medium | SW |
| 20.1 | 21.0 | Gravel-Sand mixtures/ poorly graded gravel | GW |
| 21.0 | 25.6 | No recovery | |

**Well id: MPA-13**

| Depth (m) | | Description | Classification |
|---|---|---|---|
| From | To | | |
| 0.0 | 14.6 | Blind drill to 14.9 | |
| 14.6 | 14.9 | Blind drill to 14.9 | |
| 14.9 | 17.4 | No recovery | |
| 17.4 | 19.9 | Medium to coarse sand/ more medium | SW |
| 19.9 | 20.8 | Gravel-Sand mixtures/ poorly graded gravel | GW |
| 20.8 | 21.0 | Medium to coarse sand | SW |
| 21.0 | 22.3 | No recovery | |
| 22.3 | 24.5 | Medium to coarse sand w/ big pebbles and cobbles | GP |
| 24.5 | 25.6 | Gray clay, stiff, dry, cohesive | CL |

**Well id: MPA-14**

| Depth (m) | | Description | Classification |
|---|---|---|---|
| From | To | | |
| 0.0 | 14.6 | Blind drill to 14.9m | |
| 14.6 | 14.9 | Blind drill to 14.9m | |
| 14.9 | 19.8 | Brown fine sand, saturated | SW |
| 19.8 | 20.7 | Brown coarse sand and gravel | GW |
| 20.7 | 21.5 | Brown coarse sand, trace gravel, saturated | SW |
| 21.5 | 24.8 | Mixture of medium to coarse sand w/ big pebbles and cobbles | GP |
| 24.8 | 25.6 | Clay | CL |

**Well id: MPA-15**

| Depth (m) From | To | Description | Classification |
|---|---|---|---|
| 0.0 | 14.6 | Blind drill to 14.9m | |
| 14.6 | 14.9 | Blind drill to 14.9m | |
| 14.9 | 16.2 | Medium to coarse sand/ more medium | SW |
| 16.2 | 17.5 | Gravel-Sand mixtures/ poorly graded gravel | GW |
| 17.5 | 22.6 | No recovery | |
| 22.6 | 22.8 | Coarse gravel | GP |
| 22.8 | 25.0 | Medium to coarse sand w/ big pebbles and cobbles | GP |
| 25.0 | 25.6 | Gray clay, stiff, dry, cohesive | CL |

**Well id: MPS-1**

| Depth (m) From | To | Description | Classification |
|---|---|---|---|
| 0.0 | 14.9 | Blind drill to 15.2m | |
| 14.9 | 15.2 | Blind drill to 15.2m | |
| 15.2 | 17.7 | No recovery | |
| 17.7 | 19.7 | Medium to Coarse Sand/ more medium | SW |
| 19.7 | 20.4 | Gravel-Sand Mixtures/ more gravel, well graded gravel | GW |
| 20.4 | 21.0 | Medium to coarse Sand/ well mixed sand | SW |
| 21.0 | 22.9 | No recovery | |
| 22.9 | 23.9 | Medium to coarse sand /w big pebbles and cobbles | GP |
| 23.9 | 25.3 | Gray clay, stiff, dry, cohesive | CL |

**Well id: MPS-2**

| Depth (m) From | To | Description | Classification |
|---|---|---|---|
| 0.0 | 14.6 | Blind drill to 15.2m | |
| 14.6 | 14.9 | Blind drill to 15.2m | |
| 14.9 | 18.0 | No recovery | |
| 18.0 | 18.6 | Fine to medium sand/ more fine | SW |
| 18.6 | 19.6 | Fine to medium sand/ more medium | SW |
| 19.6 | 20.2 | Gravel-Sand Mixtures/ more gravel, well graded gravel | GW |
| 20.2 | 21.0 | No recovery | |
| 21.0 | 23.2 | No recovery | |
| 23.2 | 23.5 | Medium gravel w/ large pebbles and cobbles, mixed material | GP |
| 23.5 | 24.8 | Medium to coarse sand /w large pebbles and cobbles | GP |
| 24.8 | 25.6 | Gray clay, stiff, dry, cohesive | CL |

141

**Well id: MPS-3**

| Depth (m) | | Description | Classification |
|---|---|---|---|
| From | To | | |
| 0.0 | 14.6 | Blind drill to 15.2m | |
| 14.6 | 14.9 | Blind drill to 15.2m | |
| 14.9 | 16.5 | Medium to coarse sand/ more medium | SW |
| 16.5 | 18.0 | No recovery | |
| 18.0 | 18.6 | Medium to coarse sand/ more medium | SW |
| 18.6 | 19.2 | Gravel-Sand Mixtures/ more gravel, well graded gravel | GW |
| 19.2 | 21.0 | No recovery | |
| 21.0 | 21.9 | No recovery | |
| 21.9 | 24.5 | Gravel-Sand Mixtures, Coarse sand w/ gravel at the top, Coarse sand w/ big pebbles and cobbles at bottom | GP |
| 24.5 | 25.3 | Gray clay, stiff, dry, cohesive | CL |

**Well id: MPS-4**

| Depth (m) | | Description | Classification |
|---|---|---|---|
| From | To | | |
| 0.0 | 14.6 | Blind drill to 49' | |
| 14.6 | 14.9 | Blind drill to 49' | |
| 14.9 | 16.8 | No recovery | |
| 16.8 | 21.0 | Available on Dr. Zhao's log book, not found in the field | |
| 21.0 | 23.8 | Medium to coarse sand/ Probable mixture of gravel | SW |
| 23.8 | 25.1 | Gravel-Sand Mixtures/ Poorly graded gravel | GP |
| 25.1 | 25.6 | Clay | CL |

**Well id: MPS-5**

| Depth (m) | | Description | Classification |
|---|---|---|---|
| From | To | | |
| 0.0 | 14.6 | Blind drill to 15.2m | |
| 14.6 | 14.9 | Blind drill to 15.2m | |
| 14.9 | 18.3 | Medium to coarse sand/ more medium | SW |
| 18.3 | 19.2 | Gravel-Sand mixtures/ more gravel, well graded gravel | GW |
| 19.2 | 21.0 | Medium to coarse sand, well-mixed sands | SW |
| 21.0 | 22.3 | No recovery | |
| 22.3 | 22.7 | Gravel-Sand mixtures/ poorly graded gravel | GP |
| 22.7 | 25.1 | Medium to coarse sand/ w big pebbles and cobbles | GP |
| 25.1 | 25.6 | Gray clay, dry, stiff, cohesive | CL |

**Well id: MPS-6**

| Depth (m) | | Description | Classification |
|---|---|---|---|
| From | To | | |
| 0.0 | 14.6 | Blind drill to 14.9m | |
| 14.6 | 14.9 | Blind drill to 14.9m | |
| 14.9 | 16.8 | No recovery | |
| 16.8 | 19.4 | Medium to coarse sand, more medium | SW |
| 19.4 | 21.0 | Gravel-Sand Mixtures/ well graded gravel | GW |
| 21.0 | 22.7 | No recovery | |
| 22.7 | 23.2 | Medium to coarse sand | SW |
| 23.2 | 23.8 | Gravel-Sand Mixtures/ poorly graded gravel | GP |
| 23.8 | 25.3 | Medium to coarse sand / w big pebbles and cobbles | GP |

**Well id: MPS-7**

| Depth (m) | | Description | Classification |
|---|---|---|---|
| From | To | | |
| 0.0 | 14.6 | Blind drill to 14.9m | |
| 14.6 | 14.9 | Blind drill to 14.9m | |
| 14.9 | 18.7 | No recovery | |
| 18.7 | 20.6 | Medium to coarse sand/ more medium | SW |
| 20.6 | 21.0 | Gravel-Sand Mixtures/ well graded gravel | GW |
| 21.0 | 21.8 | No recovery | |
| 21.8 | 22.1 | Gravel-Sand Mixtures/ well graded gravel | GW |
| 22.1 | 25.1 | Medium to coarse sand/ w big pebbles and cobbles | GP |

**Well id: MPS-8**

| Depth (m) | | Description | Classification |
|---|---|---|---|
| From | To | | |
| 0.0 | 14.6 | Blind drill to 14.9m | |
| 14.6 | 14.9 | Blind drill to 14.9m | |
| 14.9 | 17.4 | No recovery | |
| 17.4 | 19.8 | Medium to coarse sand/ more medium | SW |
| 19.8 | 21.0 | Gravel-sand mixtures/ well graded gravel | GW |
| 21.0 | 22.6 | No recovery | |
| 22.6 | 23.0 | Medium to coarse sand/ more coarse sand | SW |
| 23.0 | 23.3 | Gravel-Sand mixtures/ poorly graded gravel | GP |
| 23.3 | 25.0 | Medium to coarse sand /w big pebbles and cobbles | GP |
| 25.0 | 25.6 | Gray clay, stiff, dry, cohesive | CL |

**Well id: MPS-9**

| Depth (m) | | Description | Classification |
|---|---|---|---|
| From | To | | |
| 0.0 | 14.6 | Blind drill to 14.9m | |
| 14.6 | 14.9 | Blind drill to 14.9m | |
| 14.9 | 17.1 | No recovery | |
| 17.1 | 19.8 | Medium to coarse sand/ more medium | SW |
| 19.8 | 20.4 | Gravel-Sand mixtures/ well graded gravel | GW |
| 20.4 | 21.0 | Medium to coarse sand / more coarse | SW |
| 21.0 | 22.6 | No recovery | |
| 22.6 | 22.9 | Med to coarse sand/ more coarse | SW |
| 22.9 | 23.2 | Gravel-sand mixtures/ poorly graded gravel | GP |
| 23.2 | 25.0 | Medium to coarse sand /w big pebbles and cobbles | GP |

**Well id: MPS-10**

| Depth (m) | | Description | Classification |
|---|---|---|---|
| From | To | | |
| 0.0 | 14.6 | Blind drill to 14.9m | |
| 14.6 | 14.9 | Blind drill to 14.9m | |
| 14.9 | 17.1 | No recovery | |
| 17.1 | 19.8 | Medium to coarse sand/ more medium | SW |
| 19.8 | 21.0 | Gravel-Sand mixtures/ more gravel; well graded gravel | GW |
| 21.0 | 22.9 | No recovery | |
| 22.9 | 23.2 | Medium to coarse sand | SW |
| 23.2 | 25.3 | Medium to coarse sand /w big pebbles and cobbles; material gravelly at the bottom | GP |
| 25.3 | 25.6 | Gray clay, stiff, dry, cohesive | CL |

**Well id: MPS-11**

| Depth (m) | | Description | Classification |
|---|---|---|---|
| From | To | | |
| 0.0 | 14.6 | Blind drill to 14.9m | |
| 14.6 | 14.9 | Blind drill to 14.9m | |
| 14.9 | 18.0 | No recovery | |
| 18.0 | 19.8 | Medium to coarse sand/ more medium | SW |
| 19.8 | 21.0 | Gravel-Sand mixtures/ well graded gravel | GW |
| 21.0 | 22.4 | No recovery | |
| 22.4 | 25.1 | Medium to coarse sand/ with big pebbles and cobbles | GP |
| 25.1 | 25.6 | Gray clay, stiff, dry, cohesive | CL |

**Well id: MPS-12**

| Depth (m) | | Description | Classification |
|---|---|---|---|
| From | To | | |
| 0.0 | 14.6 | Blind drill to 14.9m | |
| 14.6 | 14.9 | Blind drill to 14.9m | |
| 14.9 | 17.7 | No recovery | |
| 17.7 | 19.7 | Medium to coarse sand/ more medium | SW |
| 19.7 | 20.4 | Gravel-Sand mixtures/ more gravel; well graded gravel | GW |
| 20.4 | 21.0 | Medium to coarse sand/ more coarse | SW |
| 21.0 | 22.4 | No recovery | |
| 22.4 | 25.1 | Medium to Coarse sand w/ fine gravel; big pebbles and cobbles | GP |
| 25.1 | 25.6 | Gray clay, stiff, dry, cohesive | CL |

**Well id: MPS-13**

| Depth (m) | | Description | Classification |
|---|---|---|---|
| From | To | | |
| 0.0 | 14.6 | Blind drill to 14.9m | |
| 14.6 | 14.9 | Blind drill to 14.9m | |
| 14.9 | 17.4 | No recovery | |
| 17.4 | 19.7 | Medium to coarse sand/ more medium | SW |
| 19.7 | 21.0 | Gravel-Sand mixtures/ more gravel; well graded graved | GW |
| 21.0 | 22.9 | No recovery | |
| 22.9 | 25.6 | Medium to coarse sand /w fine gravel; big pebbles and cobbles | GP |

**Well id: MPS-14**

| Depth (m) | | Description | Classification |
|---|---|---|---|
| From | To | | |
| 0.0 | 14.6 | Blind drill to 14.9m | |
| 14.6 | 14.9 | Blind drill to 14.9m | |
| 14.9 | 17.1 | No recovery | |
| 17.1 | 19.8 | Medium to coarse sand/ more medium | SW |
| 19.8 | 20.4 | Gravel-Sand Mixtures / well graded gravel | GW |
| 20.4 | 23.5 | No recovery | |
| 23.5 | 24.1 | Coarse Sand | SW |
| 24.1 | 25.6 | Gravel Sand mixtures / poorly graded gravel | GP |

**Well id: MPS-15**

| Depth (m) | | Description | Classification |
|---|---|---|---|
| From | To | | |
| 0.0 | 14.6 | Blind drill to 14.9m | |
| 14.6 | 14.9 | Blind drill to 14.9m | |
| 14.9 | 18.3 | No recovery | |
| 18.3 | 20.7 | Medium to coarse Sand w/ fine gravel | SW |
| 20.7 | 21.0 | Gravel-Sand Mixtures/ well graded gravel | GW |
| 21.0 | 22.9 | No recovery | |
| 22.9 | 24.7 | Medium to coarse sand, more medium | SW |
| 24.7 | 25.3 | Gravel-Sand mixtures; poorly graded gravel | GP |
| 25.3 | 25.6 | Medium to coarse sand/ w gravel and big pebbles | GP |

# APPENDIX B - MatLab SCRIPT FOR THE OPTIMIZATION OF AQUIFER PARAMETERS

\*\*\*\*\*\*\*\*\*\*\*\*\*\*\*\*\*\*\*\*\*\*\*\*\*\*\*\*\*\*\*\*\*\*\*\*\*\*\*\*\*\*\*\*\*\*\*\*\*\*\*\*\*\*\*\*\*\*\*\*\*\*\*\*\*\*\*\*\*\*\*\*\*\*\*\*\*\*\*\*\*\*\*\*\*

This function optimizes aquifer physical parameters given a series of tracer observations in an aquifer

Created by: Jaime A Graulau (2001)
Please send comments to: graulaus@egr.msu.edu
\*\*\*\*\*\*\*\*\*\*\*\*\*\*\*\*\*\*\*\*\*\*\*\*\*\*\*\*\*\*\*\*\*\*\*\*\*\*\*\*\*\*\*\*\*\*\*\*\*\*\*\*\*\*\*\*\*\*\*\*\*\*\*\*\*\*\*\*\*\*\*\*\*\*\*\*\*\*\*\*\*\*\*\*\*

```
function f = funtest(alpha)
persistent Cobs iter disper restfile layers

if (iter > 0)

else
    % load the observed data file only one time
    % and read relevant data for the first time from
    % the dispersion file for MT3Dms....
    iter = 0;
    load observed.dat
    Cobs = observed;
    %read and write to the dispersion file
    fid = fopen('optim.dsp','rt');

    %---change for the no. of layers in the model---
    layers = 1
    for k = 1:layers
        disper(k,:)=fscanf(fid,'%f %f', [layers 2]);
    end
    restfile = fscanf(fid,'%c');
    fclose(fid);
end

iter = iter + 1;
%--- substitute the values of the x array and run MT3DMS_recirc2
for k=1:layers
    %if (9 <= k < 15)   --- remove this coment when running the optimization for more
                layers
        disper(k,2) = alpha(1);
end

fid = fopen('optim.dsp','wt');
for k=1:layers
    if (k==layers)
```

147

```
        fprintf(fid,'%10.0f %9.7f',disper(k,:));
    else
        fprintf(fid,'%10.0f %9.7f\n',disper(k,:));
    end
end
fprintf(fid,'%c',restfile);
fclose(fid);


%----- Run MT3DM -----
!MT3D_recirc_imp optim.mts
%--------------------

modeldata = (read_obs_file('MT3D001.OBS                    INITIAL CO',1,-1))';
Ccalc = interp1(modeldata(:,2), modeldata(:,3),Cobs(:,1));

sumtot = 0.0;
for i=1:5
    Fconc(i)=abs(Cobs(i,2) - Ccalc(i));
    sumtot = sumtot + Fconc(i);
end
f = sumtot;

if (iter == 1)
    fid = fopen('optim_rout.out','wt');
    fprintf(fid, 'Iteration    long dispers(ft)    f  \n');
    fprintf(fid, '---------    ----------------    --- \n');
    fclose(fid);
end
fid= fopen('optim_rout.out', 'at');
fprintf(fid, '%i %f %6.4f\n', iter, alpha(1), f);
fclose(fid);
```

# APPENDIX C - RT3D USER DEFINED REACTION CODE FOR THE EVALUATION OF REDUCTIVE DECHLORINATION LINKED TO CARBON SOURCE DEGRADATION

```
SUBROUTINE rxns(ncomp,nvrxndata,j,i,k,y,dydt,
     &        poros,rhob,reta,rc,nlay,nrow,ncol,vrc)
C*Block 1:*****************************************************************
c List of calling arguments
c ncomp - Total number of components
c nvrxndata - Total number of variable reaction parameters to be input via RCT file
c J, I, K - node location (used if reaction parameters are spatially variable)
c y - Concentration value of all component at the node [array variable y(ncomp)]
c dydt - Computed RHS of your differential equation [array variable dydt(ncomp)]
c poros - porosity of the node
c reta - Retardation factor [ignore dummy reta values of immobile species]
c rhob - bulk density of the node
c rc - Stores spatially constant reaction parameters (can dimension upto 100 values)
c nlay, nrow, ncol - Grid size (used only for dimensioning purposes)
c vrc - Array variable that stores spatially variable reaction parameters
C*End of Block 1**********************************************************


C*Block 2:****************************************************************
c*   *Please do not modify this standard interface block*
     !DEC$ ATTRIBUTES DLLEXPORT :: rxns
     IMPLICIT NONE
     INTEGER ncol,nrow,nlay
     INTEGER ncomp,nvrxndata,j,i,k
     INTEGER, SAVE :: First_time=1
     DOUBLE PRECISION y,dydt,poros,rhob,reta
     DOUBLE PRECISION rc,vrc
     DIMENSION y(ncomp),dydt(ncomp),rc(100)
     DIMENSION vrc(ncol,nrow,nlay,nvrxndata),reta(ncomp)
C*End of block 2**********************************************************


C*Block 3:****************************************************************
c   *Declare your problem-specific new variables here*
c   INTEGER
c jgs   DOUBLE PRECISION pce ,tce,dce,vc,kpce,ktce,kdce,kvc
c jgs   DOUBLE PRECISION ytcepce,ydcetce,yvcdce


C-------------------------------------------------------------------
C     Comment previous declaration statements and declare pertinent
C     variables for the Plume G Model here
c
       DOUBLE PRECISION tol, qtol, X, KsTOL
```

```
            DOUBLE PRECISION tolsorb, Etol, KdTOL
            DOUBLE PRECISION miu, Yxtol, b
            DOUBLE PRECISION PCE, qPCE, KsPCE, Epce, PCEsorb, KdPCE
            DOUBLE PRECISION TCE, qTCE, KsTCE, Ytcepce, TCEsorb, KdTCE, Etce
            DOUBLE PRECISION DCE, qDCE, KsDCE, Edce, DCEsorb, KdDCE, Ydcetce
            DOUBLE PRECISION VC, qVC, KsVC, Evc, VCsorb, KdVC, Yvcdce

C     end of declaration statements for Plume G particular Model
c-------------------------------------------------------------------

C*End of block 3****************************************************************

C*Block 4:*********************************************************************
c     *Initilize reaction parameters here, if required*
            IF (First_time .EQ. 1) THEN
C     --------------------------------------------------------------
C     Plume G particular variables
            KsTOL = 3.50E+01   !half-veloc coeff. for toluene degradation [mg/L]
            qtol = 3.00E-01    !Max spec. toluene utilization rate [1/d]
            Yxtol = 1.52E+00   !Yield coefficient for pce degraders [mg VSS/ mg tol]
            b = 1.00E-01       !Decay coefficient for toluene degraders [1/d]
            Etol = 1.00E-01    !Toluene mass transfer coefficient [1/d]
            KdTOL = 6.60E-07   !Toluene partitioning coefficient [L/mg]
            qPCE = 4.0E-2      !Max specific PCE utilization rate [1/d]
            KsPCE = 8.00E-03   !Half-veloc. coefficient for PCE dehalogenation [1/d]
            Epce = 1.00E-01    !PCE mass transfer coeff [1/d]
            KdPCE = 1.00E-07   !PCE partitioning coefficient [L/mg]
            qTCE = 6.00E-02    !Max. specific TCE utilization rate [1/d]
            Ytcepce = 7.90E-01 !PCE to TCE yield coefficient [mg TCE/mg PCE]
            KsTCE = 1.8E-01    !Half-velocity coeff. for TCE dehalogenation [mg/L]
            Etce = 1.00E-01    !TCE mass transfer coefficient [1/d]
            KdTCE = 9.00E-08   !TCE partitioning coefficient [L/kg]
            qDCE = 9.00E-02    !Max. specific DCE utilization rate [1/d]
            Ydcetce = 5.70E-01 !TCE to DCE yield coefficient [mg DCE/mg TCE]
            KsDCE = 2.88E-01   !Half velocity coefficient for DCE dehalogeation [mg/L]
            Edce = 1.00E-01    !DCE mass transfer coefficient [1/d]
            KdDCE = 5.00E-08   !DCE partitioning coefficient [L/kg]
            qVC = 5.00E-03     !Max. specific VC utilization [1/d]
            Yvcdce = 6.50E-01  !DCE to VC yield coefficient [mg VC/mg DCE]
            KsVC = 1.61E-01    !Half-velocity coefficient for VC dehalogenation [mg/L]
            Evc = 1.00E-01     !VC mass transfer coefficient [1/d]
            KdVC = 2.00E-09    !VC partitioning coefficient [L/kg]
            miu = qtol*Yxtol

!           KsTOL = rc(1)     !Half-veloc coeff. for toluene degradation [mg/L]
!           qtol = rc(2)      !Max spec. toluene utilization rate [1/d]
```

```
!        Yxtol = rc(3)    !Yield coeff. for pce degraders [mg VSS/ mg tol]
!        b = rc(4)        !Decay coefficient for microorganisms [1/d]
!        Etol = rc(5)     !Toluene mass transfer coefficient [1/d]
!        KdTOL = rc(6)    !Toluene partitioning coefficient [L/kg]
!        qPCE = rc(7)     !Max specific PCE utilization rate [1/d]
!        KsPCE = rc(8)    !Half-veloc. coefficient for PCE dehal. [1/d]
!        Epce = rc(9)     !PCE mass transfer coeff [1/d]
!        KdPCE = rc(10)   !PCE partitioning coefficient [L/kg]
!        qTCE = rc(11)    !Max. specific TCE utilization rate [1/d]
!        Ytcepce = rc(12) !PCE to TCE yield coefficient [mg TCE/mg PCE]
!        KsTCE = rc(13)   !Half-velocity coefficient for TCE dehalog. [mg/L]
!        Etce = rc(14)    !TCE mass transfer coefficient [1/d]
!        KdTCE = rc(15)   !TCE partitioning coefficient [L/kg]
!        qDCE = rc(16)    !Max. specific DCE utilization rate [1/d]
!        Ydcetce = rc(17) !TCE to DCE yield coefficient [mg DCE/mg TCE]
!        KsDCE = rc(18)   !Half velocity coefficient for DCE dehalog. [mg/L]
!        Edce = rc(19)    !DCE mass transfer coefficient [1/d]
!        KdDCE = rc(20)   !DCE partitioning coefficient [L/kg]
!        qVC = rc(21)     !Max. specific VC utilization [1/d]
!        Yvcdce = rc(22)  !DCE to VC yield coefficient [mg VC/mg DCE]
!        KsVC = rc(23)    !Half-velocity coefficient for VC dehal. [mg/L]
!        Evc = rc(24)     !VC mass transfer coefficient [1/d]
!        KdVC = rc(25)    !VC partitioning coefficient [L/kg]
!        miu = rc(2)*rc(3) !Maximum specific bacterial growth rate [1/d]


C    end of variable initialization for Plume G model
C    --------------------------------------------------------------------
     First_time = 0 !reset First_time to skip this block later
        END IF
C*End of block 4**********************************************************************


C*Block 5:***************************************************************************
c     *Assign or compute values for new variables, if required*
c        Assign the Plume G model statements in this sub-block
         tol = y(1)
         X = y(2)
         PCE = y(3)
         TCE = y(4)
         DCE = y(5)
         VC = y(6)
         tolsorb = y(7)
         PCEsorb = y(8)
         TCEsorb = y(9)
         DCEsorb = y(10)
         VCsorb = y(11)
c     end of assignment statements for plume G model
```

```fortran
c      --------------------------------------------------------------------

C*End of block 5*****************************************************************

C*Block 6:**********************************************************************
c      *Differential Reaction Equations*
C      Plume G particular reactions here

       dydt(1)=-qtol*X*(tol/(tol+KsTOL))-(Etol*rhob/poros)*
     &      (KdTOL*tol-tolsorb)

       dydt(2)=miu*X*(tol/(tol+KsTOL))-b*X

       dydt(3)=-qPCE*X*(PCE/(PCE+KsPCE))-(Epce*rhob/poros)*
     &      (KdPCE*PCE-PCEsorb)

       dydt(4)=Ytcepce*qPCE*X*(PCE/(PCE+KsPCE))-
qTCE*X*(TCE/(TCE+KsTCE))-
     &      (Etce*rhob/poros)*(TCE*KdTCE-TCEsorb)

       dydt(5)=Ydcetce*qTCE*X*(TCE/(TCE+KsTCE))-
qDCE*X*(DCE/(DCE+KsDCE))-
     &      (Edce*rhob/poros)*(DCE*KdDCE-DCEsorb)

       dydt(6)=Yvcdce*qDCE*X*(DCE/(DCE+KsDCE))-qVC*X*(VC/(VC+KsVC))-
     &      (Evc*rhob/poros)*(VC*KdVC-VCsorb)

       dydt(7)=Etol*(tol*KdTOL-tolsorb)

       dydt(8)=Epce*(PCE*KdPCE-PCEsorb)

       dydt(9)=Etce*(TCE*KdTCE-TCEsorb)

       dydt(10)=Edce*(DCE*KdDCE-DCEsorb)

       dydt(11)=Evc*(VC*KdVC-VCsorb)
!
C*End of block 6************************************************************
      RETURN
      END
```